Characterisation of the Homogeneity of Thiol-Ene Hydrogels by Light Scattering Methods

Doctoral Thesis

(Dissertation)

to be awarded the degree
Doctor rerum naturalium (Dr. rer. nat.)

submitted by

Svenja Grube

from Osterode am Harz

approved by the Faculty of Natural and Materials Sciences,
Clausthal University of Technology

date of oral examination:

15.06.2012

This thesis was written at the Institute of Physical Chemistry at Clausthal University of Technology, Clausthal-Zellerfeld, Germany, in the time between September 2008 and January 2012.

Chairperson of the Board of Examiners: Prof. Dr. D. Kaufmann

Chief Reviewer: Prof. Dr. W. Oppermann

Reviewer: PD Dr. J. Adams

Name, Vorname: **Datum:**

Grube, Svenja   **24.01.2012**

EIDESSTATTLICHE ERKLÄRUNG

Hiermit erkläre ich an Eides Statt, dass ich die bei der Fakultät für Natur- und Materialwissenschaften der Technischen Universität Clausthal eingereichte Dissertation selbständig und ohne unerlaubte Hilfe verfasst und die benutzten Hilfsmittel vollständig angegeben habe.

Name, Vorname: **Datum:**

Grube, Svenja   **24.01.2012**

EIDESSTATTLICHE ERKLÄRUNG

Hiermit erkläre ich an Eides Statt, dass die eingereichte Dissertation weder in Teilen noch in ihrer Gesamtheit einer anderen Hochschule zur Begutachtung vorliegt oder vorgelegen hat und dass ich bisher noch keinen Promotionsversuch unternommen habe.

"I have a friend who's an artist and has sometimes taken a view which I don't agree with very well. He'll hold up a flower and say "look how beautiful it is," and I'll agree. Then he says "I as an artist can see how beautiful this is but you as a scientist take this all apart and it becomes a dull thing," and I think that he's kind of nutty. First of all, the beauty that he sees is available to other people and to me too, I believe. Although I may not be quite as refined aesthetically as he is ... I can appreciate the beauty of a flower. At the same time, I see much more about the flower than he sees. I could imagine the cells in there, the complicated actions inside, which also have a beauty. I mean it's not just beauty at this dimension, at one centimeter; there's also beauty at smaller dimensions, the inner structure, also the processes. The fact that the colors in the flower evolved in order to attract insects to pollinate it is interesting; it means that insects can see the color. It adds a question: does this aesthetic sense also exist in the lower forms? Why is it aesthetic? All kinds of interesting questions which the science knowledge only adds to the excitement, the mystery and the awe of a flower. It only adds. I don't understand how it subtracts."

— Richard P. Feynman

Abstract

The aim of this thesis was to prepare hydrogels that possess a spatially homogeneous network structure. To reach this aim the thiol-ene polymerisation (TEP) was used. This reaction is a radical step-growth polymerisation with additional characteristics of an end-linking polymerisation and should thus be capable of forming homogeneous networks. As a reference a common free radical crosslinking copolymerisation (FCC) was utilised, usually yielding rather inhomogeneous structures. For the TEP three series each consisting of the same crosslinker (a trithiol) but different network chain precursors (three linear dienes with different molar masses) were used. The monomer used for the FCC was acrylamide combined in two series with a low and a high concentration of a tetrafunctional crosslinker.

The mainly used characterisation methods were rheology, to find out about the macroscopic properties of the gels, and dynamic light scattering, to determine the underlying network structure. The gels were examined in reactor batch state, i.e. directly after preparation, and in equilibrium swollen state.

The results for the reactor batch state demonstrated that the thiol-ene gels were more homogeneous than the polyacrylamide gels. Especially the thiol-ene gels with the longer diene precursor chains showed virtually no spatial inhomogeneity at all possessing a remarkably uniform concentration distribution. In contrast, the spatial inhomogeneity of the polyacrylamide gels was rather pronounced, particularly for the samples with the higher crosslinker concentration.

Swelling the hydrogels to equilibrium led to an increase in inhomogeneity, especially pronounced for the formerly very homogeneous thiol-ene gels. All the gels, thiol-ene and polyacrylamide, now exhibited the same, rather high spatial inhomogeneity. In the state of preparation the thiol-ene gels exhibited an evenly distributed polymer concentration and potential defects did not have an impact on the light scattering intensity. However, subjecting them to equilibrium swelling brought out the non-uniformity within the network. Zones that were more highly crosslinked did not swell as much as the less crosslinked ones. This yielded systems with much greater concentration differences than before, leading to stronger scattering.

In conclusion, it can be said that in the state of preparation the thiol-ene hydrogels certainly exhibited a very homogeneous network structure with a uniform concentration distribution. However, in the equilibrium swollen state inhomogeneities appeared that could not be detected before. In this state both the thiol-ene and the polyacrylamide gels showed the same, high network inhomogeneity.

TABLE OF CONTENTS

1   Introduction

Hydrogels are important materials in today's everyday life[1,2]. They are used as scaffolds in tissue engineering[3,4], soft contact lenses[5], superabsorbent material in diapers[6], drug delivery systems[7,8], wound dressing[9], sensors and actuators[10], chemical valves[11], optically transparent materials[12], metal particle preparation[13], chromatography[14], agriculture (controlled release of fertiliser)[15] and probably many more areas.

This wide variety of applications shows the importance of hydrogels. For some of these applications the inner structure of the hydrogel is not the decisive factor. Others may have the additional requirement for the network structure to be homogeneous, since a high degree of inhomogeneity can negatively affect properties like the permeability, the stiffness or the optical properties of the gel. For applications that rely on these factors, it is crucial to be able to know the structure of the underlying network and to be able to generate it in a reproducible way.

Polymer networks and gels are complex, not yet fully understood systems that can exhibit a variety of defects and imperfections leading to an inhomogeneous structure. The existence of inhomogeneities in polymer networks is well-known and has been investigated extensively. It has of course also been attempted to control the formation of networks with regard to decreasing the inhomogeneity (chapters 2.1.4.2 & 2.1.4.3).

The aim of this thesis is the formation of hydrogels that possess a homogeneous network structure. It is commonly known that network structures formed from the conventional free radical crosslinking copolymerisation (FCC) tend to be spatially inhomogeneous, the degree of inhomogeneity depending on the reaction conditions. Although this kind of polymerisation has the advantage of being easily conducted, the formation of inhomogeneities is one of its inherent features. Thus, to achieve the aim of homogeneous networks in this study another reaction mechanism is used for the crosslinking polymerisation, namely the thiol-ene polymerisation (TEP).

The thiol-ene polymerisation was chosen because it is known to form rather homogeneous networks (chapter 2.2.3) and it is also carried out very easily. As the FCC, it is a radical polymerisation, however it does not proceed by chain growth but by step growth of

the polymer chains. Further more it is oxygen insensitive which is certainly an advantage over the FCC, which should be carried out in an inert gas atmosphere.

One of the requirements for a successful thiol-ene polymerisation is the fact that the monomers are not capable of homopolymerising. Thus, a thiol and an ene alternately react with each other. The substances used for this study are a trithiol that acts as the crosslinker and dienes that are the precursors for the network chains. Hence, due to ruling out homopolymerisation, the polymerisation proceeds in an end-linking fashion. Employing suitable reaction conditions, especially a sufficiently high monomer concentration and sufficiently long network chain precursors, end-linking polymerisations have the potential of producing highly homogeneous structures. So, in addition to the advantages of a step-growth polymerisation this system also possesses the benefits of an end-linking polymerisation. Thus, the TEP is rather promising concerning the formation of highly homogeneous network structures.

The homogeneous structure built up by the TEP is, according to literature, only verified for polymer networks without any solvent and was proved by dynamic mechanical analysis, which is a macroscopic method (chapter 2.2.3). This thesis will now focus on determining the network homogeneity in gels mainly ascertained by light scattering methods, which can describe the microstructure of the underlying network. The macroscopic properties will be measured with oscillatory rheology.

2 Theoretical Background

This thesis addresses an approach to decrease inhomogeneity in polymer networks by using a dedicated reaction mechanism, the thiol-ene polymerisation. The samples were hydrogels, thus networks swollen in water. To determine their degree of inhomogeneity, light scattering measurements were conducted. Comparative studies on a macroscopic scale were carried out by rheometry. The next chapters will be concerned with elucidating the theoretical background of these topics.

2.1 Polymer Networks and Gels

2.1.1 Basic Structure and Formation Methods

A system of three-dimensionally interconnected polymer chains is called a polymer network[16,17]. The junctions that connect the polymer chains are the crosslinks and the strands between them are the network chains. The number of network chains emanating from a junction is its functionality. Basically, a polymer network consists of one single polymer molecule with an extremely high molar mass. If the observed system does not solely consist of the network itself but is swollen in an additional liquid, it is a polymer gel. Gels comprising water as the second phase are called a hydrogels. Polymer gels can be pictured as a certain amount of liquid kept in shape by a three-dimensional polymer mesh. It often consists of a very small percentage of the polymer itself and hence, a very large fraction of the system is taken up by the liquid. It can be dimensionally stable down to less than one percent, by weight, of polymer[18]. It simultaneously exhibits solid and liquid properties and thus belongs to the category of soft matter[19].

The junctions holding together the strands of a network can be either of chemical or of physical nature, giving rise to chemical or physical networks[20,21]. Chemical crosslinks are intramolecular, covalent bonds which irreversibly connect the network chains. Physical crosslinks are non-covalent, intermolecular bonds. Strong physical networks are formed if the polymer chains partially crystallise[22,23], form micelles[24,25] or helical structures[26,27], thereby generating domains that act as crosslinks. The crystallised domains often exhibit lamellar structures. They cover more than just one segment of a network chain and may thus be

relatively strong junctions, or rather junction zones. Weak physical networks are held together by physical crosslinks like entanglements among the network chains (e.g. in a polymer melt[28]) or physical interactions like hydrogen bonds[29-31], ionic[32,33], dipole-dipole or VAN-DER-WAALS interactions[34,35]. Ionic interactions can be rather strong physical bonds with energies of $\cong 250$ kJ/mol[36]. However, physical junctions are usually weaker ($\cong 1$ to 50 kJ/mol[20,37]) than the covalent bonds in chemical crosslinks ($\cong 250$ to 350 kJ/mol[38]). They dynamically break and reform repeatedly[20]. Forming a chemical network is irreversible and it cannot be taken apart to form uncrosslinked polymer chains without destroying it further. If the network strands in a chemical network are long enough, it is possible for them to entangle. That yields trapped entanglements, which introduce additional, physical crosslinks into the network. This thesis focuses on gels consisting of chemical networks.
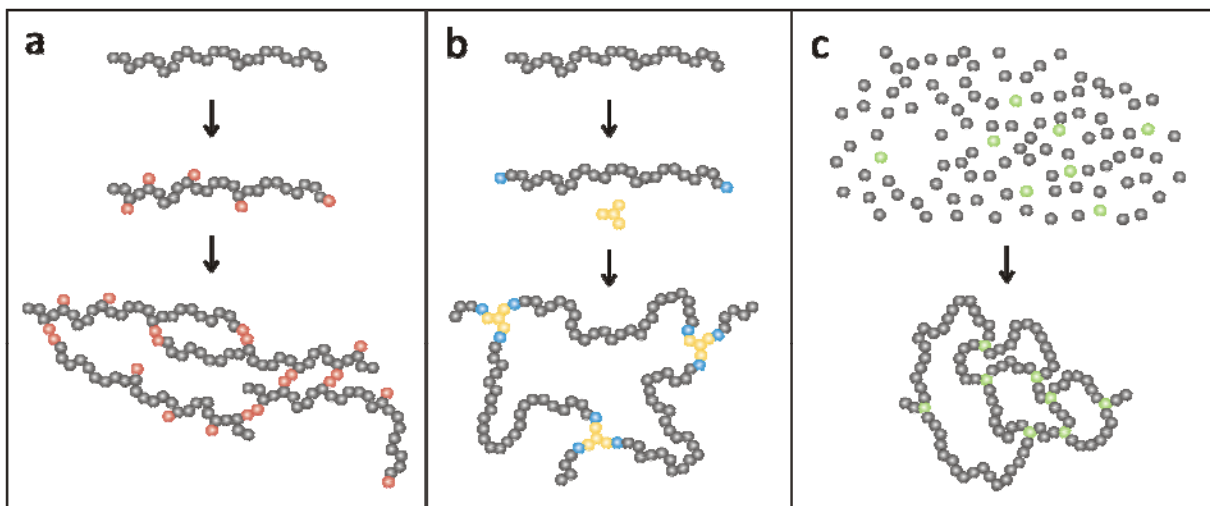
Fig. 1: Different ways of preparing polymer networks; **a:** random crosslinking of already existing polymer chains, red spheres: crosslinking functional group, grey spheres: monomer units; **b:** end-linking of already existing polymer chains, blues spheres: functional end-groups, yellow spheres: trifunctional crosslinker; **c:** crosslinking copolymerisation from monomers as smallest unit, green spheres: trifunctional crosslinker molecules, grey spheres: monomers

Fig. 1 shows different options to prepare chemical polymer networks. They can be formed by random crosslinking of already existing, randomly functionalised polymer chains that act as network chains afterwards. The functional groups at the polymer backbones couple and form network junctions (Fig. 1 a). Furthermore, end-linking of pre-existing polymer chains can be used. These chains have to be suitably functionalised at both ends, enabling them to

react with an appropriate crosslinker molecule which has to be at least trifunctional (Fig. 1 b). Another possibility is the crosslinking copolymerisation that starts out from monomers and multifunctional crosslinker molecules. Due to a similar structure, the monomers and crosslinkers usually have comparable reactivities. During the polymerisation, the crosslinker molecules are inserted into the growing polymer chains, at the same time connecting them to form a network (Fig. 1 c).

2.1.2 Formation of Polymer Gels and Swelling

A permanent, chemical polymer *network* cannot be dissolved by any liquid but it can swell, thus becoming a polymer *gel*[39]. Usually, polymer gels are not formed by swelling dry networks but by adding a liquid to the reaction mixture. During the formation of a polymer gel, the gelation, the sol-gel transition takes place, at which the initially liquid sample (sol) becomes solid (gel)[20]. In the sol state, the growing molecules are still soluble in the surrounding medium. However, they become longer and more and more branched. At a certain point of the reaction, the whole volume of the sample is spanned by one continuous, "infinite" molecule, the incipient gel. This molecule is not soluble anymore but can merely swell in the surrounding liquid. The point at which this transition occurs is called the gel point. Shortly after it, there is still a high fraction of low molecular weight, branched chains that are soluble. As the reaction proceeds they get connected to the incipient gel and to each other forming a fully developed polymer gel. Directly after preparation, without further swelling or drying, polymer gels are called reactor-batch gels.

Reactor batch gels usually still have the potential to swell further. Swelling is thermodynamically the same process as dissolving but with a different macroscopic outcome[40,41]. The network is maintained but, immersing it in a liquid that is a good solvent for that particular polymer, it typically shows a substantial increase in volume. Superabsorbent hydrogels, for instance, can imbibe water to as much as 100,000 %[18] of the mass of their underlying network. Important factors that determine the degree of swelling are the length of the network chains, the network chain density, the temperature and the thermodynamic interactions between network and solvent[42]. The equilibrium swelling is reached when the energy that is released due to the solvation of the network chains equals

the energy needed to counteract the elastic forces of the system so to extend the network chains[43].

The volume-related degree of swelling, Q_V, is defined as the quotient of the volume of the gel in swollen state, V_{sw}, and the volume in the dry state without any solvent, V_{dry} (eq. 1). The inverse of the degree of swelling Q_V is the volume fraction, ϕ_V, of the network in swollen state, $Q_V = 1/\phi_V$.

$$Q_V = \frac{V_{sw}}{V_{dry}} \qquad\qquad (1)$$

Since it is difficult to exactly determine the volume of a swollen gel sample, it is favourable to work with the mass-related degree of swelling, Q_m (eq. 2), because weighing a sample is much more precise. The mass of the swollen gel, m_{sw}, is the sum of the mass of the solvent and the mass of the dry network, m_{dry}.

$$Q_m = \frac{m_{sw}}{m_{dry}} \qquad\qquad (2)$$

The relation between the volume- and mass-related degree of swelling (eq. 3) requires the density of the solvent, ρ_{solv}, and the density of the dry network, ρ_{net}. If the densities are the same it is $Q_V = Q_m$ [44].

$$Q_V = 1 + \frac{(Q_m - 1) \cdot \rho_{net}}{\rho_{solv}} \qquad\qquad (3)$$

2.1.3   Network Rheology

One of the most important properties of a polymer network above the glass transition temperature is its rubber elasticity[45]. It can usually be deformed to a great extent without being destroyed and recover its original shape afterwards. For a network to be capable of being deformed without being broken, it needs to have access to a large number of network chain conformations. This is achievable by flexible, sufficiently long network chains. The kind of elasticity that originates from this fact is called entropic elasticity as opposed to energy elasticity. The latter exists with metals, for instance. Elastically deforming or stretching a metal, takes it out of its energetic equilibrium to a state of higher energy with an increased distance between the metal atoms. Due to the system wanting to decrease its energy again, it reforms to its original state as soon as the deforming force is released. Deforming a polymer network involves another effect. The number of different conformations a network chain can adopt if it is elongated, is a lot smaller than in the undeformed state, giving rise to a reduction of the entropy of the system. Accordingly, reforming the original state leads to an increase in entropy. This is highly favourable and therefore causes a restoring force yielding elasticity.

2.1.3.1   Network Viscoelasticity

Polymer networks are certainly no ideal elastic materials as described by HOOKE's law of elasticity. In fact, they are viscoelastic, combining both viscous and elastic properties[46,47]. In general, deforming a material can cause different reactions, depending on its type. Elastic behaviour involves instantaneous response to deformation and complete storage of the energy of deformation. The original shape is fully recovered afterwards, without delay (limited by inertia). HOOKE's law of linear elasticity for a shear experiment (eq. 4) describes this behaviour with the shear stress, σ, the shear modulus, G, and the shear strain, γ. The shear modulus can be described as the resistance of a material against deformation. Empirically, HOOKE's law is applicable to all solids, as long as the shear strain is sufficiently low.

$$\sigma = G \cdot \gamma \qquad\qquad\qquad (\, 4 \,)$$

The deformation of an ideal viscous liquid is associated with a retarded response and complete irreversibility. The energy of deformation is dissipated as heat. Afterwards, the material remains in the fully deformed state. Such liquids are described by NEWTON's law of viscosity (eq. 5) with the dynamic viscosity, η, and the shear rate, $\dot{\gamma}$.

$$\sigma = \eta \cdot \dot{\gamma} \qquad\qquad (5)$$

For ideally elastic materials, the relation between stress and strain is time-independent. The rate at which the deformation is carried out, does not affect the response. However, in the case of viscoelasticity it is important, as can be seen in Fig. 2. For high shear frequencies, ω (region I), which corresponds to short times, the shear modulus adopts very high values, describing samples in the glassy state. In region II the viscoelastic material softens, passing through the glass transition. At medium frequencies, the rubber-elastic plateau (region III) illustrates entropically elastic materials. For linear polymers, the rubber-elastic plateau becomes broader with increasing molar mass, since longer polymer chains exhibit a higher entanglement lifetime. Reducing the frequency further, linear polymers start to flow, with G sharply decreasing (region IV). Permanently crosslinked networks retain their rubberlike elasticity even for very low frequencies (region V). For $\omega \rightarrow 0$ the equilibrium shear modulus, G_0, is reached.
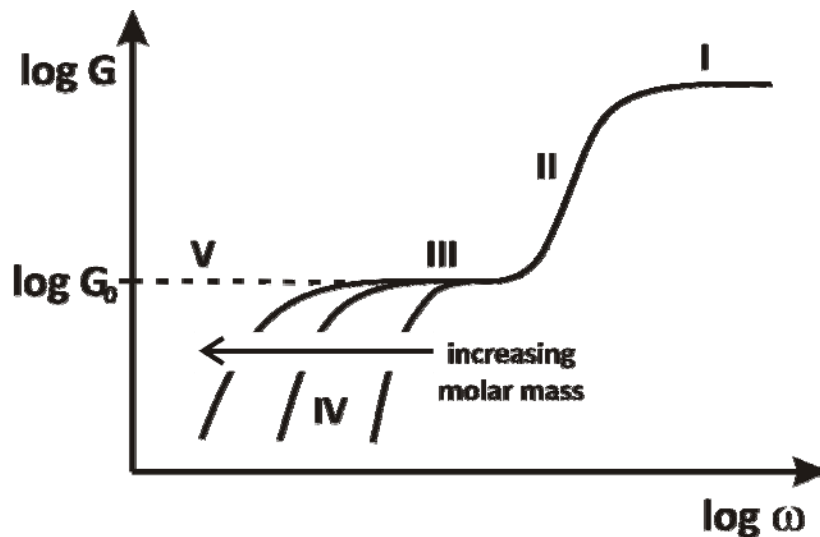

Fig. 2: Shear modulus G changing with shear frequency, ω; **I** – glassy region, **II** – glass transition region, "leathery" region, **III** – rubber-elastic plateau, **IV** – viscous flow region, **V** – polymer network behaviour; G_0: equilibrium modulus of a permanently crosslinked network at $\omega \rightarrow 0$

Viscoelastic materials can be subdivided into two cases, viscoelastic liquids and viscoelastic solids. Deforming a viscoelastic *liquid* is irreversible, since it cannot entirely regain its initial shape, due to viscous energy dissipation. Yet, the elastic fraction of the material yields partial energy storage, so that it does not remain completely deformed. However, it has to be considered at which time scale the deformation is carried out. For very low shear frequencies, ω, viscoelastic liquids this viscously flow during distortion (Fig. 2, IV). A polymer melt is an example of a viscoelastic liquid. A viscoelastic *solid* shows full reversibility of its shape after deformation. What distinguishes it from a purely elastic solid is a delay in the recovery of the initial shape. For very low shear frequencies, ω, viscoelastic solids do not flow during distortion (Fig. 2, V). Chemical gels can be characterised as viscoelastic solids. Their equilibrium shear modulus strongly depends on the amount of crosslinks and the length of the network chains. At frequencies below the glassy state, a gel becomes stiffer if the number of network junctions is increased, resulting in a higher shear modulus.

To measure the viscoelastic properties of a sample, different rheological methods can be used depending on the sample and the required information. The main types are displayed in table 1. The only one that shall be presented in more detail is the oscillation experiment, since it was used as a characterisation method within the scope of this thesis.

Table 1: Different kinds of rheological experiments, their properties and their applications; sin.: sinusoidal; dep.: dependent; exp.: experiment; const.: constant

Technique	Applied Quantity	Measured Quantity	Mainly Used For
viscometry exp.	const. shear rate	const. stress	liquid samples
creep exp.	const. stress	time-dep. strain	liquid samples, also gels
relaxation exp.	const. strain	time-dep. stress	liquid samples, also gels
oscillation exp.	sin. stress or strain	sin. strain or stress	any kind of soft matter

2.1.3.2 Oscillation Measurements[46,47]

In a rheological oscillation measurement the examined sample is deformed sinusoidally, oscillating at the angular frequency, ω. A specific shear strain, $\gamma(t)$, (eq. 6), with the strain amplitude, γ_0, can be applied to the sample, by letting the instrument dynamically deform it to a certain extent and then measure the necessary shear stress, $\sigma(t)$.

$$\gamma(t) = \gamma_0 \cdot \sin(\omega t) \tag{6}$$

For an ideally elastic material HOOKE's law still applies, the shear stress and shear strain now being time-dependent. Eq. 7 accordingly shows that the measured quantity, the shear stress, is in-phase with the applied strain. The elastic material instantly reacts to the deformation that is imposed upon it. This is illustrated in fig. 3, top left. The applied strain and the responding stress exhibit the same frequency and the same phase.

$$\sigma(t) = G \cdot \gamma(t) = G \cdot \gamma_0 \cdot \sin(\omega t) \tag{7}$$

For a NEWTONian liquid the resulting shear stress can be determined by eq. 8. Strain and stress are phase-shifted by $\pi/2$, meaning that if the strain passes through a maximum or minimum the stress and the shear rate are zero and vice versa (Fig. 3, top right). The response of the viscous material to the applied strain is delayed.

$$\sigma(t) = \eta \cdot \frac{d\gamma(t)}{dt} = \eta \cdot \gamma_0 \cdot \omega \cdot \cos(\omega t) = \eta \cdot \gamma_0 \cdot \omega \cdot \sin\left(\omega t + \frac{\pi}{2}\right) \tag{8}$$

In the viscoelastic case the phase-shift, δ, of stress with respect to strain is in between the two above-mentioned extreme examples, $0 < \delta < \pi/2$ (eq. 9, σ_0: stress amplitude,).

$$\sigma(t) = \sigma_0 \cdot \sin(\omega t + \delta) \tag{9}$$

The applied strain and the resulting stress are out-of-phase with each other, but they always oscillate at the same frequency (Fig. 3, bottom).
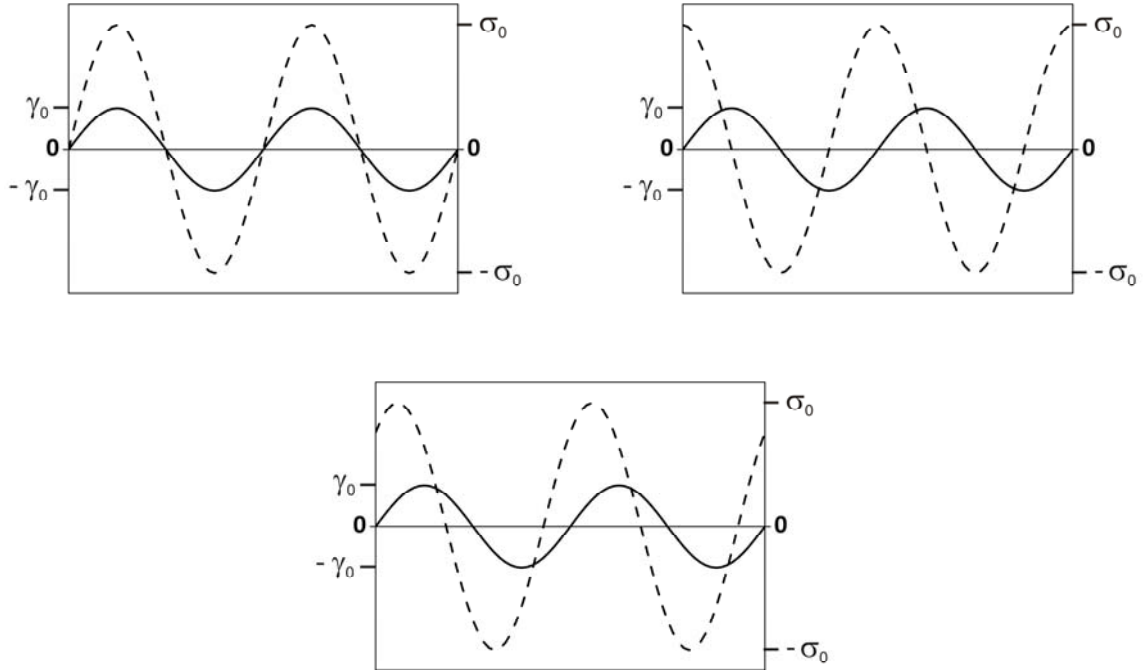

Fig. 3: Phase relations between the applied strain, $\gamma(t)$ (solid line), and the resulting stress, $\sigma(t)$ (dashed line), in an oscillation measurement, top left: elastic material; top right: viscous material; bottom: viscoelastic material; σ_0: stress amplitude, γ_0: strain amplitude

Since viscoelasticity describes a state which involves two entirely opposed properties, elasticity and viscosity, the stress can be split up into an elastic component being in phase ($\delta = 0$) and a viscous component by $\delta = \pi/2$ out-of-phase with respect to the strain. Yet, both of them exhibit the same oscillation frequency (eq. 10). Accordingly, the shear modulus has to be separated into two values, G′ being the elastic modulus and G″ the viscous modulus. G′ is also called the storage modulus. It is a measure for the deformation energy that is stored within the system and is afterwards used to recover the original state. Correspondingly, G″ is the loss modulus characterising the energy dissipated by deformation and thus converted into thermal energy.

$$\sigma(t) = \gamma_0 \left[G'(\omega) \cdot \sin(\omega t) + G''(\omega) \cdot \cos(\omega t) \right] \qquad (10)$$

The shear modulus determined in a dynamic measurement, like an oscillation experiment, is a complex quantity, G*. The real part is the elastic modulus, G′, and the imaginary part is the viscous modulus, G′′ (eq. 11).

$$G^*(\omega) = G'(\omega) + i \cdot G''(\omega) \qquad (\,11\,)$$

The ratio of the viscous to the elastic modulus is the so-called loss tangent, $\tan\delta$, (eq. 12). It is also called the damping factor and can be used as a measure of viscoelasticity.

$$\tan\delta = \frac{G''}{G'} \qquad (\,12\,)$$

Corresponding to the phase angle, δ, the loss tangent, $\tan\delta$, can be divided into different ranges that are related to certain material properties (Table 2).

Table 2: Material properties connected to different value ranges of the loss tangent, $\tan\delta$; δ: phase angle between G′ (elastic modulus) and G′′ (viscous modulus)

Loss Tangent	Phase Angle	Modulus	Properties
$\tan\delta \to \infty$	$\delta = \pi/2$	G′ = 0	ideally viscous
$\infty > \tan\delta > 1$	$\pi/2 > \delta > \pi/4$	G′′ >> G′	viscoelastic liquid
$\tan\delta = 1$	$\delta = \pi/4$	G′ = G′′	gel point
$0 < \tan\delta < 1$	$\pi/4 > \delta > 0$	G′ >> G′′	viscoelastic solid
$\tan\delta = 0$	$\delta = 0$	G′′ = 0	ideally elastic

As can be seen in table 2, an ideally viscous NEWTONian liquid is only characterised by the loss modulus, G′′, consistent with the fact that all deformation energy is dissipated during the process. An ideally elastic HOOKEan solid stores all that energy to recover its initial state, so it is solely described by the storage modulus, G′. In the more realistic case of a viscoelastic liquid or solid both moduli exist. In a viscoelastic liquid G′′ exceeds G′ accounting for the fact that such materials can relax to zero stress after a sudden increase in strain. In contrast, a viscoelastic solid retains part of the stress, reflected in the fact that G′ adopts a greater value

than G''. However, it has to be kept in mind that for viscoelastic materials, the relation between G' and G'' usually depends on the observed time scale and temperature.

A special case with regard to the network structure is the gel point, which in table 2 is denoted as the situation when G' and G'' are equal. During the formation of a chemical network the gel point is reached when the weight-average molar mass, M_w, diverges and thus becomes virtually infinite[48]. This is the point when the sample turns from liquid to solid. WINTER and CHAMBON[49] investigated the phenomenon and found out that the assumption concerning the equality of G' and G'' only holds if both have the same value over a wide range of frequencies. Generally, at the gel point both moduli are proportional to the frequency according to a power law (eq. 13).

$$G' \propto G'' \propto \omega^n$$ (13)

The network specific exponent, n, is called the relaxation exponent and can adopt values between 0 and 1[50]. Eq. 13 indicates that at the gel point in a double logarithmic plot G' and G'' exhibit the same slope, n, at all frequencies in the linear viscoelastic region. Consequently, the loss tangent is independent of frequency (eq. 14). If n = 0.5, the loss tangent becomes unity and thus G' = G''. According to WINTER[51], this is either the case for end-linking polymerisations that are stoichiometrically balanced or in which the concentration of the functional groups of the crosslinker exceeds the concentration of the functional groups of the difunctional molecule. If the system is short of functional groups stemming from the crosslinker, then n > 0.5. This results in the gel point occuring before the intersection of G' and G''. Generally, the loss tangent becomes frequency independent precisely at the gel point[52].

$$\tan\delta = \frac{G''}{G'} = \tan\left(\frac{n \cdot \pi}{2}\right)$$ (14)

For this thesis only stoichiometrically balanced systems were used. Accordingly, it is assumed that n = 0.5. The gel point can thus be determined by monitoring crosslinking reactions in a time-course experiment at constant frequency and strain, hence recording the

evolution of the moduli G′ and G′′ during the reaction (Fig. 4). When G′ and G′′ intersect the gel point is reached.
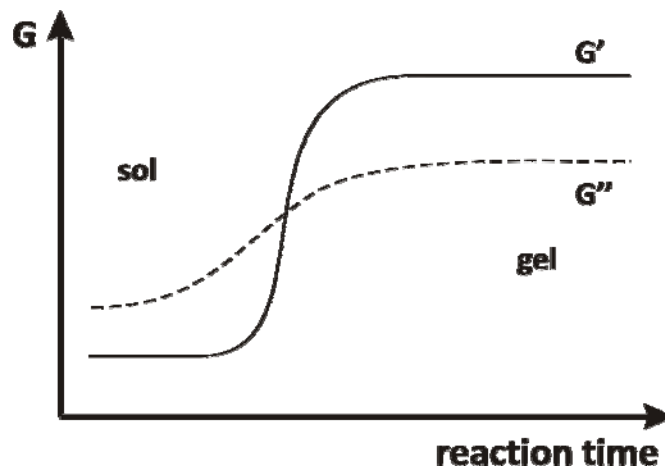

Fig. 4: Typical plot of the elastic modulus G′ and the viscous modulus G′′ versus the reaction time of a crosslinking polymerisation; the system passes from the liquid sol to the solid gel state; the intersection of the curves is often considered to be (a sufficiently good estimate for) the gel point; the y-axis is scaled logarithmically; continuous line: G′; dashed line: G′′

A special experiment that can be performed is the frequency sweep. It is carried out at a constant deformation while the shear frequency changes. Frequency sweeps can be used to investigate the time-dependent rheological behaviour of viscoelastic materials, as shown in fig. 2. The elastic modulus of a fully developed, permanent polymer network (which usually adopts almost the same value as G*, since G′′ is comparatively small) should not decline with decreasing shear frequency. If it still does, it may be concluded that the present sample is not a permanently crosslinked system.

14

2.1.4   Theoretical Models and Structural Inhomogeneity

The structure of a perfect network[53] involves a GAUSSIAN distribution of the end-to-end distances of the network chains and does not exhibit any defects or inhomogeneities. All crosslinker molecules have reacted according to their functionality and all their reactive sites are connected to an elastically active network chain (Fig. 5). There are no trapped entanglements, loops, dangling chains or unreacted functional groups. This way all network chains contribute to the elasticity of the polymer network.
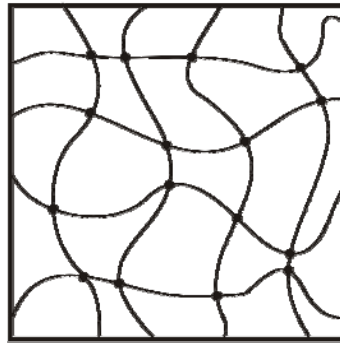

Fig. 5: Perfect network structure, no topological imperfections or spatial inhomogeneities present, each crosslinker has reacted according to its functionality (in this case tetrafunctional) and each chain contributes to the network elasticity

The following relation (eq. 15) between the molar density of network chains, ν, the functionality, f, of the crosslinker and the molar density of crosslinker molecules, μ, holds true for a perfect network[54].

$$\mu = \frac{2\nu}{f}$$

(15)

There are two basic statistical models to describe polymer networks theoretically[55,56]. Both of them consider the network chains to be monodisperse and are based on the structure of a perfect network. Moreover, the network chains are phantom chains that can freely pass through each other. The main difference is the way the crosslinks are defined.

The *affine* network model developed by WALL and FLORY assumes that the crosslinks are embedded in the network without being able to fluctuate. If the network is deformed on a macroscopic scale the crosslinks carry out a directly related, affine movement on the

molecular scale. The volume of the network does not change upon deformation. The other model is the more complicated *phantom* network model by JAMES and GUTH in which only the crosslinks at the surface are fixed and the ones inside the network are capable of fluctuating. Both models characterise the deformation behaviour of polymer networks and yield similar results. However, they can be seen as two limiting examples for the description of network properties. At rather low deformations the affine model is superior in characterising a given network. The phantom model suits the situation of higher deformations better, since stretching of the network chains leads to disentangling, enabling the crosslinks to fluctuate more strongly[57]. Both models lead to an expression that relates the shear modulus, G, with the molar network chain density, ν, (eqs. 16 & 17), ρ being the density of the network in mass per unit volume, M_s the number-average molar mass of the network strands, R the universal gas constant and T the absolute temperature. The contribution of each network chain to the shear modulus is the thermal energy, $k_B T$, with k_B the BOLTZMANN constant. The only difference between the calculation of the shear modulus for the affine network, G_{af}, (eq. 16) and the phantom network, G_{ph}, (eq. 17) is a factor that takes into account the functionality, f, of the crosslinker for the phantom network. At the smallest possible crosslinker functionality, which is three, only one third of each network chain in the phantom network contributes to the network elasticity, owing to the fluctuation of the junctions.

$$G_{af} = \nu \cdot RT = \frac{\rho}{M_s} \cdot RT \qquad (16)$$

$$G_{ph} = \nu \cdot RT \cdot \frac{(f-2)}{f} = \frac{\rho}{M_s} \cdot RT \cdot \left(1 - \frac{2}{f}\right) \qquad (17)$$

Due to the additional factor the modulus of the phantom network, G_{ph}, is always lower than the affine network modulus, G_{af}, if both networks have the same network chain density, ν. Only in the case of a very high crosslinker functionality G_{af} and G_{ph} are practically equal. The reason is the fact that the junctions are allowed to fluctuate in a phantom network which yields a softer system. However, at very high functionalities there are a lot of chains emanating from one crosslink which restricts its capability to fluctuate. As a general rule the affine network model may be used for very highly concentrated or even bulk networks, whereas the phantom network model is more appropriate for lower concentrations or

swollen networks. Most real networks have shear moduli that lie in between the predicted values of the affine and phantom networks[55].

The structure of a perfect network can hardly be obtained in a *real* system. The formation of a polymer network is a random process and so the generation of defects is inevitable. There will always be topological imperfections like loops (a network chain emanating from and ending up in the same junction), dangling chains (only connected to a network junction at one end, often exhibiting an unreacted functional group) or trapped entanglements (additional physical crosslinks between tangled network chains, that cannot be loosened) (Fig. 6 a). All these imperfections affect the elasticity of a network. Loops and dangling chains do not contribute to the elastic properties. Thus they decrease the stiffness of a network compared to the perfect structure. In contrast, trapped entanglements add to the elasticity of the network by introducing further, physical crosslinks to the system. These imperfections can be taken into consideration by only regarding the elastically effective network chains. Instead of the molar network chain density, ν, the effective molar network chain density, ν_{eff}, has to be applied (eqs. 18 & 19).

$$G_{af,eff} = \nu_{eff} \cdot RT \qquad\qquad (18)$$

$$G_{ph,eff} = \nu_{eff} \cdot RT \cdot \left(1 - \frac{2}{f}\right) \qquad\qquad (19)$$

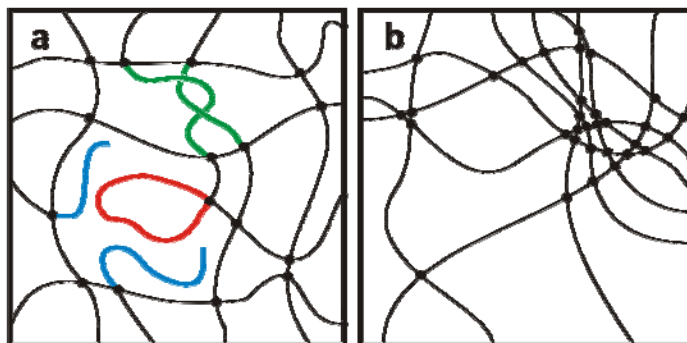Polymer networks are very often spatially inhomogeneous[58], as well (Fig. 6 b).

Fig. 6: Different kinds of network inhomogeneities; **a**: topological network defects, blue: dangling chains, red: loop, green: entanglement; **b**: spatial inhomogeneity

In these cases the concentration of the network chains and the junctions is non-uniform. There are areas that possess a very high network chain density and are therefore rather stiff, exhibiting a rather high shear modulus. Thus, compared to a perfect network with an even crosslink distribution, these areas show a low degree of swelling[59]. They can withstand relatively high stresses, if exposed to strain or deformation. Other sections have a very low crosslink concentration rendering them much less stiff. They are highly swellable and therefore, compared to a perfect network, much more likely to break if the network is subjected to strain. Consequently, with respect to deformation, these sections are the weak point of a spatially inhomogeneous network or gel[60]. Depending on the application it may therefore be desirable to form networks with a network structure that is as homogeneous as possible.

2.1.4.1   Network Properties Affected by Spatial Inhomogeneity

Compared to a matching polymer solution, spatial inhomogeneities in a network or gel typically lead to an excess scattering of light[60]. Depending on the degree of inhomogeneity the scattering can be very strong[59], meaning that the particular network or gel can become turbid even to the point of being fully opaque[61]. In certain situations, e.g. for optical applications such as contact lenses or intraocular lenses[62], the material has to be clear to see through. An overly inhomogeneous polymer gel would not be suitable for such applications. The fact that spatial inhomogeneities increase the extent of scattered light still is rather valuable for detecting them. This can be accomplished by carrying out light scattering measurements (chapter 2.3).

Another property of a polymer network affected by spatial inhomogeneities is its permeability. Preparing polyacrylamide hydrogels by free radical crosslinking copolymerisation using N,N'-methylene bis-acrylamide (BIS) as crosslinker with a constant total monomer concentration, WEISS and SILBERBERG[63] unexpectedly found out that raising the crosslinker concentration leads to a strongly increasing permeability for water. They attributed this to an increasing extent of spatial inhomogeneity. Highly crosslinked and thus hardly permeable regions become more pronounced and regions that are much less crosslinked expand as well, being able to overcompensate the poor permeability. Such behaviour makes it almost impossible to predict material properties from reaction conditions.

2.1.4.2   Spatial Inhomogeneity in FCC

The issue of polymer network inhomogeneities has been thoroughly studied. Since the free-radical crosslinking copolymerisation (FCC) is a simple way to prepare polymer networks it has been investigated very extensively. This reaction is simply a radical chain growth reaction starting from vinyl monomers, often acrylates or acrylamides. The crosslinker molecules usually have a structure similar to the monomers, only with a higher functionality. It is well-known that this kind of network formation often leads to rather strong spatial inhomogeneity[58,64-68]. Due to its chain-growth nature, a relatively small amount of very long, high-molecular chains are formed at low conversions, already. These few chains mainly carry out intramolecular crosslinking which yields small domains, sometimes called microgels. These domains grow with conversion and eventually become loosely interconnected to a macroscopic, continuous network[69,70]. On the one hand, the network formed in this manner exhibits highly crosslinked regions, stemming from the former microgels that barely swell in a suitable solvent. On the other hand, there are regions, which are only slightly crosslinked and thus highly swellable, rendering the network rather frail.

The homogeneity of networks or gels formed by FCC has been examined with respect to various reaction conditions. The type of crosslinker is important, considering its reactivity towards the monomer[71]. A crosslinker with a structure dissimilar to the monomer exhibits a different reactivity. Hence the monomer may prefer reacting with itself, to reacting with the crosslinker which leads to an inhomogeneous distribution of network junctions. It was also shown that the structure of the crosslinker in terms of the distance of the functional groups from each other has an influence on the resulting network[72]. Longer chains between the functional groups account for a higher crosslinking efficiency and therefore a more homogeneous network structure. The crosslinker is likely to connect two chains, that are relatively far apart, which diminishes the probability of intramolecular crosslinking and thus leads to less spatial inhomogeneity. It is generally established that a higher crosslinker concentration yields a more inhomogeneous network, if the monomer concentration is kept constant[73]. This only holds for network preparation in a good solvent, though. Utilising a poor solvent yields the opposite outcome[74], due to the fact that in a poor solvent the network strands collaps and form cluster-like domains. Increasing the crosslink density

prevents the network from being able to form these domains since the network strands are being held in place, thus eventuating in a more homogeneous structure.

The type of monomer certainly impacts on the network structure. KURU et al. showed that hydrogels formed from a mixture of N,N-dimethylacrylamide (DMAAm) and acrylamide (AAm) exhibit a more homogeneous network structure than those only formed from AAm[75]. This is supposed to be due to a steric effect of the methyl-groups in DMAAm which diminishes the rate of crosslinking and increases the excluded volume of the polymer chains. This leads to an earlier chain-overlap, thus less intramolecular crosslinking and a delayed gel point. Increasing the monomer concentration and keeping the crosslinker concentration constant, results in a rise in crosslinking efficiency and the examined networks become more homogeneous[73]. This result is attributed to a reduced probability of cyclisation reactions and intramolecular crosslinking. However, it was also reported that increasing the monomer concentration lets the inhomogeneity of a FCC network pass through a maximum value if the ratio of monomer and crosslinker concentration is kept constant[76].

Adding a chain transfer agent usually gives rise to more homogeneous networks since the chains formed in the early stages of the reaction are shorter and thus less prone to carry out intramolecular crosslinking. Moreover, it delays the gel point towards higher conversions[77].

The degree of swelling influences the homogeneity insofar as in a gel, swollen to equilibrium, the spatial inhomogeneities become even more pronounced, compared to a reactor-batch gel (in the state of preparation)[42,78]. Regions that exhibit a high crosslink density are not capable of absorbing a significant amount of solvent due to very high elastic restoring forces. However, a high degree of swelling will be accomplished in the lowly crosslinked regions. This increases the already existing concentration differences within a gel even more and leads to an increased scattering intensity. Hence, by swelling, spatial inhomogeneities that may not have been noticed before, are emphasised and more easily observable.

2.1.4.3 Polymerisation Mechanisms to Improve Network Homogeneity

There are certainly other ways to prepare networks apart from FCC. It is for instance possible to use living crosslinking copolymerisation which can nowadays also be performed radically rather easily, relative to the ionic alternatives[69,70,79,80]. This kind of polymerisation involves simultaneous, slow growth of the polymer chains yielding a delayed gel point and thus a well-defined network structure. However, compared to the simple FCC, performing a living radical polymerisation is still comparatively intricate.

Another approach that is known to form fairly homogneous networks is their preparation from already existing, randomly functionalised polymer chains[81,82]. This method is thus called random crosslinking. An important prerequisite for homogeneous, continuous networks to be formed this way is for the polymer concentration to be well above the overlap concentration, c*. Getting too close to c* leads to inhomogeneous structures and below c* no continuous network formation is possible.

A similar way is the end-linking process[53,83]. The preexisting polymer chains are suitably functionalised at both chain-ends to react with a crosslinking molecule of a certain functionality. This can for example be carried out by sequential anionic polymerisation or by step-growth polymerisation with one of the monomers being a difunctional linear polymer and the other monomer a multifunctional crosslinker with corresponding functional groups. Owing to the fact that the linear chains should only react with the crosslinker and not with their own kind, the networks formed this way can be very well-defined, possessing a rather homogeneous network structure. This method has for instance been used to form model networks exhibiting structures similar to a perfect network, including low polydispersity of the network chains and homogeneously distributed crosslinker and chain segment density. However, topological defects like trapped entanglements, dangling chains or loops have to be accepted since they cannot be entirely avoided by any method. In fact, particularly loop formation is an issue with end-linking polymerisations[84]. It becomes likely especially with dilute systems or short precursor chains. This has to be taken into account if homogeneous network structures are required.

The step-growth crosslinking method can also be carried out as a copolymerisation from monomers, i.e. a difunctional monomer with the functional group A, and a difunctional monomer and a multifunctional crosslinker each with the functional group B[85-87]. Compared

to the FCC, the polymer chains grow more slowly, the number of growing chains is higher at the start of the reaction and very long chains are only formed at rather high conversions. Thus, in the early stages the viscosity of the reaction mixture is relatively low and the mechanism exhibits less intramolecular crosslinking so that highly crosslinked domains are formed to a lesser extent. Moreover, the gel point is delayed to higher conversions, enabling chain relaxations into an entropically favoured state for a comparatively long time. All in all, this kind of crosslinking should theoretically improve the homogeneity of the prepared networks or gels in relation to the FCC.

2.2   Thiol-Ene Polymerisation

The reaction employed for this thesis was the thiol-ene polymerisation. It was first described by POSNER in 1905[88]. In 1938, KHARASCH et al.[89] were the first to publish findings about the free radical mechanism of the thiol-ene polymerisation (TEP). The mechanism they proposed is still accepted nowadays (Scheme 1)[85]. The thiol-ene polymerisation has been used for several applications such as relief printing (Letterflex process), wear layers for floor tiles or optical and electronic adhesives. Other applications which are currently being researched on are e.g. injectable intraocular lenses[90] (implantation of artificial eye lenses with minimal incision), dental restorative materials[91], marine antifouling coatings[92], cellular microarrays[93] (to detect interactions of cells with certain biological or synthetic compounds) or microfluidic devices[94,95].

2.2.1   Reaction Mechanism and Critical Conversion

The thiol-ene polymerisation[85,96] is a free radical step-growth polymerisation and as its name implies it is a polymerisation between a thiol and an ene. To form a polymer it is necessary for both monomers to be at least difunctional. A linear polymer is thus formed by using a dithiol and a diene. To build a polymer network at least one of the monomers has to have three or more functional groups. The reaction mechanism consists of four main steps as shown in scheme 1. In the first step a hydrogen atom is abstracted from a thiol group by appropriate initiation. The thereby generated thiyl radical attacks the double bond of an ene,

forming a carbon-centred radical in step two. In a chain transfer step, this carbon-centred radical abstracts a hydrogen atom from another thiol group, transferring the radical function to form another thiyl radical (step 3). This process repeats itself. The fourth step is the inevitable termination of radical functions and thus growing chains by radical recombination where all kinds of occurring radicals can react with each other (Scheme 1, Termination). Disregarding the termination reactions, this mechanism is an anti-MARKOVNIKOV addition[97] of the thiol to the double bond yielding a thioether with a fairly flexible sulfide bond.

1. Initiation:

R—SH $\xrightarrow{\text{Ini}}$ R—S•
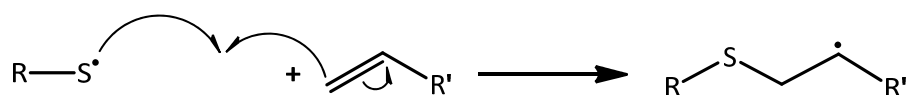
2. Propagation:

3. Chain Transfer:

4. Termination:

RS• + RS• $\longrightarrow$ RS—SR
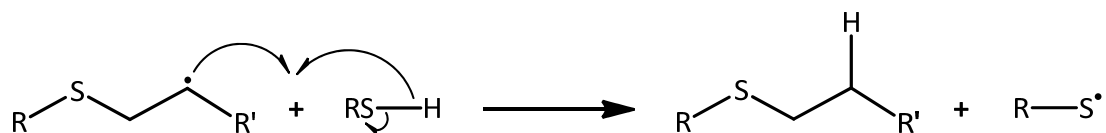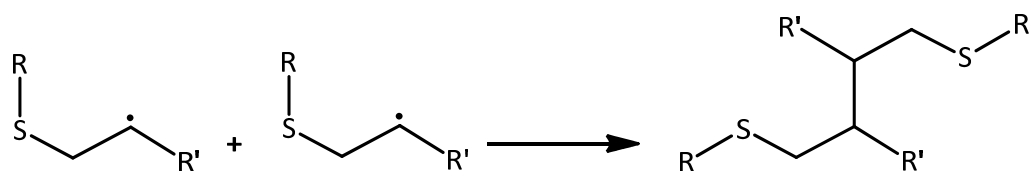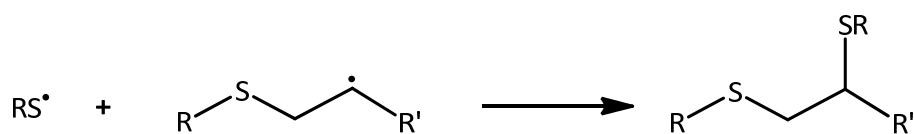
Scheme 1: The four main steps of the thiol-ene reaction mechanism; initiation, chain growth comprising the propagation step and the chain transfer step and termination by radical coupling

Since the TEP is a step growth polymerisation, another important prerequisite to attain reasonable degrees of polymerisation, especially for linear polymers, is to use the monomers in stoichiometric ratio. This means that there has to be the same number of thiol groups and double bonds within the reaction mixture. The degree of polymerisation, x_n, can then be calculated by the CAROTHERS equation (eq. 20) which applies to the formation of linear polymers[98]. It is simply dependent on the conversion, p, of the reaction. Reasonable values for x_n can only be obtained at very high conversions, $p \geq 0.99$.

$$x_n = \frac{1}{(1-p)}$$ (20)

In a crosslinking system this equation has to be modified[98]. Due to the additional functional groups that are introduced in such systems there are more sites for chain growth which lead to branching and eventually crosslinking. An important parameter to determine the conversion dependence of x_n for a crosslinking system (eq. 21) is the average functionality per molecule, f_{av}. This parameter is defined by eq. 22 with N_i the number of the different molecules and f_i the respective functionality. For linear polymer growth it is $f_{av} = 2$ but if crosslinking is intended it is $f_{av} > 2$. The system mostly used in this thesis consists of a trifunctional crosslinker and a difunctional monomer yielding the value $f_{av} = 2.4$ if stoichiometrical balance is assumed.

$$x_n = \frac{2}{\left(2 - p \cdot f_{av}\right)}$$ (21)

$$f_{av} = \frac{\sum_i N_i \cdot f_i}{\sum_i N_i}$$ (22)

Consequently, for the formation of linear polymers, eq. 21 changes into the normal CAROTHERS equation (eq. 20).

Comparing both equations graphically (Fig. 7), with f_{av} = 2.4 for the crosslinking system, it is evident that the conversion which is needed to form polymers with a reasonable degree of polymerisation is far lower if network formation is intended.
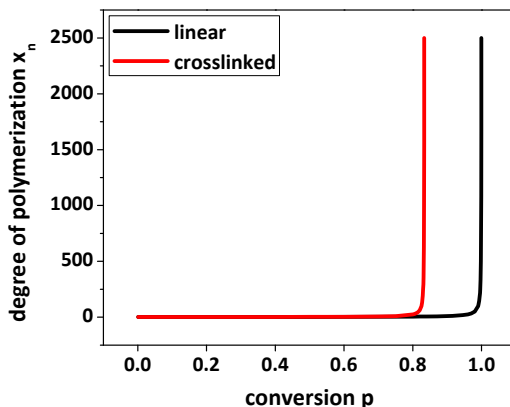
Fig. 7: Conversion dependence of the degree of polymerisation x_n in step-growth polymerisations; the black curve depicts the formation of linear polymers, as calculated by eq. 20; the red curve depicts the formation of crosslinked polymers as calculated by eq. 21 with f_{av} = 2.4

The critical conversion, p_{crit}, corresponding to a theoretically infinite degree of polymerisation can be determined by eq. 23. For a linear polymer with f_{av} = 2 it is p_{crit} = 1 meaning that almost complete conversion is needed to form polymers with a reasonable molar mass. The critical conversion for network formation with f_{av} = 2.4 is only p_{crit} = 0.8$\bar{3}$. Even at minor stoichiometric imbalances, it is still possible to form a continuously crosslinked sample. A conversion of $p = 0.8\bar{3}$ would lead to a degree of polymerisation of no more than x_n = 6 in a linear step-growth polymerisation.

$$p_{crit} = \frac{2}{f_{av}}$$

(23)

Due to utilising only a diene and a trifunctional thiol for the most part of this thesis, the actual mechanism of the conducted reactions was an *end-linking* step-growth crosslinking polymerisation.

## 2.2.2   Initiation Methods and Monomers

The preparation of linear polymers via thiol-ene polymerisation is rarely done, it is rather used to form networks. It is also often carried out without additional solvent which is possible because many of the utilised monomers are liquid. This approach leads to quantitative yields, very high reaction rates and stiff networks. Avoiding the use of solvent significantly reduces the potential damage to the environment. Research has also been done in the field of thiol-ene hydrogels, e.g. concerning their degradability[99,100] or preparing hydrogels from biopolymers[101,102].

The most common way to initiate a thiol-ene polymerisation is photochemical initiation. It is also possible to use thermal initiation[103] but this method is seldomly employed. There are basically three different ways of photoinitiation[85]. The first is to use a cleavage-type initiator (type-I) that disintegrates into two radicals if it is irradiated with light of an appropriate wavelength. Both radicals can start a reaction by either abstracting a hydrogen atom from a thiol group or by adding to a double bond[104] (Scheme 2).
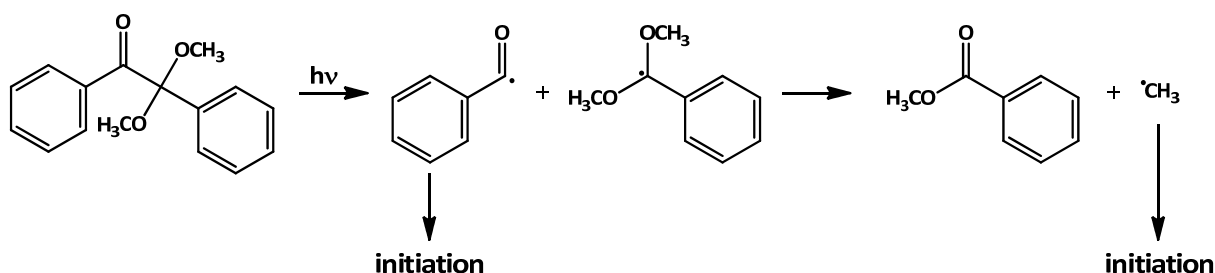
Scheme 2: Typical type-I photoinitiator 2,2-dimethoxy-2-phenyl acetophenone; by irradiation at a suitable wavelength the molecule undergoes unimolecular bond cleavage yielding two radicals that can initiate a radical reaction

Another option is the utilisation of type-II photoinitiators[105,106], which are typically aromatic ketones. Camphorquinone (Scheme 3) is frequently used as well and shall be considered, henceforth[107,108]. Upon irradiation with the correct wavelength (400 to 500 nm) camphorquinone is excited to its singlet state by an (n,π*)-transition and by intersystem crossing (ISC) it proceeds to the respective triplet state. It is then capable of abstracting a hydrogen atom from the relatively weak SH-bond (338 kJ/mol[38]), creating a thiyl radical which can subsequently start the polymerisation[109]. The additionally formed hydrogenated

camphorquinone radical cannot initiate a polymerisation since its steric hindrance is too high.
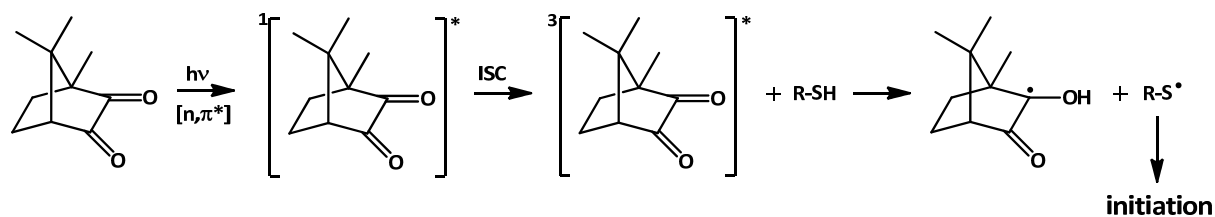
Scheme 3: Type-II photoinitiator camphorquinone (CQ); by irradiation at a suitable wavelength CQ undergoes an (n,π*)-transition, thereby being excited to the singlet state, which by intersystem crossing (ISC) forms a triplet state; the triplet state is capable of abstracting a hydrogen atom from a thiol group yielding a thiyl radical which initiates the radical reaction

Initiation by camphorquinone, and by type-II photoinitiators in general, is thus the less efficient method of the two yet mentioned, because one photon only produces one growing chain whereas one molecule of a type-I photoinitiator can start two chains. The third possibility to photochemically initiate a thiol-ene polymerisation is to use no photoinitiator at all[110-113]. This way is less efficient than both above-mentioned methods but it has the advantage of a smaller number of reactants influencing the system. Two wavelengths are used for this technique, 254 nm and 365 nm. On irradiation at 254 nm the reaction rate is proportional to the thiol group concentration which can be explained by the homolytic cleavage of the SH-bonds. The reaction rate observed when irradiated at 365 nm is directly proportional to the double bond concentration. Using 254 nm has the benefit of a faster reaction rate, but due to strong absorption at this wavelength the samples that shall be cured, should not have a high thickness.

Polymerisations are strongly influenced by the kind of monomers that are used. In case of the enes virtually any of the class can be used. In order for a *pure* thiol-ene polymerisation to take place the ene should not be able to undergo free radical chain-growth homopolymerisation[85]. This means that acrylates, acrylamides and other monomers that are known to easily homopolymerise are not an appropriate choice. They can of course still be used keeping in mind that the reaction is then characterised by a combination of two distinct polymerisation mechanisms[114]. Furthermore, it can be said that molecules with double bonds of high electron density are more reactive than others. Compounds that are

often used are vinyl ethers, plain alkenes and allyl ethers. There are some molecules that do not follow this rule, e.g. norbornene which, although its electron density does not seem high enough, reacts much faster than the other above-mentioned enes due to relief of ring strain during thiol addition. Molecules that are able to stabilise the carbon-centred radical which is formed by the addition of the thiyl radical to the double bond have a rather low overall reactivity. Those kinds of compounds are, for instance, conjugated dienes, styrene or methacrylates whereas the two latter are also readily capable of homopolymerising. An additional factor concerning the reactivity of enes is steric hindrance. The higher the degree of substitution of the double bond the lower the reactivity of the ene. Moreover, the addition of a thiyl radical to a multiply substituted, internal ene is reversible. If possible only enes with terminal double bonds should be used.
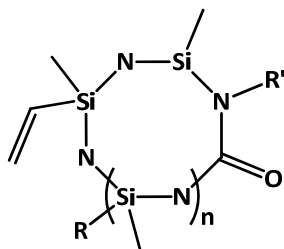
Fig. 8: Vinyl silazanes, used as enes in thiol-ene polymerisation; they make the propagation step rate determining

As for the question of the rate determining step of the chain growth, three different situations were found[85,115]. The chain transfer is slower than the propagation step for allyl ethers, plain alkenes, acrylates and, particularly pronounced, styrene. The styrene radical is especially stable due to strong conjugation. In these cases, the reaction rate, r_p, solely depends on the thiol concentration (eq. 24).

$$r_p \propto c_{thiol} \qquad\qquad (24)$$

Both steps exhibit approximately the same rate with vinylethers or norbornenes so the thiol- and the ene-concentration both influence r_p (eq. 25).

$$r_p \propto c_{thiol}^{1/2} \cdot c_{ene}^{1/2}$$ (25)

The propagation step being rate determining is rather seldom, it can however be observed for vinyl silazanes (Fig. 8) and r_p is then only dependent on the ene concentration (eq. 26). The overall reaction rate for chain growth is always first order in monomer concentration.

$$r_p \propto c_{ene}$$ (26)

Three different kinds of compounds are mainly utilised as thiols, namely alkyl thiols, mercaptopropionates (Fig. 9, left hand side) and mercaptoacetates (Fig. 9, right hand side). The two latter types usually lead to faster reaction rates, owing to hydrogen bonding between the ester carbonyl groups and the hydrogen of the thiol groups yielding a weaker sulfur-hydrogen bond. Often multifunctional thiols are applied, with up to 64 thiol groups. Usually, thiols with three or four functional groups are used.

Fig. 9: Molecules frequently used as thiols in TEP; left hand side: mercaptopropionates; right hand side: mercaptoacetates

2.2.3   Properties That Characterise Thiol-Ene Systems

As previously mentioned (chapter 2.1.4.3), step-growth crosslinking polymerisations have the potential to yield networks that exhibit a comparatively homogeneous structure. Due to the step growth character of the polymerisation, the gel point is delayed towards higher conversions compared to a conventional FCC. This means that most of the reaction-induced shrinkage of the mixture happens before the system passes into the gel state, thus resulting in a lower buildup of stress within the sample[85]. Reduced stress increases the ability of a thus formed film to adhere to the surface of a substrate. The conversion for a reaction between one thiol and one ene, at which the gel point occurs, p_{gp}, can theoretically be calculated by eq. 27, with r the molar ratio of thiol groups to double bonds, f_{thiol} the thiol functionality and f_{ene} the ene functionality[87,116].

$$p_{gp} = \frac{1}{\sqrt{(r \cdot (f_{thiol} - 1) \cdot (f_{ene} - 1))}} \qquad\qquad (27)$$

For the system of a diene and a trithiol combined in stoichiometric ratio concerning the functional groups (r = 1), the gel point theoretically occurs at a conversion of 71 %. In FCCs the gel point is known to occur much earlier. Even in a thiol-ene system of both a tetrafunctional thiol and ene the gel point conversion is calculated to a rather high 33 %. FCC systems that are comparable in terms of functionality already gel at conversions of down to below 5 %[117,118], which is not desirable if the aim is a homogeneous network structure.

To determine whether the thiol-ene networks are indeed more homogeneous than others, dynamic mechanical analysis (DMA) has been employed, measuring $\tan\delta$[119,120]. Investigating the glass transition can give information on the uniformity of the network chain density within the examined network. For this purpose the sample is dynamically deformed at an either fixed or varying frequency over a certain temperature range. In the glass transition region a plot of $\tan\delta$ versus temperature exhibits a peak. The narrower and more symmetrical the peak is, the more well-defined is the network structure. It was found that such peaks are much narrower for thiol-ene than for pure acrylate networks demonstrating that the former exhibit more homogeneous networks. The maximum of the peak which

indicates the glass transition temperature, T_g, is also affected, insofar that it is often positioned at much lower temperature values for the thiol-ene networks (Fig. 10).
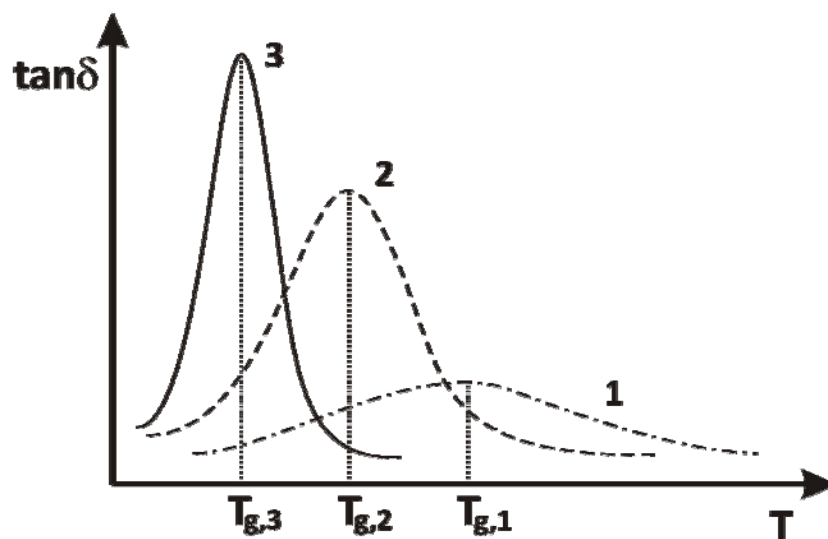

Fig. 10: The loss tangent, tanδ, at the glass transition of differently prepared networks plotted vs. temperature, T; **1**: pure FCCs with acrylates exhibit a rather broad tanδ-peak and a high glass transition temperature, $T_{g,1}$; **2**: a combination of TEP and homopolymerisation yields a lower glass transition temperature, $T_{g,2}$, and a narrower peak demonstrating improved uniformity of the network chain density in the network, **3**: pure TEP results in the narrowest peak with the lowest glass transition temperature, $T_{g,3}$, indicating a rather homogeneous crosslink distribution[119,120]

Blending in an increasing amount of thiol (binary mixture), or thiol and non-homopolymerisable ene (ternary mixture), to a system of a multifunctional acrylate, lets the tanδ-peak of the resulting network grow narrower. The glass transition temperature mostly decreases as well (Fig. 10). This indicates that adding thiols to an acrylate polymerisation mixture, which usually yield rather non-uniform structures, leads to a rising network homogeneity since the acrylate monomer does not only carry out fast chain-growth steps anymore but also participates in a step-growth mechanism. This was shown for a binary mixture of pentaerythritol tetra(3-mercaptopropionate) (a tetrafunctional thiol, Fig. 11, left hand side) and hexanediol diacrylate (Fig. 11, right hand side)[85]. The acrylate is evidently consumed faster than the thiol because it takes part not only in the thiol-ene polymerisation but it also homopolymerises leaving unreacted thiol. Ternary mixtures are less sensitive to the stoichiometric ratio of the components' functional groups and can yield materials that, compared to pure acrylate systems, have a more uniform structure but still an equally high glass transition temperature[121]. Generally, combining thiols and homopolymerisable enes at

different ratios renders it possible to tailor networks to the requirements necessary for particular applications by adjusting physical and mechanical properties.
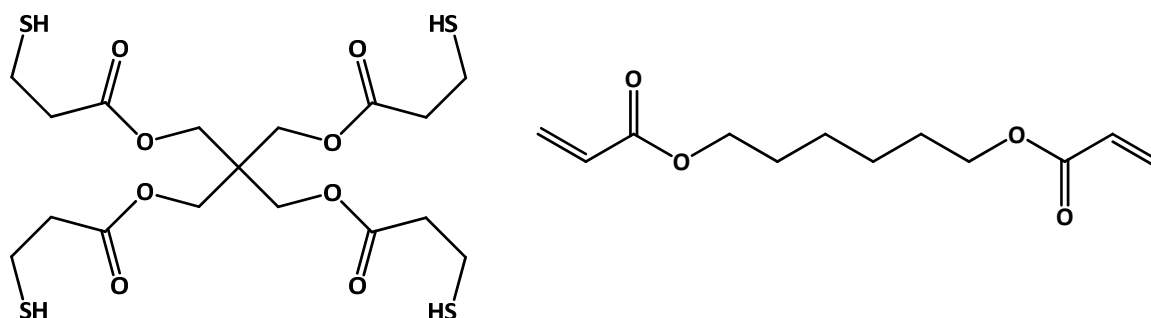
Fig. 11: Monomers; left hand side: pentaerythritol tetra(3-mercaptopropionate); right hand side: hexanediol diacrylate

One of the major advantages of the thiol-ene polymerisation especially over the free radical chain-growth polymerisation is its insensitivity towards oxygen inhibition[85]. In the latter type of polymerisation the reaction rate is significantly reduced if oxygen is not kept from the reaction mixture. By addition to a carbon centred radical of a growing chain it forms a peroxy radical which does not easily react with a double bond to continue the polymerisation. Therefore, this polymerisation should be carried out in a nitrogen atmosphere or at least be purged with nitrogen. This is not necessary in a thiol-ene polymerisation because the peroxy radical can abstract a hydrogen atom from a thiol group, so that the radical chain is not terminated. The generated thiyl radical can carry on reacting by adding to a double bond, as usual (Scheme 4).
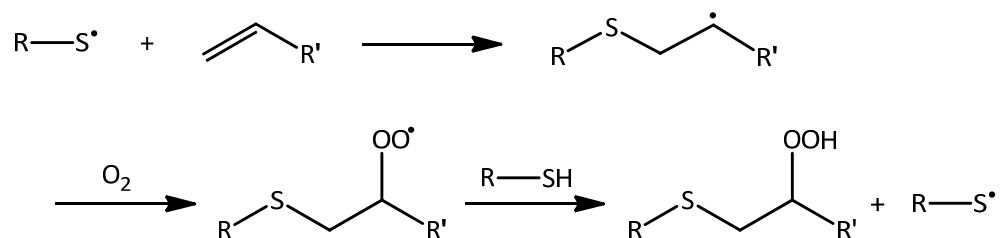
Scheme 4: Oxygen scavenging mechanism in thiol-ene polymerisation; the peroxy radical formed by the attack of oxygen to a carbon-centred radical is capable of abstracting a hydrogen atom from a thiol group so that the polymerisation carries on

In fact, it is possible to reduce the negative influence of oxygen on free radical chain growth polymerisations by simply adding some thiol to the reaction mixture[85,113,120-122]. It increases the polymerisation rate by taking over the radical function of a peroxy radical and starting a new growing chain. Thus it decreases the amount of initiator needed, but it also acts as a chain transfer agent, in all probability leading to a lower average molar mass.

The most important disadvantage of the thiol-ene polymerisation is probably the fact that a mixture of thiol and ene has a relatively low shelf-life stability (ranging from hours to months depending on the monomers) meaning that such mixtures begin to react of their own accord[85]. This can happen to a considerable extent, even at room temperature without any radiation or external initiation of any kind. Disregarding impurities in the reaction mixture, this circumstance is mainly due to the generation of a charge-transfer complex between a thiol and an ene molecule (Scheme 5), whereby radicals are formed that spontaneously initiate a polymerisation[123-126].

R——SH   +   (ene, R')   ⇌   [charge-transfer complex]   →   R——S•   +   (radical, R')

Scheme 5: Spontaneous formation of a charge-transfer complex between an ene and a thiol yielding radicals that unintendedly initiate polymerisation

This kind of dark reaction is not as fast as a deliberately initiated polymerisation but it can lead to an increase in the viscosity of the reaction mixture and furthermore, preclude long-time storage of already mixed samples. The most unstable mixtures in terms of shelf-life comprise vinyl ethers. However, it is also relevant what kind of molecule structure separates the double bonds, how the ene was synthesised and how exactly the mixture is stored.

This difficulty, which is strongly reduced if solvent is used, can be counteracted by adding appropriate stabilisers e.g. reducing agents like pyrogallol, triarylphosphites, the aluminium salt of N-nitrosophenylhydroxylamine, phosphoric acid (all Fig. 12) and many more.
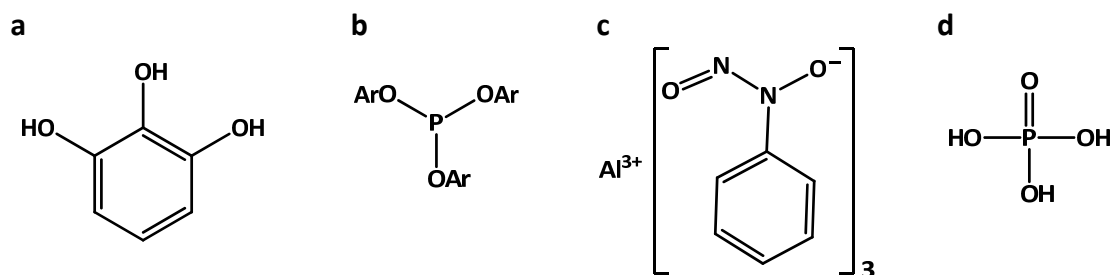
Fig. 12: Stabilisers used to prevent the self-initiation in thiol-ene polymerisations due to formation of charge-transfer complexes; **a**: pyrogallol; **b**: triaryl phosphyte; **c**: aluminium salt of N-nitroso-phenylhydroxylamine; **d**: phosphoric acid

In summary, the thiol-ene polymerisation has many positive aspects. The formation of fairly homogeneous polymer networks, rapid reaction rates, mild reaction conditions, insensitivity to atmospheric oxygen and water, the possibility to work without ecologically harmful solvents, high yields and the availability of a high amount of thiol- and ene-reactants make this method a very valuable approach to form a wide variety of functional crosslinked materials.

2.3   Light Scattering[127]

Polymer networks formed by thiol-ene polymerisation are rather uniform in their network chain density considering it being a free radical reaction (chapter 2.2.3). DMA-measurements showed very narrow glass-transition regions as determined by the loss-tangent. The DMA-method is closely related to rheometry, both being macroscopic techniques. Hence, to make a statement about the network homogeneity based on DMA-measurements is principally an extrapolation from macroscopic data to microscopic material properties. It is reasonable to assume that the broadness of the glass-transition region is connected to the polydispersity of the network chains and consequently the crosslink density. Still, it is desirable to apply a method, capable of examining properties at smaller length scales. The method used for this purpose, within the scope of this thesis, is light scattering.

The extent of light scattered by a polymer network strongly depends on its structure as holds true for all material. A perfectly homogeneous, infinitely extended crystal does not scatter any light at all and is thus optically absolutely transparent. Gases and liquids exhibit density fluctuations due to thermal motion of the particles whereby both systems scatter light to a small extent. In a solution, e.g. of a polymer in a good solvent, there are additional concentration fluctuations of the diffusing polymer coils that exceed the density fluctuations of the solvent itself greatly and yield a much stronger scattering[128,129]. If the coils can diffuse freely this is an ergodic system, since the time-average of the scattered light intensity, is the same as the ensemble-average.

Fixing the polymer coils by introducing crosslinks in a polymer solution, thus creating a polymer gel, the concentration fluctuations within the solution become frozen-in. Hence, there are sites exhibiting a high polymer concentration and sites with a low concentration, resulting in a spatially inhomogeneous structure. The properties of a gel are thereby affected in such a way that it usually scatters light even more strongly than the corresponding polymer solution[73-77,81,130]. It is the same situation that arises for gels formed by FCC (chapter 2.1.4). Since the coils, or rather network chains, cannot diffuse freely but merely fluctuate about a main area the inhomogeneities cannot dissipate. This results in a non-ergodic sample in which it makes a significant difference whether a property is measured infinitely long but only at one position or the whole ensemble is measured at once.

Basically, there are two ways in which to perform light scattering measurements, one is static light scattering (SLS) and the other the dynamic light scattering (DLS). Since the latter was the mostly used method in this thesis it will be considered more thoroughly.

2.3.1 Dynamic Light Scattering[128,131]

Static and dynamic light scattering are distinguished by the way the samples are measured. For SLS the angle-dependence of the scattered light intensity is vital and the scattering volume is comparatively large, because one is not interested in the fluctuations of the intensity but in an average of it. Usually, only one scattering angle, mostly 90°, is used for DLS. Moreover, the scattering volume is smaller than for SLS, since the aim is to detect the time-dependent scattering behaviour of the sample, which is autocorrelated, subsequently.

Thus, the central element in dynamic light scattering is the autocorrelation function (ACF). It illustrates the similarity of a property (e.g. the scattering intensity) of the observed system to itself. The scattering intensity of a polymer *solution* statistically fluctuates with time about an average value, generating a noise pattern. Comparing this fluctuating intensity with itself, without any lag time, τ, obviously the similarity or correlation is maximal. Shifting the curve by a certain lag time, it is less likely for the original curve to possess the same values as the shifted curve at the same time, t. They begin to deviate more and more from each other with increasing τ, leading to a decay in correlation. According to this, in the fully coherent case the normalised intensity correlation function (ICF) $g^{(2)}(q,\tau)$ can be calculated by eq. 28, I being the scattering intensity and $\langle...\rangle_T$ indicating a time-average[132,133]. The coherence factor, β, is unity in this case and can thus be omitted. For deviations from full coherence, hence $\beta < 1$, see chapter 3.7.

$$g^{(2)}(q,\tau) = \frac{\langle I(q,t) \cdot I(q,t+\tau)\rangle_T}{\langle I(q,t)\rangle_T^2}$$

(28)

The length of the scattering vector, q, as shown in eq. 29, is determined by the refractive index, n, of the solvent, the wavelength, λ_0, of the light source (usually a laser) in vacuum and the scattering angle, θ.

$$q = \frac{4\pi \cdot n}{\lambda_0} \cdot \sin\frac{\theta}{2} \tag{29}$$

The correlation decay of the light scattering intensity is assumed to be exponential. The normalised ICF then exhibits the intensity correlation time, $\tau_{(2)}$, (eq. 30), the time at which the ICF has decayed to e^{-1} of the initial value.

$$g^{(2)}(q,\tau) = \exp\left(-\frac{\tau}{\tau_{(2)}}\right) + 1 \tag{30}$$

Usually, the intensity of the scattered light is measured, however, the actually important property is the experimentally not accessible electric field of the scattered light, $\vec{E}$. Fortunately, the square of the electric field is proportional to the corresponding intensity. Thus, the field correlation function (FCF) $g^{(1)}(q,\tau)$ (eq. 31), where E is the field amplitude and E* the conjugate field amplitude, is easily obtained by the so-called SIEGERT-relation (eq. 32).

$$g^{(1)}(q,\tau) = \frac{\left\langle E(q,t) \cdot E^*(q,t+\tau) \right\rangle_T}{\left\langle E(q,t) \right\rangle_T^2} \tag{31}$$

$$g^{(2)}(q,\tau) = \left| g^{(1)}(q,\tau) \right|^2 + 1 \tag{32}$$

Accordingly, the FCF is also an exponentially decaying function but with the field correlation time $\tau_{(1)}$ (eq. 33).

$$g^{(1)}(q,\tau) = \exp\left(-\frac{\tau}{\tau_{(1)}}\right) \tag{33}$$

It follows that $\tau_{(1)}$ is twice as high a value as $\tau_{(2)}$ (eq. 34).

$$\tau_{(1)} = 2 \cdot \tau_{(2)} \hspace{3cm} (34)$$

Both the intensity and the field correlation time can be expressed by means of the diffusion coefficient, D, of the observed scatterers and the length of the scattering vector, q (eqs. 35 & 36).

$$\tau_{(1)} = \frac{1}{D \cdot q^2} \hspace{3cm} (35)$$

$$\tau_{(2)} = \frac{1}{2 \cdot D \cdot q^2} \hspace{3cm} (36)$$

Dynamic light scattering is primarily known as a convenient method to determine hydrodynamic radii of polymer coils or other particles in a solvent[134-136]. The correlation times $\tau_{(1)}$ or $\tau_{(2)}$ derived from the autocorrelation function of the fluctuating scattering intensity can be converted into the corresponding translational diffusion coefficient, D_{trans}, of the observed particles in the particular solvent by eqs. 35 and 36. Afterwards the diffusion coefficient is used to determine the particle size, or rather the hydrodynamic radius R_H of the particles by the STOKES-EINSTEIN equation (eq. 37), with η the dynamic viscosity of the solvent[133]. The higher the hydrodynamic radius of the particles, the lower their diffusion coefficient, which results in a higher correlation time.

$$R_H = \frac{k_B T}{6 \pi \eta \cdot D_{trans}} \hspace{3cm} (37)$$

The simple SIEGERT-relation is only valid for homodyne measurements. These are measurements in which only light scattered from fluctuating components in the sample is detected and correlated. In a purely homodyne situation, e.g. dilute polymer solutions or particle dispersions which are both ergodic, no static, non-decaying part appears in the ACF. The correlation of the scattered light intensity experiences a certain exponential decay at a characteristic correlation time because of the diffusive movement of the particles. The y-axis

intercept of the ICF adopts the value two in the homodyne case and it decays to unity. Usually, reducing it by one, the ICF is conveniently adjusted, so that it decays from unity to zero. Thus, the resulting intercept, σ^2 (eq. 38, $\tau = 0$), is unity, as it is for the FCF (Fig. 13). However, the characteristic correlation times $\tau_{(2,ho)}$ and $\tau_{(1)}$ differ (eq. 39, see also eq. (34)).

$$\sigma^2 = g^{(2)}(q,0) - 1 \tag{38}$$

$$\tau_{(1)} = 2 \cdot \tau_{(2,ho)} \tag{39}$$

In the case of a sample that also comprises a non-fluctuating static component (a so-called local oscillator), e.g. hardly moving, frozen-in network inhomogeneities or reflections from a surface the SIEGERT-relation no longer applies[137-139]. Light scattering measurements are then inherently heterodyne or at least partially heterodyne. The static scatterer adds a time-independent component to the system and the correlation of the light scattered from it does not decay. It is possible to intentionally render a homodyne measurement heterodyne e.g. by blending radiation of the initial, unscattered laser beam into the detected light, since the laser light itself is time-independent. The y-axis intercept of a heterodyne ICF is lower than unity. Systems with a dominating heterodyne regime are considered to show intercepts below 0.1[140]. Instead of the SIEGERT-relation for both heterodyne and partial heterodyne systems one has to utilise another, more complicated equation, that takes into account the two different kinds of scatterers, in order to explain the relation between the ICF and the corresponding FCF (eq. 40)[131,141-144]. In this equation $\langle I_F \rangle$ is the average scattering intensity arising from thermal concentration fluctuations and $\langle I_S \rangle$ is the average scattering intensity of the static component, probably stemming from the spatial inhomogeneities. The unit of the scattering intensities is hertz (Hz) due to measuring the count rate. In the homodyne case $\langle I_S \rangle$ = 0 which converts eq. 40 into the SIEGERT-relation again.

$$g^{(2)}(q,\tau) - 1 = \frac{2 \cdot \langle I_F \rangle \cdot \langle I_S \rangle}{\left(\langle I_F \rangle + \langle I_S \rangle\right)^2} \cdot g^{(1)}(q,\tau) + \left(\frac{\langle I_F \rangle}{\langle I_F \rangle + \langle I_S \rangle} \cdot g^{(1)}(q,\tau)\right)^2 \tag{40}$$
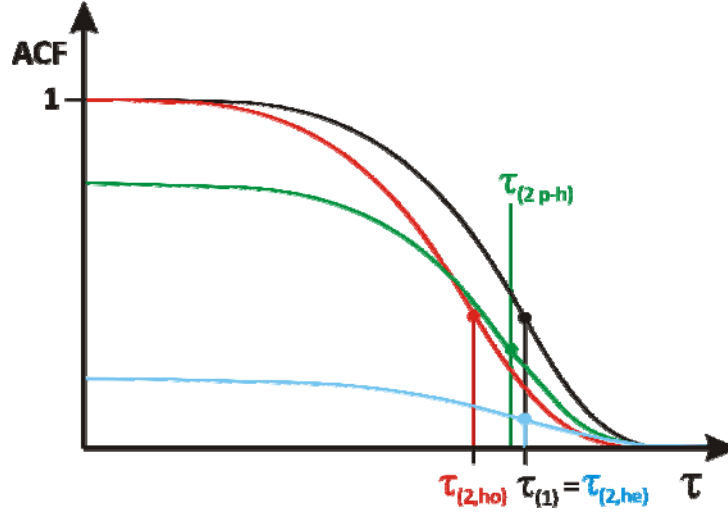
Fig. 13: The y-axis intercept and the correlation time of an ICF depend on the type of scatterers in the sample that yield either homodyne (red curve), partial-heterodyne (green curve) or heterodyne scattering (blue curve); the FCF (black curve) always remains the same

If $\langle I_F \rangle$ is negligible compared to $\langle I_S \rangle$ the light scattering of the observed system is fully heterodyne and the intercept of the ICF decreases appreciably (Fig. 13, blue curve). The squared term in eq. 40 becomes negligibly small and except for a prefactor the ICF becomes equal to the FCF (eq. 41). Thus, the correlation time of a heterodyne correlation function, $\tau_{(2,he)}$, is the same as the one for the corresponding FCF (eq. 42). Consequently, using a heterodyne mode has the advantage that by measuring the ICF one simlutaneously obtains the correlation time of the FCF and the directly related diffusion coefficient (eq. 35).

$$\left(g^{(2)}(q,\tau) - 1 \right)_{he} \cong \frac{2 \cdot \langle I_F \rangle}{\langle I_S \rangle} \cdot g^{(1)}(q,\tau) = \frac{2 \cdot \langle I_F \rangle}{\langle I_S \rangle} \cdot \exp\left(-\frac{\tau}{\tau_{(1)}} \right) \qquad (41)$$

$$\tau_{(1)} = \tau_{(2,he)} \qquad (42)$$

A partially heterodyne situation may be the most complex of the three, because it is mostly an inherent quality of the investigated samples and thus not intended. It can be circumvented by converting the system into being predominantly heterodyne. If that is impossible or unwanted, eq. 40 has to be utilised without simplifications because the intensities $\langle I_F \rangle$ and $\langle I_S \rangle$ do not sufficiently deviate from one another, and no term may be disregarded. Non-ergodic sytems, like polymer gels, comprising static spatial

inhomogeneities typically induce partially heterodyne light scattering. In such a measurement the now position dependent intercept, σ_p^2, of the ICF decreases compared to the FCF, but not as much as for the predominantly heterodyne situation (Fig. 13, green curve). The characteristic correlation time yielded by the partially heterodyne ICF, $\tau_{(2,p\text{-}h)}$, lies in-between $\tau_{(1)}$ and $\tau_{(2,ho)}$. Thus, to be able to derive the correct diffusion coefficient it is essential to find out the exact value.

Consequently, what has to be determined are the two intensities, $\langle I_F \rangle$ and $\langle I_S \rangle$, where the sum is the total scattering intensity, $\langle I \rangle$. Two methods for the analysis of light scattering measurements of polymer gels will be elucidated in the next two chapters. Both of them can separate the scattering intensities caused by fluctuating and static components of the investigated system from each other.

2.3.1.1   *Partial-Heterodyne Method*[58,132,145,146]

Polymer gels usually possess a more or less inhomogeneous structure. On the one hand, there are sites that are highly crosslinked thus being incapable of performing any detectable motion. The static fraction of the scattering intensity, $\langle I_S \rangle$, arises from this immobile part of the gel. On the other hand, there are sites where the network chains can diffuse or thermally fluctuate, although this diffusion is restricted due to the chains being tethered to the network junctions. This part of the gel is responsible for the fluctuating fraction of the scattering intensity, $\langle I_F \rangle$. The partial-heterodyne method is able to separate the overall scattering intensity into those two fractions. In a fairly homogeneous gel the fraction of scattered light from fluctuating network chains should be high compared to the light scattered from the immobile domains.

Generally it can be said that the higher the proportion of heterodyneity, the smaller the y-axis intercept of the ICF. The degree of heterodyneity in a light scattering measurement from a polymer gel (without scattering or reflection from external static elements) depends on its spatial inhomogeneity. The more inhomogeneous the underlying network of a polymer gel is, the higher is the heterodyneity and it is possible to assess the network homogeneity from the intercept of the ICF.

For the partial-heterodyne method the polymer gel has to be measured at a high number of different positions. Due to its non-ergodicity each position exhibits a different structure and thus yields a different time-average scattering intensity $\langle I \rangle_{T,p}$ with p denoting the position dependence. Plotting $\langle I \rangle_{T,p}$ versus the number of positions at which the measurements are taken yields a speckle pattern as can be seen in fig. 14. The average of all the time-average scattering intensities is considered to be a rather precise estimate of the ensemble-average scattering intensity $\langle I \rangle_E$ with $\langle ... \rangle_E$ denoting the ensemble-average.
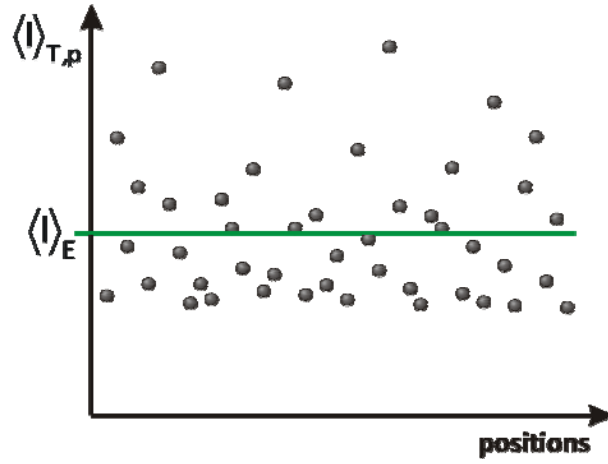
Fig. 14: The speckle pattern of a polymer network or gel; within a non-ergodic system different positions yield different time-average scattering intensities $\langle I \rangle_{T,p}$, $\langle I \rangle_E$ is the ensemble-average scattering intensity which is the average of all $\langle I \rangle_{T,p}$

The fluctuating part of the network is considered to act like polymer coils in dilute solution, thus being ergodic[147]. Consequently, the scattering intensity of this fluctuating part is an ergodic property as well, so that $\langle I_F \rangle_T = \langle I_F \rangle_E = \langle I_F \rangle$. Subtracting this scattering intensity arising from the thermal fluctuations, $\langle I_F \rangle$, from the total ensemble-average scattering intensity, $\langle I \rangle_E$, leads to the ensemble-average intensity arising from frozen-in spatial inhomogeneities $\langle I_S \rangle_E$ (eq. 43). This implies that $\langle I_F \rangle$ cannot adopt values higher than $\langle I \rangle_E$, because $\langle I_S \rangle_E$ cannot become negative. If $\langle I_F \rangle = \langle I \rangle_E$ the gel exhibits no scattering intensity from static inhomogeneities. This theoretically means the gel is ergodic and has virtually no spatial inhomogeneity.

$$\langle I \rangle_E = \langle I_F \rangle + \langle I_S \rangle_E \qquad\qquad (\,43\,)$$

Since $\langle I_F \rangle$ is an ergodic quantity it is not position dependent which signifies that it cannot be higher than the lowest of all measured time-average scattering intensities, $\langle I \rangle_{T,p}$, either, since it always has to adopt the same value. The time-average intensity of the static component, $\langle I_S \rangle_{T,p}$, is position dependent and according to eq. 44 varies with the position, p, as $\langle I \rangle_{T,p}$ does.

$$\langle I \rangle_{T,p} = \langle I_F \rangle + \langle I_S \rangle_{T,p} \tag{44}$$

In summary, the value of the fluctuating part of the scattering intensity has to be the same as or smaller than the lowest overall time-average scattering intensity, $\langle I \rangle_{T,p}$ (Fig. 15). If the fluctuating part of the scattering intensity equals the overall ensemble-average scattering intensity, $\langle I \rangle_E$, the observed gel exhibits no speckle pattern since its scattering intensity is the same at all positions. Thus the relation between $\langle I_F \rangle$ and $\langle I \rangle_E$ or similarly $\langle I_S \rangle_E$ and $\langle I \rangle_E$ provides information about the non-ergodicity and correspondingly inhomogeneity of the observed polymer gels.
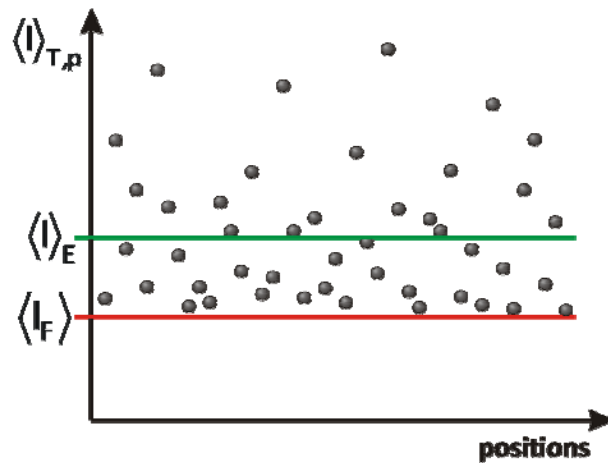
Fig. 15: By means of the partial-heterodyne analysis method it is possible to determine the average scattering intensity of the fluctuating proportion, $\langle I_F \rangle$, within a network or gel. $\langle I_F \rangle$ theoretically has to be less than or equal to the lowest $\langle I \rangle_{T,p}$ value.

Each of the positions at which $\langle I \rangle_{T,p}$ is measured exhibits a correlation function that has to be analysed. For this purpose the natural logarithm of the ICFs is plotted versus the non-logarithmic time scale yielding a straight line with a negative slope at short times due to the

decay being exponential. At longer time scales the slope gradually increases (Fig. 16). The next step is to calculate an apparent diffusion coefficient, D_A, according to eq. 45.

$$D_A = -\frac{1}{2q^2} \cdot \lim_{\tau \to 0} \left(\frac{d}{d\tau} \ln \left(g^{(2)}(q,\tau) - 1 \right) \right)$$ (45)

This diffusion coefficient is only apparent because eq. 45 assumes the observed system to be homodyne (eq. 36). Since it is not homodyne, D_A exhibits too small a value because the initial slope of the partial-heterodyne ICF is smaller than in the homodyne case, which can be seen in fig. 16. The black line shows the FCF and the red line shows the ICF in the homodyne case, when eq. 45 is valid. It is visible that the absolute value of the slope of the FCF is smaller by half than that of the ICF. If the same factor is assumed to hold true for the initial slope of the ICF in the partial-heterodyne case, which is illustrated by the green line in fig. 16, the slope of the resulting, apparent FCF (grey line) and hence the diffusion coefficient are smaller than for the actual, black FCF.
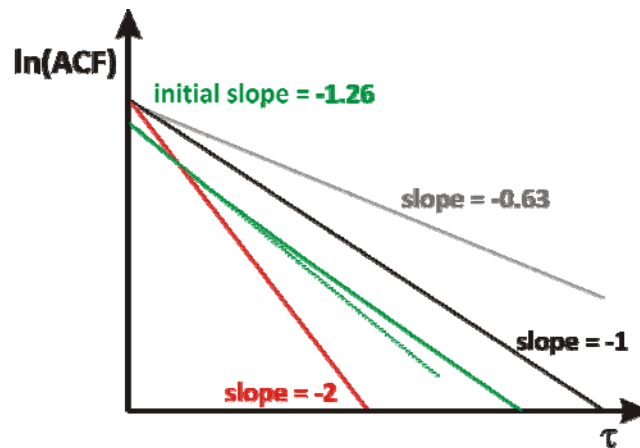
Fig. 16: Logarithmised autocorrelation functions (ACF) plotted versus the non-logarithmic time scale; black line: FCF; red line: homodyne ICF; solid, green curve: partial-heterodyne ICF, dotted green line: fitted line to determine the initial slope of the partial-heterodyne ICF; grey line: apparent FCF determined by eq. 45 in the partial-heterodyne case, its slope results in D_A

The real factor by which to divide the slope of the partial-heterodyne ICF must be between 1 and 2 ($D_A < D < 2D_A$). The lower the heterodyneity, and so the higher the fluctuating proportion of the system, the more D_A approaches the real diffusion coefficient, D. Accordingly, the relation between D and D_A is influenced by the proportion of fluctuation

within the investigated system. The ratio of the fluctuating part of the scattering intensity, $\langle I_F \rangle$, and the overall time-average, position-dependent scattering intensity, $\langle I \rangle_{T,p}$, is utilised according to eq. 46. It can be derived by differentiating the ICF with respect to τ as described in eq. 45. After rearranging one obtains eq. 46 which yields the diffusion coefficient for each position. A fully fluctuating, ergodic and thus homogeneous and homodyne system ($\langle I_F \rangle = \langle I \rangle_{T,p}$) yields $D = D_A$. In a predominantly static, non-ergodic, inhomogeneous and heterodyne system ($\langle I_F \rangle << \langle I \rangle_{T,p}$) it is $D = 2D_A$.

$$D = D_A \cdot \left(2 - \frac{\langle I_F \rangle}{\langle I \rangle_{T,p}} \right) \tag{46}$$

Subsequently, a linearised equation can be yielded (eq. 47) by plotting $\langle I \rangle_{T,p} / D_A$ versus $\langle I \rangle_{T,p}$. The slope of the resulting straight line yields the diffusion coefficient, D, and $\langle I_F \rangle$ can be attained from the y-axis intercept. This way one diffusion coefficient is obtained, averaged over all positions. Knowing $\langle I_F \rangle$ and $\langle I \rangle_E$, now $\langle I_S \rangle_E$ can be calculated according to eq. 43.

$$\frac{\langle I \rangle_{T,p}}{D_A} = \frac{2}{D} \cdot \langle I \rangle_{T,p} - \frac{\langle I_F \rangle}{D} \tag{47}$$

The light scattering intensity of different systems can vary substantially even if they are absolutely homogeneous, due to differences in their refractive index increment, dn/dc, which, at the same ambient conditions, depends on the combination of polymer and solvent. Thus, it is not as simple as assuming that the stronger a system scatters light, the more inhomogeneous it is. If dn/dc and so the contrast between polymer and solvent differs for two systems their scattering intensities cannot be directly compared. That is why the scattering intensity of the fluctuating component of the network, $\langle I_F \rangle$, itself has no universal significance. It needs to be normalised, e.g. by combining it with the overall ensemble-average scattering intensity, $\langle I \rangle_E$. This means that the ratios $\langle I_F \rangle / \langle I \rangle_E$ and $\langle I_S \rangle_E / \langle I \rangle_E$ are both equally suitable measures for the network inhomogeneity, even if two different systems are compared. A homogeneous system is existent if $\langle I_F \rangle / \langle I \rangle_E = 1$ or $\langle I_S \rangle_E / \langle I \rangle_E = 0$.

Additionally, it is possible to determine a characteristic length scale, the dynamic correlation length, ξ_D, of the gel by means of the diffusion coefficient, D, according to a slightly modified STOKES-EINSTEIN equation (eq. 48). This correlation length is the radius of an unpervaded, spherical particle that has the same diffusive properties as the fluctuating network chains. The correlation length does not make a statement about the length of the network chains but it is a measure for the distance between the crosslinks, that are connected by the network chains. It is important to note that the diffusion coefficient thus determined for a polymer network is a cooperative diffusion coefficient, D_{coop}. It does not describe the centre-of-mass movement of the whole coil, as D_{trans} does, but the relaxation of the network chain segments.

$$\xi_D = \frac{k_B T}{6\pi\eta \cdot D_{coop}} \tag{48}$$

2.3.1.2 Non-ergodic Medium Method[132,137,148]

The aforementioned method focuses on the fact that polymer networks usually yield partially heterodyne light scattering. The heterodyneity results from the static scatterers within those networks. This very reason also leads to the non-ergodicity of polymer networks. A technique that exploits the non-ergodicity was devised by PUSEY and VAN MEGEN. Again, the SIEGERT-relation cannot be employed to ascertain the diffusion coefficient for non-ergodic samples. The equation that PUSEY and VAN MEGEN developed instead (eq. 49) is not concerned with the initial slope of the ICF but with its position dependent y-axis intercept, σ_p^2. They determined the FCF, $f(q,\tau)$, by using a modified version of the SIEGERT-relation.

$$f(q,\tau) = 1 + \frac{\langle I \rangle_{T,p}}{\langle I \rangle_E}\left[\sqrt{\left(\left(g^{(2)}(q,\tau)-1\right)-\sigma_p^2+1\right)}-1\right] \tag{49}$$

As can be seen in fig. 17, by converting the ICF (green curve) into the FCF (black curve) it is shifted up to a y-axis intercept with the value of one resulting in an offset, $f(q,\infty)$, different from zero. An important factor in this equation is the relation between σ_p^2 and the intensity-ratio $\langle I \rangle_{T,p} / \langle I \rangle_E$. The lower the intercept is, the more static scatterers are located within the

scattering volume resulting in a higher scattering intensity and a higher intensity-ratio. Thus, a decreasing value for σ_p^2 is compensated by an increasing $\langle I \rangle_{T,p} / \langle I \rangle_E$ - value and vice versa. It would theoretically be sufficient to measure an ICF at only one position if in addition the overall ensemble-average scattering intensity is determined as well.
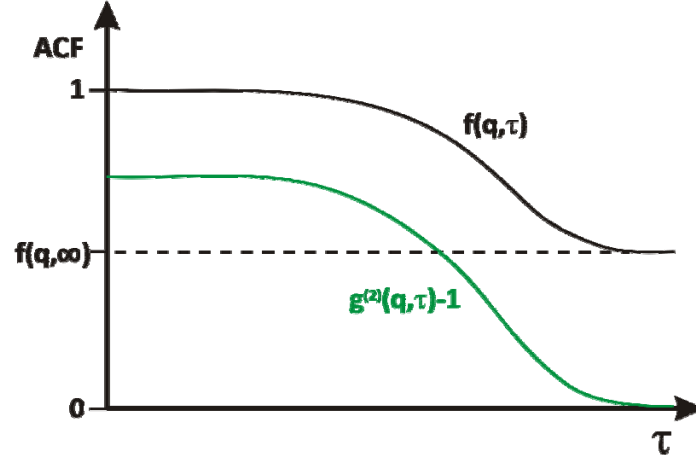
Fig. 17: In order to obtain the FCF, f(q,τ) (black curve), by the non-ergodic analysis method the ICF, $g^{(2)}$(q,τ)-1 (green curve), is shifted to a y-axis intercept of 1 and altered according to eq. 49

When the ICF has been transformed into the FCF, a function of the type of eq. 50 has to be fitted to it. The offset value, f(q,∞), and the correlation time, $\tau_{(1)}$, can be obtained from the resulting fit-curve. The amplitude of the FCF is A = 1 - f(q,∞).

$$f(q,\tau) = f(q,\infty) + A \cdot \exp\left(-\frac{\tau}{\tau_{(1)}}\right)$$

(50)

Hence, similar to the partial-heterodyne method, the main result is the separation of the static and fluctuating part of the investigated sample, however not in terms of intensity but as percentages. The offset, f(q,∞), represents the static, frozen-in proportion of the network and the amplitude, A, corresponds to the fluctuating part. The lower the plateau value of the offset, the more homogeneous is the observed polymer gel.

According to eqs. 35 and 48, it is possible to determine the dynamic correlation length, ξ_D, from the correlation time $\tau_{(1)}$.

47

2.3.2 Static Light Scattering

The SLS technique can be used to ascertain network inhomogeneity as well. As already mentioned (chapters 2.1.4 & 2.3), polymer networks generally scatter light stronger than their corresponding polymer solutions. That is due to the static inhomogeneities within polymer networks. Depending on how pronounced those frozen-in inhomogeneities are, they can even be visible to the naked eye by rendering the network or gel opaque which suggests rather strong light scattering[59,61]. The excess scattering of polymer networks compared to their corresponding solutions, can thus be seen as a measure for the network inhomogeneity.

In SLS, it is unusual to work with the scattering intensity itself. The typically used quantity is the RAYLEIGH-ratio $R(q)$[129]. For vertically polarised light it is defined in eq. 51 with the intensity of the scattered light, $I(q)$, at the scattering vector, q, the intensity of the incident radiation, I_0, the scattering volume, V_{sc}, and the distance between the detector and the scattering volume, u.

$$R(q) = \frac{I(q) \cdot u^2}{I_0 \cdot V_{sc}}$$

(51)

Conducting light scattering measurements from polymer gels yields $R_{gel}(q)$. It is the sum of the excess scattering ratio $R_{ex}(q)$, originating from the static inhomogeneities, and $R_T(q)$, the part of the scattered light arising from thermal concentration fluctuations of the network chains (eq. 52). $R_T(q)$ is supposed to be ergodic.

$$R_{gel}(q) = R_T(q) + R_{ex}(q)$$

(52)

The c*-theorem[149,150] implies that the network chains in a neutral, swollen gel adopt the same conformation that comparable polymer chains have in solution. Thus, it is possible to replace the thermal term $R_T(q)$ by $R_{sol}(q)$, which originates from the scattering intensity of the polymer solution. For this purpose, a polymer solution and gel have to be prepared identically at a concentration that gives rise to overlapping chains, the only difference being the lack of crosslinker in the solution. The excess RAYLEIGH-ratio can then easily be determined by measuring $R_{gel}(q)$ and $R_{sol}(q)$ and thereafter substracting the latter from the former

(eq. 53). This is not an exact procedure, however the inaccuracy can be tolerated and becomes less significant the stronger the excess scattering is[58,73-77,81,127,151].

$$R_{ex}(q) = R_{gel}(q) - R_{sol}(q)$$ (53)

This excess scattering can be used to ascertain the static correlation length, ξ_S, which is a measure for the spatial extent of the inhomogeneities, and the mean square fluctuation of the refractive index, $\langle \delta n^2 \rangle$, which extends over ξ_S^3 and can be related to concentration fluctuations within the gel.

DEBYE and BUECHE[152] worked on light scattering by inhomogeneous solids, like Lucite®, and developed an equation for the scattering intensity which SONI and STEIN[153] refined for application to swollen networks (eq. 54).

$$R_{ex}(q) = 4\pi \cdot K \cdot \langle \delta n^2 \rangle \int \frac{\gamma(r) \cdot \sin(qr) \cdot r^2}{qr} dr$$ (54)

They showed that the excess RAYLEIGH-ratio depends on refractive index fluctuations, $\langle \delta n^2 \rangle$, within the gel, on the scattering vector, q, and also on a spatial correlation function, $\gamma(r)$, that is specified in eq. 55. Therein, $\langle \delta n_i \delta n_j \rangle_r$ is the average product of pairs of refractive index fluctuations at the positions i and j, which are all separated by the distance, r. It was found that it often holds true for $\gamma(r)$ to be an exponentially decaying function with the correlation length ξ_S. K is a constant in which n is the refractive index of the medium and λ_0 the wavelength of the incident radiation in vacuum (eq. 56).

$$\gamma(r) = \frac{\langle \delta n_i \delta n_j \rangle_r}{\langle \delta n^2 \rangle} = \exp\left(-\frac{r}{\xi_S}\right)$$ (55)

$$K = 4\pi^2 n^2 \lambda_0^{-4}$$ (56)

Solving eq. 54 by inserting the exponential function of eq. 55 yields a simple expression for $R_{ex}(q)$ (eq. 57).

$$R_{ex}(q) = \frac{8\pi \cdot K \cdot \xi_S^3 \cdot \left\langle \delta n^2 \right\rangle}{\left(1 + q^2 \cdot \xi_S^2\right)^2}$$

(57)

In a typical DEBYE-BUECHE graph, the inverse of the square root of the excess Rayleigh-ratio $(R_{ex}(q))^{-1/2}$ is plotted versus q^2. According to eq. 58 this results in a straight line with a positive slope and intercept that can be used to determine ξ_S and $\langle \delta n^2 \rangle$.

$$\frac{1}{\sqrt{R_{ex}(q)}} = \frac{\xi_S^2}{\sqrt{8\pi \cdot K \cdot \xi_S^3 \cdot \left\langle \delta n^2 \right\rangle}} \cdot q^2 + \frac{1}{\sqrt{8\pi \cdot K \cdot \xi_S^3 \cdot \left\langle \delta n^2 \right\rangle}}$$

(58)

Thus, by means of the q-dependence of the excess scattering of a gel its inhomogeneity can be determined. The static correlation length ξ_S is a measure for the size of the inhomogeneities and the mean square refractive index fluctuation, $\langle \delta n^2 \rangle$, provides information about how pronounced the inhomogeneities are.

Assuming the local refractive index in a gel only depends on the local polymer concentration and the crosslinker concentration to be sufficiently small, it is possible to relate the fluctuations in refractive index to fluctuations in concentration (eq. 59). For that purpose, it is necessary to know the refractive index increment, dn/dc, of the observed system. Concentration fluctuations on the molecular scale can then be compared to the known macroscopic concentration. This is favourable, since it is easier to conceive than fluctuations in refractive index[81].

$$\sqrt{\left\langle \delta c^2 \right\rangle} \cong \frac{\sqrt{\left\langle \delta n^2 \right\rangle}}{dn/dc}$$

(59)

3 Experimental Part

The general strategy followed for this thesis was to determine the homogeneity of the network structure of thiol-ene hydrogels prepared from a trithiol and three different dienes. A minor challenge in this process was to render these basically organic molecules water soluble. Moreover, it was considered important to have a point of reference, regarding network inhomogeneity for the purpose of comparison. Thus, not only thiol-ene hydrogels were investigated but also polyacrylamide hydrogels prepared by FCC, which are known to exhibit a rather non-uniform structure concerning spatial inhomogeneity[154-156].

The formation mechanisms of the two kinds of gels are rather different from each other. The network chains in an FCC-gel are made up of a varying, but high, number of monomers whereas in the thiol-ene gels each network chain primarily consists of only one diene-monomer, thus yielding an end-linking polymerisation. The hydrogels were characterised by mechanical measurements to determine their macroscopic qualities. This way it was possible to prepare gels that exhibited similar elastic properties and were thus macroscopically comparable. Light scattering experiments, primarily DLS, were used to ascertain the microscopic structure of the different hydrogels. Concerning the origin and purity of the chemicals see Appendix C.

3.1 Monomers

3.1.1 Thiol-Ene Polymerisation

All thiol-ene polymerisations were carried out with the same trifunctional thiol, an ethoxylated trimethylolpropane tri(3-mercaptopropionate) (ETTMP1300, Scheme 6, right hand side). ETTMP1300 acts as a crosslinker. Since the aim was to prepare hydrogels, ethoxylation of the three branches in ETTMP1300 was employed to render the molecule water-soluble. As opposed to most other polyethers, polyethylene glycol (PEG), which only consists of ethoxy groups, is water-soluble at moderate temperatures due to the distance of its oxygen atoms[157]. They are approximately as far apart from each other as the space

between the oxygen atoms in liquid water yielding effective hydrogen bonding. Each of the three branches possesses seven ethoxy groups, on average.
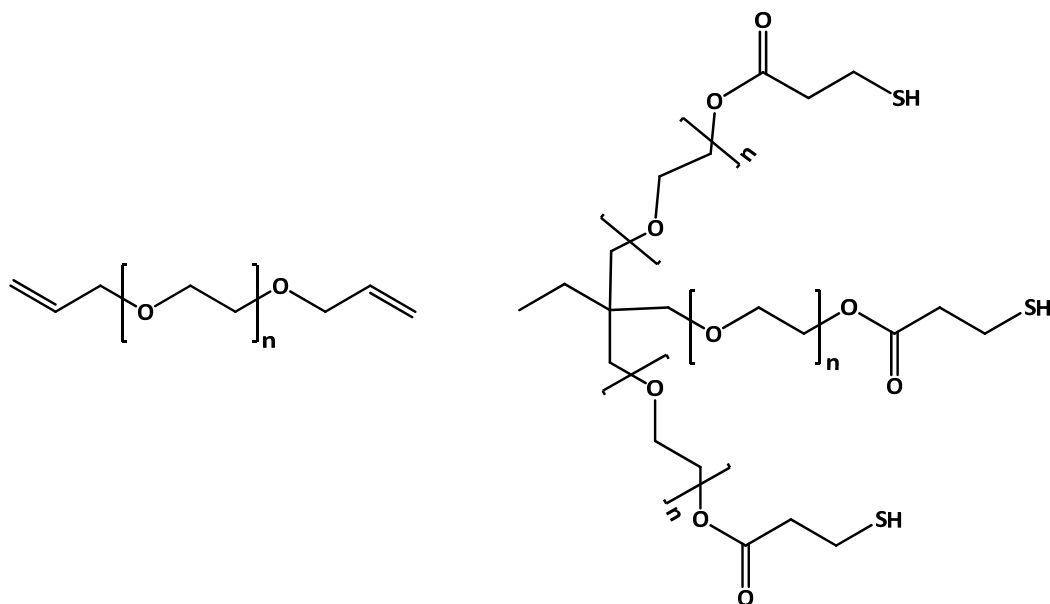
Scheme 6: Monomers for the TEP; left hand side: the diene DAPX000, DAP1000: n $\cong$ 23, DAP2000: n $\cong$ 45, DAP3000: n $\cong$ 68; right hand side: the trithiol ETTMP1300, n $\cong$ 7

As ene-components water-soluble diallylated PEGs (DAP, Scheme 6, left hand side) were used. They were synthesised from PEG (PEG1000, PEG2000 and PEG3000) by deprotonation and subsequent nucleophilic substitution to allyl bromide[100]. The reaction mechanism is illustrated in scheme 7.
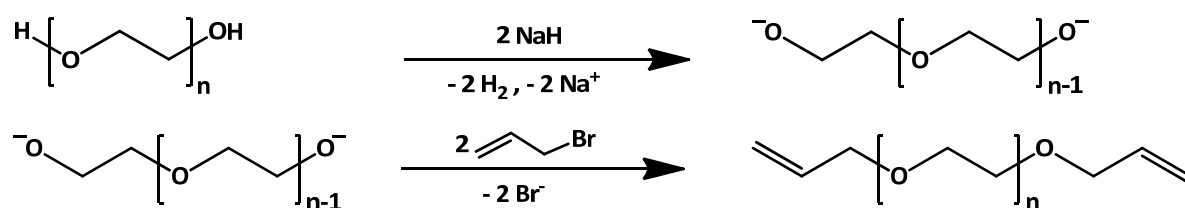
Scheme 7: Formation mechanism of DAPX000; in the first step NaH deprotonates the hydroxyl-groups of the PEG-molecules which then attacks the allylbromide, nucleophilicly substituting the bromide

Synthesis of diallylated PEG (DAP)[100]:

400 mL of dried THF were utilised to dissolve 40 g of PEG which was used in three different molar masses, M_n = 1000, 2000 and 3000 g/mol. The mixture was heated by a water bath (T $\cong$ 50 °C) to accelerate the dissolving process. Dried *n*-hexane was employed in an appropriate amount (ca. 50 mL) to purify sodium hydride (NaH), which was available as a 60 % suspension in mineral oil. This was done by placing the required amount of NaH (1.1 molar equivalents of NaH for each hydroxyl group in PEG) in a SCHLENK flask purged with nitrogen and then successively adding *n*-hexane, stirring, letting NaH sediment and removing the supernatant mixture of *n*-hexane and mineral oil with a pipette. This procedure was repeated four times, followed by drying the NaH in a nitrogen stream. Subsequently, the purified NaH was slowly added in small portions to the solution of PEG in THF while stirring. The reaction mixture turned turbid due to the generation of a beige precipitate. Once the evolution of hydrogen had ceased, the flask was purged with nitrogen followed by dropwise addition of a 10:1 - mixture of THF and allylbromide (1.1 molar equivalents of allylbromide for each hydroxyl group in PEG), while constantly stirring. After this, the flask was transferred to an 85 °C hot oil bath and was heated overnight, under reflux conditions. The turbid, yellowish reaction mixture was then alowed to cool to room temperature (22 °C ± 1 °C) and was centrifuged for 30 min, at 6000 rpm, to let the precipitate sediment. This was followed by partial evaporation of THF in a rotary evaporator to increase the concentration of the product. In the last step the product was precipitated by slowly adding the clear mixture to iced diethyl ether in a ratio of 10:1 $\hat{=}$ v:v $\hat{=}$ ether:product solution.

The yielded diallylated PEGs, namely DAP1000 (M_n = 1080 g/mol) produced from PEG1000, DAP2000 (M_n = 2080 g/mol) from PEG2000 and DAP3000 (M_n = 3080 g/mol) from PEG3000, were analysed by ^{1}H NMR-spectroscopy. Additionally, MALDI-TOF measurements were carried out for PEG1000 and DAP1000.

NMR results:

^{1}H-NMR (400 MHz, CDCl$_3$): δ = 3.65 (m, 95 H (DAP1000), 183 H (DAP2000) or 290 H (DAP3000), [OCH_2CH_2]$_n$), 4.00 (d, 4.14 H, 4.15 H or 4.27 H, PEG-OCH_2CH=CH$_2$), 5.17 (d, 2.05 H, 2.01 H or 2.05 H, PEG-OCH$_2$CH=CH_2), 5.27 (d, 2.05 H all three, PEG-OCH$_2$CH=CH_2), 5.91 (q, 2.00 H all three, PEG-OCH$_2$CH=CH$_2$) ppm.

The NMR-results show degrees of functionalisation with allyl ether end-groups of 96 % for DAP1000, 99 % for DAP2000 and 94 % for DAP3000. For the NMR spectra see Appendix D, 1. Only the one of DAP1000 is presented because all three spectra are very similar.

MALDI-TOF results:

The MALDI-TOF mass spectrometry measurements (Matrix Assisted Laser Desorption Ionisation - Time Of Flight) were carried out by Lars Nothdurft on a Biflex III instrument by Bruker with the matrix *trans*-2-[3-(4-*tert*-butylphenyl)-2-methyl-2-propenylidene]malono-nitrile (DCTB). The metal adduct was potassium trifluoroacetate (KTFA). The samples PEG1000 and DAP1000 were investigated in order to see whether changes in molar mass or molar mass distribution due to the diallylation could be detected.
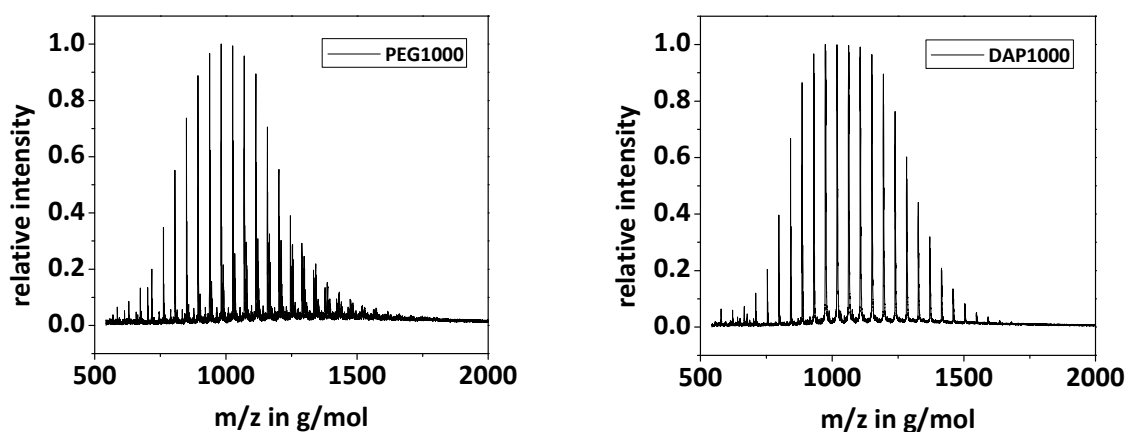

Fig. 18: MALDI-TOF spectra of PEG1000 (left hand side) and DAP1000 (right hand side); m/z: ratio of the molar mass, m, to the charge of the molecules, z, where z is assumed to be unity

As can be seen in fig. 18 the spectra of the two compounds, PEG1000 and DAP1000, do not differ significantly from each other. The number-average molar mass, M$_n$, the weight-

average molar mass, M_w, and the polydispersity taken from the MALDI-TOF data can be seen in table 3. Due to the functionalisation, the molar mass increases from PEG1000 to DAP1000, although by less than the expected 80 g/mol, which is the molar mass of two allyl groups. The polydispersity of 1.03 is very low and does not change during the functionalisation reaction. Furthermore, the spectrum of DAP1000 exactly coincides with the theoretical simulation.

Table 3: Results from the MALDI-TOF spectra of PEG1000 and DAP1000; M_n: number-average molar mass, M_w: weight-average molar mass

Sample	M_n in g/mol	M_w in g/mol	Polydispersity
PEG1000	1023	1056	1.03
DAP1000	1070	1102	1.03

3.1.2 Free Radical Crosslinking Copolymerisation

The FCC was used to prepare polyacrylamide (PAAm) hydrogels that could be compared to the thiol-ene hydrogels concerning their inhomogeneity. The reagents that were used for the syntheses of these gels were acrylamide (AAm, Scheme 8, left hand side) as the monomer and N,N'-methylene-bisacrylamide (BIS, Scheme 8, right hand side) as the crosslinker. Used in an free radical crosslinking copolymerisation, BIS is a tetrafunctional crosslinker because it comprises two double bonds.
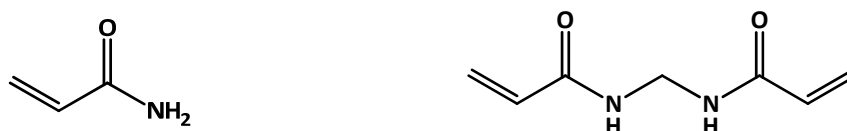
Scheme 8: Monomers for the FCC; left hand side: AAm; right hand side: BIS

3.2   Preparation of Hydrogels

3.2.1   Thiol-Ene Polymerisation

For the thiol-ene polymerisation three series of hydrogels were prepared. The thiol that was utilised as crosslinker for these sets was always ETTMP1300, but as enes either DAP1000, DAP2000 or DAP3000 were used. Each series was prepared at various concentrations (7.5 - 20 wt% total monomer concentration with regard to the entire solution, Table 4). If not otherwise specified, the concentration indications in weight percent (wt%) for the thiol-ene gels always denote the overall monomer concentration, c_{TEP}.

Table 4: Concentrations $c_{DAPX000}$ and c_{ETTMP} of the monomers employed in the three series of the TEP; c_{cross} is the concentration of crosslinker functional groups resulting from c_{ETTMP}, $c_{cross} = 3 \cdot c_{ETTMP}$

overall monomer concentration c_{TEP} in wt%		7.5	10	12.5	15	17.5	20
DAP1000	$c_{DAP1000}$ in mmol/g	0.042	0.058	0.074	0.091	0.110	0.130
	c_{ETTMP} in mmol/g	0.028	0.038	0.049	0.061	0.073	0.086
	c_{cross} in mmol/g	0.084	0.115	0.148	0.183	0.220	0.259
DAP2000	$c_{DAP2000}$ in mmol/g	0.028	0.038	0.049	0.060	0.072	0.085
	c_{ETTMP} in mmol/g	0.018	0.025	0.032	0.040	0.048	0.057
	c_{cross} in mmol/g	0.055	0.076	0.098	0.120	0.145	0.171
DAP3000	$c_{DAP3000}$ in mmol/g	0.021	0.028	0.036	0.045	0.054	0.064
	c_{ETTMP} in mmol/g	0.014	0.019	0.024	0.030	0.036	0.042
	c_{cross} in mmol/g	0.041	0.057	0.073	0.090	0.108	0.127

Thiol and ene were used in stoichiometric ratio concerning the number of functional groups. Since the molar mass of DAP3000 is higher than that of DAP1000, the molar concentration in both mixtures differs if compared at the same weight concentration. Under these circumstances a hydrogel formed from DAP3000 comprises fewer crosslinks and should thus be less elastic than a hydrogel prepared from DAP1000. Table 4 shows the

concentrations of ETTMP1300 (c_{ETTMP}) and the DAPs of the three series ($c_{DAPX000}$) in wt% and the concentration of crosslinker functional groups, c_{cross}, in mmol/g. The density of the reaction mixtures at room temperature (always 22 °C ± 1 °C) is $\cong$ 0.98 g/mL.

The polymerisations could not be carried out in pure water as solvent, since ETTMP1300 does not completely dissolve in it. This was probably due to an uneven distribution of the ethoxy groups, either among the molecules or between the branches of one molecule. Therefore, the polymerisations were conducted in a mixture of water (ultrapurified water) and ethanol (v:v $\cong$ 3:1) which could overcome this problem. The density of this solvent mixture at room temperature is $\cong$ 0.96 g/mL.

As photoinitiator camphorquinone-10-sulfonic acid monohydrate (CQS, Scheme 9) was employed. The sulfonic acid side-group is necessary to render the photoinitiator water soluble. It was used in a stock solution at a concentration of c_{CQS} = 0.4 g/L (chapter 3.2.1.1), in the water-ethanol mixture.
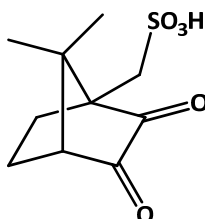
Scheme 9: The photoinitiator for the TEP samples, camphorquinone sulfonic acid (CQS)

The reaction mixtures were prepared by weighing out ETTMP1300 and the particular DAP, adding the stock solution of the photoinitiator and stirring it until a clear solution was formed. During this procedure, the reaction mixture was protected from light by wrapping the vial up in aluminium foil. The further course of action was dependent on what the solution was going to be used for (chapters 3.3, 3.4, 3.5).

3.2.1.1 UV-Vis Measurements Concerning the Photoinitiation

The UV/Vis-measurements were performed at a Jasco V-550 UV/Vis spectrometer. Since the aim was to prepare hydrogels with a homogeneous network structure utilising photoinitiation, UV/Vis-measurements were carried out to determine the light absorption of

the reactants. This way an appropriate initiator and initiator concentration could be ascertained which, in addition, influenced the choice of the radiation source.

An important prerequisite was to minimise absorption of the exciting light within the gel, either by the monomer or the initiator. If that were the case the light intensity would decrease on its way through the cuvette, leading to an inhomogeneous reaction rate within the reaction mixture and thus an inhomogeneous network structure. As can be seen in fig. 19, the monomers (green curve) mainly absorb in the UV-region. Accordingly, for the absorption range of the initiator not to coincide with that of the monomer, it was not possible to use a UV-initiator.
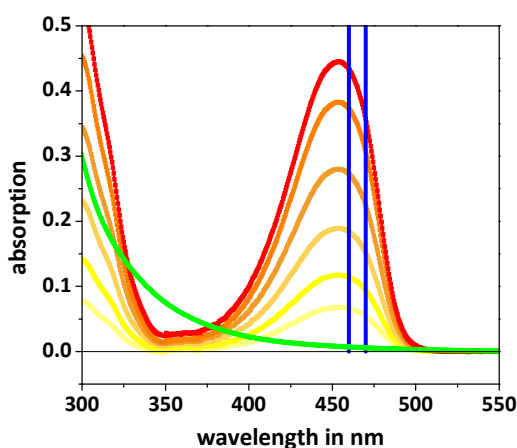
Fig. 19: Absorption spectrum of CQS at different concentrations (red curve: high concentration, yellow curve: low concentration); the blue lines indicate the emission wavelength range of the LED-lamp ($\lambda \cong 465$ nm); the green curve indicates the absorption of a 10 wt% mixture of ETTMP1300 and DAP1000 in water-ethanol (v:v $\hat{=}$ 3:1), at the wavelength of the LED-lamp there is virtually no monomer absorption

The initiator that met the requirements, which were absorption at visible wavelengths (avoiding an inner filter effect) and being water soluble, was CQS. It has an absorption maximum of 453 nm in the above-mentioned water-ethanol mixture. The light that was used to excite CQS was emitted by blue LEDs exhibiting a wavelength of around 465 nm (Fig. 19, blue lines). At this wavelength there was virtually no monomer absorption (Fig. 19, green curve). CQS was used in such a concentration ($c_{CQS} = 0.4$ g/L, extinction coefficient $\varepsilon_{465nm} = 22.8$ L/(mol·cm)) that the light absorption throughout the reaction mixture was less than 10 % at an optical path of 1 cm. Thus, the formation of a significant gradient of the light intensity was prevented.

The decrease of light intensity by absorption throughout the reaction mixture was the reason why the large cuvettes for the SLS measurements had to be rotated during irradiation. At a concentration of 0.4 g/L the light absorption would have exceeded the permitted 10 % because those cuvettes have an inner diameter of 23 mm.

3.2.2 Free Radical Crosslinking Copolymerisation

Two series of PAAm hydrogels were prepared using different crosslinker concentrations. The first series was carried out with 1 mol% BIS (crosslinker) with respect to AAm (monomer). The monomer concentration, c_{AAm}, ranged from 7 to 19 wt% (with regard to the entire solution, see table 5). For the second series 0.35 mol% BIS with respect to the monomer were utilised and the concentration ranged from 7.5 to 20 wt% (with regard to the entire solution, see table 5). The concentration of crosslinker functionalities (which is four per BIS molecule), c_{cross}, in mmol/g is also displayed in table 5. In general, c_{cross} adopts lower values for the PAAm-hydrogels than for the TEP-hydrogels. This theoretically means that the network chain density should be lower for the PAAm-gels. The density of the reaction mixtures is $\cong 0.99$ g/mL.

Table 5: Concentrations c_{AAm} and c_{BIS} of the monomers employed in the two series of the FCC; c_{cross} is the concentration of crosslinker functional groups resulting from c_{BIS}, $c_{cross} = 4 \cdot c_{BIS}$

acrylamide concentration c_{AAm} in wt%		7.5	10	12.5	15	17.5	20		
0.35 mol% BIS	c_{AAm} in mmol/g	1.056	1.408	1.774	2.112	2.465	2.817		
	c_{BIS} in mmol/g	0.004	0.005	0.006	0.007	0.009	0.010		
	c_{cross} in mmol/g	0.015	0.020	0.025	0.029	0.035	0.040		
acrylamide concentration in wt%		7	10	13	14	15	16	17	19
1 mol% BIS	c_{AAm} in mmol/g	0.986	1.408	1.831	1.971	2.111	2.254	2.394	2.675
	c_{BIS} in mmol/g	0.010	0.014	0.018	0.020	0.021	0.023	0.024	0.026
	c_{cross} in mmol/g	0.040	0.057	0.074	0,079	0.084	0.090	0.096	0.105

Pure water (ultrapurified) was used as solvent for the PAAm-hydrogels. The redox initiation system consisting of ammonium peroxydisulfate (APS, Scheme 10, left hand side) and N,N,N',N'-tetramethylethylenediamine (TEMED, Scheme 10, right hand side) served as initiator. Accordingly, to start the polymerisation there was no need for heat or light. The initiator components were used in stock solutions, the concentrations of which were 0.7 g/L for the APS-solution and 1.8 g/L for the TEMED-solution. Two-thirds of the total volume of the necessary solvent were taken from the APS-solution (overall concentration: 0.47 g/L) and one-third from the TEMED-solution (overall concentration: 0.6 g/L) yielding a ratio of n(TEMED) : n(APS) = 2.5 (n: amount of substance). As opposed to the TEP, the concentration indications in weight-percent for the PAAm gels only denote the acrylamide concentration, c_{AAm}.
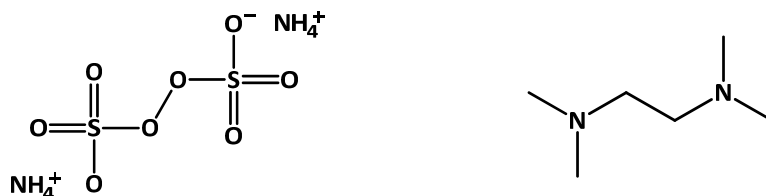
Scheme 10: The redox initiator system for the FCC comprising TEMED (left hand side) as the accelerator and APS (right hand side) as the actual initiator

The reaction mixtures were prepared by weighing out AAm and BIS, adding the APS stock solution, stirring it until a clear solution was formed, then adding the TEMED stock solution and stirring again. The further course of action was dependent on what the solution was going to be used for (chapters 3.3, 3.4, 3.5). However, since this mixture crosslinked rather rapidly, it was important to proceed fast to the next step.

3.3   Mechanical Measurements

The mechanical measurements were carried out on a rheometer (Bohlin Gemini 150 Rheometer System, Malvern Instruments Ltd), equipped with a modified quartz glass bottom plate and underneath it a blue LED-lamp exhibiting a wavelength of $\cong 465$ nm (chapter 3.2.1.1), only used for the TEP-samples. The system was a cone-and-plate configuration, with a 4° cone angle and a cone diameter of 40 mm (Fig. 20). The liquid reaction mixtures were filtered through a membrane syringe filter (always PTFE, 0.45 µm pore size) and applied to the horizontal plate. The truncated cone was lowered to a specified distance of 150 µm. The measurements were conducted at room temperature in oscillation mode at an oscillation frequency of 1 Hz and a predefined constant strain amplitude of 1 %.
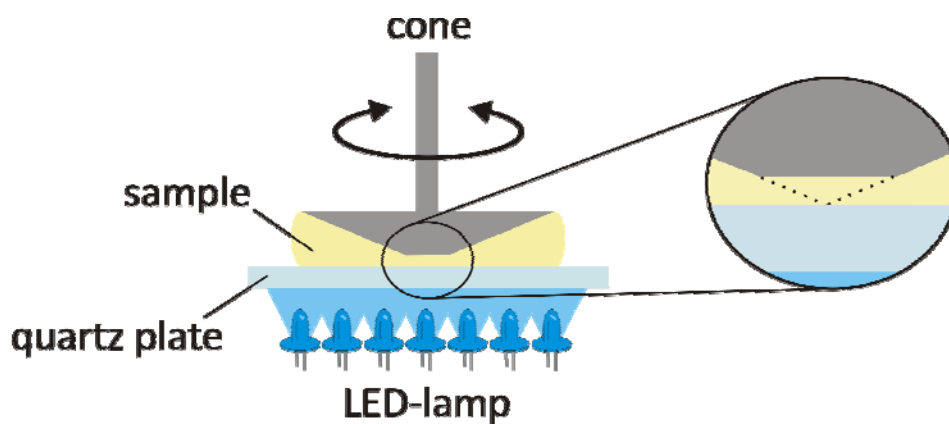
Fig. 20: Schematic illustration of the utilised rheometer; the magnification shows how the exact position of the truncated cone is determined, the distance between cone and plate is 150 µm; the LED-lamp was only used for the TEP-samples

3.3.1 Thiol-Ene Hydrogels

As already mentioned, the thiol-ene samples were irradiated from below the quartz glass bottom plate. Thus, the crosslinking process could be followed rheologically. The LED-lamp was connected to a power supply unit with which it was set to a voltage of 3.5 V. Depending on the concentration, the first increase of the elastic modulus G′ typically started after an induction period of about 20 min (high concentrations) to 2.5 h (low concentrations). The measurements lasted as long as it took for G′ to level off to a plateau value. This was usually around 20 h for the thiol-ene samples. However it has to be noted that even after 20 h the G′-value still increased slightly, but due to solvent evaporation it did not make sense to go on measuring for much longer. Fig. 21 shows the typical course of a rheology measurement of thiol-ene hydrogels using the example of DAP1000 at 15 wt%.

Fig. 21: A plot of the elastic modulus, G′, and the viscous modulus, G′′, versus time, taken with the rheometer during a crosslinking reaction of DAP1000 at 15 wt%

The gel point, estimated by the intersection of G′ and G′′, occured between half an hour for the high concentrations and up to 3.5 h for the lowest concentrations (Fig. 22).
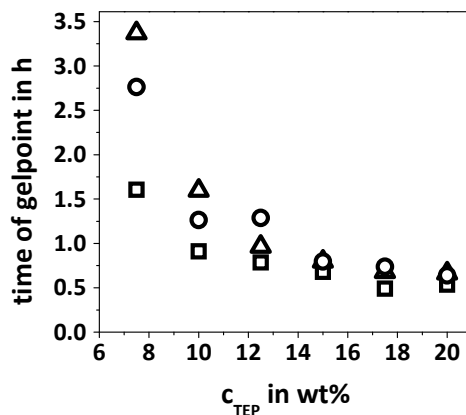
Fig. 22: Time at which the gel point (assumed to be at the intersection of G′ and G′′) occurs plotted versus the monomer concentration, c_{TEP}; squares: DAP1000, triangles: DAP2000, circles: DAP3000
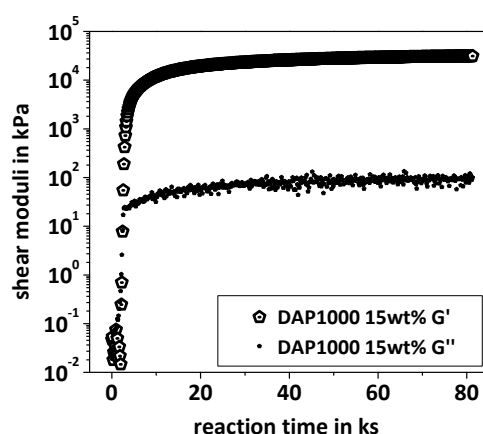
Blank experiments were carried out on the rheometer. The mixture of ETTMP1300 with non-allylated PEG and initiator stock solution irradiated by the LED-lamp, did not yield any crosslinked products or even an increase in viscosity. The same was true for only PEG10,000 and only DAP3000, dissolved in the initiator stock solution and irradiated by the LED-lamp. Thus, undesired side-reactions such as branching or homopolymerisation of the dienes could be considered negligible.

3.3.1.1 Rheology Measurements Concerning the Photoinitiation

One advantage of using photoinitiation should be the possibility to stop the reaction at any point by turning off the light. In order to examine whether this is possible for the thiol-ene systems used in this thesis, a DAP2000 17.5 wt% sample was observed rheologically while polymerising, turning the LED-lamp on and off for certain time intervals (Fig. 23).

It is evident from fig. 23 that the increase in the elastic modulus receded when the irradiation was stopped (red parts of the curve), which means that the crosslinking proceeded more slowly and thus the reaction rate decelerated. Especially at the earlier stages of the reaction, G′ was still slightly rising with time although there was no light starting

the polymerisation. This is probably due to the radical nature of the mechanism. If the radicals are not terminated, they carry on reacting even if there is no further initiation. Still, the reaction rate abated and at longer times even came to a complete halt when the sample was not irradiated.

   This behaviour shows the considerable influence of the irradiation. Since without light the reaction does not easily proceed, it is for instance possible to examine a crosslinking TEP-sample at certain conversions without it altering its structure in the meantime. Aside from that, it appears that at medium reaction times of around 11 h (40 ks), there was no change in the elastic modulus of the uninitiated sample. Thus, it can be concluded that, at least during the first half of the reaction, there was no significant solvent evaporation.
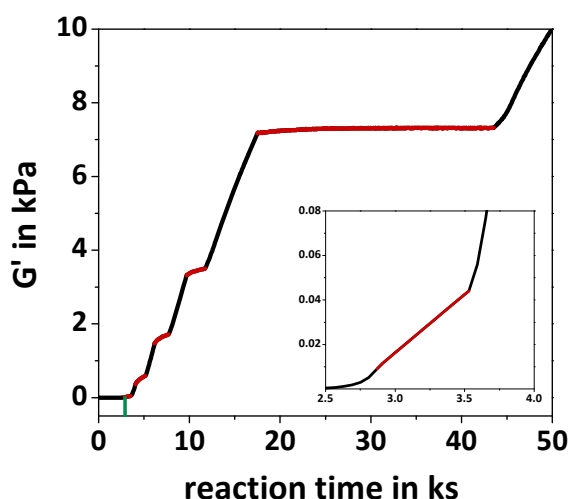
Fig. 23: Rheological measurement of a thiol-ene polymerisation of DAP2000 and ETTMP1300 at a weight concentration of 17.5 wt%; the sample was only irradiated for the black parts of the curve, during the red parts the LED-lamp was turned off; the green line indicates the gel point (intersection of G′ and G′′); note that the scale of G′ is not logarithmic

3.3.2   PAAm Hydrogels

The PAAm hydrogels were prepared on the same quartz glass plate as the thiol-ene gels but without being irradiated by the LED-lamp, because of the redox initiation system. The first increase in G′ occurred faster than in the thiol-ene polymerisation, approximately after 10 min, and the plateau was also reached much earlier, usually after about 2.5 h depending on the concentration. Moreover, once the plateau value was attained, it did not noticeably increase anymore. Fig. 24 (left hand side) shows the typical course of a rheology measurement of PAAm-hydrogels, using the example of PAAm 0.35 mol% BIS at 17.5 wt%. The difference between the run of the elastic moduli of a thiol-ene and a PAAm-gel can also be seen in fig. 24 (right hand side).
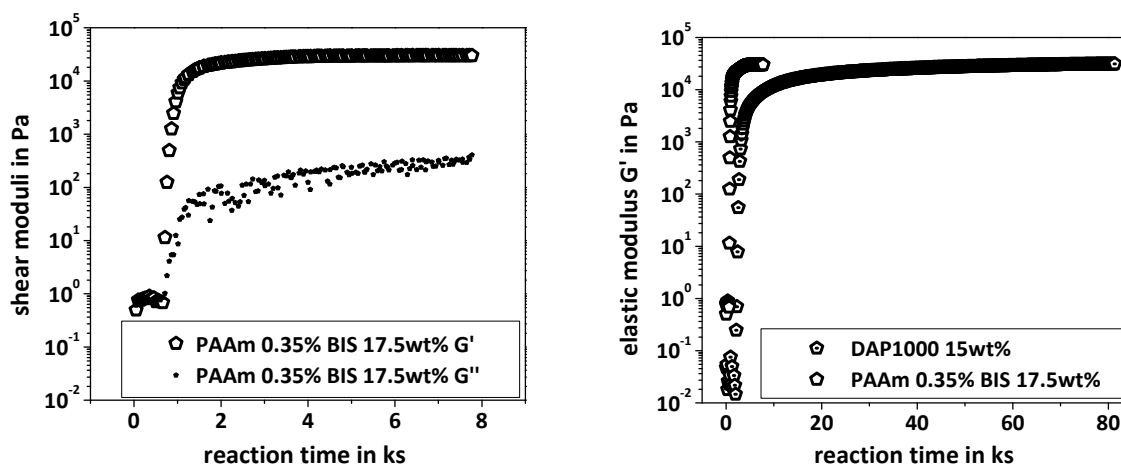
Fig. 24: Left hand side: a plot of the elastic modulus, G′, and the viscous modulus, G′′, versus time taken with the rheometer during a crosslinking reaction of PAAm at 17.5 wt% and 0.35 mol% BIS; right hand side: comparison of the elastic modulus build-up for a TEP sample (Fig. 21) and a FCC sample (this figure, left hand side), the FCC reaches its final modulus considerably faster than the TEP

65

3.4 Light Scattering Measurements

For both DLS and SLS experiments the reaction mixture was filtered through a membrane syringe filter and then introduced into an appropriate light scattering cuvette. After sealing it, the cuvette was placed in front of an LED-lamp (chapter 3.2.1.1), irradiating at a wavelength of $\cong 465$ nm for a day in the case of the thiol-ene hydrogels. For the PAAm hydrogels the cuvette was simply allowed to stand in order for the reaction to take place. The LED-lamp was connected to a power supply unit with which it was set to a voltage of 4 V. The polymerisations were carried out at room temperature.

Different cuvettes were used for the DLS- and SLS-measurements. The DLS-cuvettes (Deutero and Norell, 400 MHz NMR) have an inner diameter of $\cong 9$ mm. The SLS measurements were carried out in special quartz cuvettes with an inner diameter of $\cong 23$ mm. A higher diameter results in a lower curvature of the surface that the laser beam impinges upon. This is favourable because it reduces the influence of the glass surface on the measurement.

In the case of the thiol-ene hydrogels, the bigger cuvettes used for the SLS experiments had to be rotated around their longitudinal axis during the polymerisation procedure (see chapter 3.2.1.1).

Not only reactor-batch gels were investigated by light scattering measurements but also equilibrium swollen hydrogels. They were put into a cuvette which was filled with the particular solvent, for the gel not to be exposed to air anymore (chapter 3.5).

3.4.1 Dynamic Light Scattering

The DLS measurements were carried out with an ALV/CGS-3 compact goniometer system (ALV GmbH) equipped with a helium-neon laser ($\lambda = 632.8$ nm), a correlator of the type ALV/LSE-5003, a cuvette rotation/translation unit for measuring non-ergodic samples and fibre-optical three-mode detection optics combined with a ALV/HIGH QE avalanche photodiode detector. The majority of the measurements were performed in a 25 °C toluene bath (for index matching) and at a scattering angle of $\theta = 90°$. The cuvettes were tempered in the bath for about 5 min before the measurements were started. Furthermore, a few experiments concerning the temperature dependence of the light scattering were performed

at 35 °C and 45 °C. For all applied methods the thiol-ene gels and the PAAm-gels were treated the same way.

It is crucial to know the viscosity and the refractive index of the solvent, to calculate the dynamic correlation length, ξ_D, of a gel (eq. 48) and the scattering vector, q (eq. 29) which is essential for the determination of the diffusion coefficient (eq. 35). Both quantities are displayed in table 6 for pure water and the water-ethanol mixture.

Table 6: Properties of the utilised solvents that are relevant to light scattering measurements at 25 °C; the viscosity, η, is determining for the dynamic correlation length, ξ_D, of a gel and the refractive index, n (at 633 nm and 25 °C), that influences the scattering vector, q

	viscosity η in mPas	n_{25}^{633}
water	$0.890^{[158]}$	$1.3320^{[158]}$
water-ethanol (v:v $\,\hat{=}\,$ 3:1)	$1.880^{[159]}$	$1.3375^{[160]}$

The data of the DLS-experiments were evaluated by the partial-heterodyne and the non-ergodic method. The next two chapters explain how the measurements were conducted for those two techniques.

3.4.1.1 Partial-Heterodyne Method

For the partial-heterodyne scattering method it is necessary to perform measurements at many different sample positions in order to obtain a statistically meaningful speckle pattern. Each sample was thus measured at 100 different positions, turning and lifting or lowering the sample randomly after each measurement. The measurement time at each position was 30 s. The intensity correlation functions of all the positions were then interpreted according to chapter 2.3.1.1. Both reactor-batch and swollen gels were measured and analysed like this. Some samples were also measured at 2000 positions in order to compare the usual partial-heterodyne method to a simplified technique that can be used to determine the fluctuating part of the scattering intensity, $\langle I_F \rangle$ (chapter 4.4.2.4).

3.4.1.2   Non-Ergodic Medium Method

For the non-ergodic medium method the combination of a relatively long measurement from a rotating cuvette, which yields the ensemble-average scattering intensity $\langle I \rangle_E$, and a shorter measurement at one position should suffice to analyse the structure of the gel (chapter 2.3.1.2). Nevertheless, the gels that were analysed by this method were all measured at 10 to 15 positions, each one for 30 s, to check for the validity of this assumption with the available systems. The constant rotation measurements that were performed to determine $\langle I \rangle_E$ lasted 100 s. The intensity correlation functions of the different positions were analysed according to chapter 2.3.1.2. Unfortunately, this method did not work out for many of the observed reactor-batch gels. Only the DAP1000 and the PAAm samples could be characterised by this method.

3.4.2   Static Light Scattering

The SLS measurements were carried out at an instrument built by Gernot Baur (SLS Systemtechnik) assembled from a helium-neon laser ($\lambda = 632.8$ nm), a photomultiplier detection unit and a light scattering photometer (photo/gonio/diffusomètre by Wippler & Scheibling) manufactured by Sofica, Paris.

One distinctive feature of SLS is that it determines the angle dependence of the scattering intensity or rather the Rayleigh-ratio of a sample. The range of the detection angle that was applied for the performed measurements went from 45° to 125° in 2° steps. In the water-ethanol mixture this corresponds to a q-range of $102 \cdot 10^3$ cm^{-1} to $237 \cdot 10^3$ cm^{-1}. The temperature of the toluene bath was always 25 °C (index matching). The cuvettes were tempered in the bath for about 15 min before the measurements were started.

The SLS technique (Debye-Bueche) is based on ascertaining the excess Rayleigh-ratio by measuring the polymer gel and the corresponding polymer solution, followed by subtracting the results of the solution from those of the gel (see chapter 2.3.2). The usual procedure for such an experiment was first to measure pure toluene for the purpose of calibration and then the pure solvent (water or water-ethanol), to be able to eliminate the solvent scattering afterwards. The next step was to measure the gel and the solution, each five times at

different positions, by manually turning and lifting the cuvette, so to obtain a more accurate average.

3.4.2.1   Thiol-ene samples

The solvent utilised for the thiol-ene samples was the above-mentioned water-ethanol mixture. The linear polymer that was used to determine the RAYLEIGH-ratio of the solution was PEG35,000. Due to the step-growth nature of the TEP it was rather difficult to prepare a linear thiol-ene polymer in an amount that would have sufficed. Furthermore, the thiol-ene gels were composed of a rather high proportion of ethoxy groups, increasing from DAP1000 to DAP3000, and thus have a structure very similar to PEG. This is also reflected in the dn/dc-values of PEG and various linear thiol-ene polymers (chapter 3.6.3). Thus, it was reasonable to use PEG instead of a linear thiol-ene polymer. All three DAP-series were measured from 7.5 wt% to 20 wt%.

3.4.2.2   PAAm samples

This technique was not reasonably applicable for the PAAm-hydrogels. It was not difficult to obtain linear PAAm but the SLS-measurements showed a rather unusual behaviour of the PAAm-water system. The solutions, especially of the higher concentrated samples, scattered light stronger than the hydrogels, so that the DEBYE-BUECHE method is futile for this system. Hence, only the thiol-ene gels were characterised by SLS.

3.5   Swelling Measurements

All hydrogels were swollen until the state of equilibrium was reached. For this purpose test tubes, that had a smaller diameter than the light scattering cuvettes, were used as reaction vessels. Afterwards, the swollen gels, which were going to have a considerably higher volume than the reactor-batch gels, would still fit into the cuvettes.

After a hydrogel was formed in a test tube (as explained in chapter 3.4), the tube was carefully shattered, leaving the gel intact. The gel was then ridded of the glass shards and cut into several cylindrical samples that were first weighed and then immersed into an excess of solvent. For the PAAm-gels only ultrapurified water was used as swelling agent and for the thiol-ene gels both ultrapurified water and the water-ethanol mixture were employed. The samples were then allowed to swell for one to two weeks until equilibrium swelling was reached, discernible by a constant weight. The solvent was renewed every day and at the same time the samples were weighed.

Following the light scattering measurements, the swollen samples were dried in an oven at 55 °C, again until a constant weight was reached, in order to be able to determine the mass-related degree of swelling, Q_m, of the networks. Additionally, the ratio of the dry weight and the initially utilised mass of the monomers yields the conversion of the polymerisation in terms of the amount of monomer that contributed to the network formation. All low-molecular compounds that are not bound to the network are usually extracted from the system during a swelling procedure.

Additional swelling measurements were conducted in order to determine the course of the conversion over the reaction time. The same sample (DAP2000 17.5 wt%) was prepared nine times and subjected to light for different periods of time (Table 7) to achieve increasing conversions. After the samples were removed from irradiation, they were taken out of the test tubes, weighed and then subjected to swelling in the water-ethanol mixture until the equilibrium state was reached and the unreacted part of the reaction mixture was removed. The irradiation of the first sample was stopped at 4.5 h. At this point the gel was still very soft and stuck to the shards of the test tube it was in, rendering it difficult to leave the gel undamaged while removing them. Subsequently, the swollen gels were dried in an oven until the point of constant weight. The ratio of the dry weight and the initially used monomer

mass yields the conversion of the reaction in terms of non-extractable components, as explained in the previous paragraph.

Table 7: Data acquired from the samples that were irradiated for different periods of time in order to determine the course of conversion over time

sample number	reaction time in h	conversion
1	4.5	0.46
2	5.5	0.66
3	6.5	0.69
4	7.5	0.75
5	8.5	0.77
6	9.5	0.81
7	15.5	0.87
8	24	0.89
9	52.5	0.89

Fig. 25 shows the conversion of the samples plotted versus the reaction time. In the beginning (4.5 h to 9.5 h) it increased rather sharply and then it started to level off. After approximately 24 h the final conversion of about 89 % was reached. Irradiating one more day up to 52.5 h did not raise the conversion further.
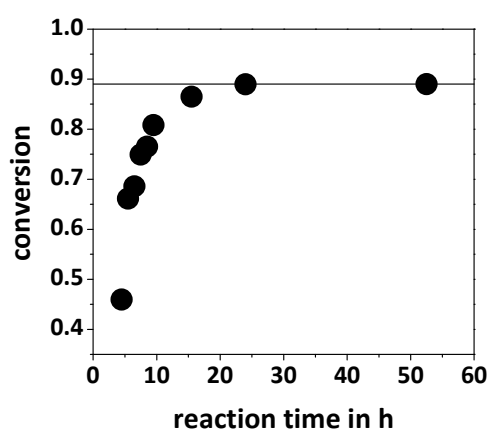

Fig. 25: Conversion of the non-extractable part of the prepared polymer network plotted versus the reaction time, for the sample DAP2000 17.5 wt%

3.6   Additional Experiments

3.6.1   Preparation of a Water Soluble Dithiol

A water soluble dithiol with a similar structure to ETTMP1300 was not readily available. It was thus prepared analogous to the preparation of the thiol-ene hydrogels with DAP1000 and DAP2000 serving as precursors. Basically, the particular DAP was supposed to react according to the normal radical mechanism as explained in chapter 2.2.1. Only an excess of a water insoluble dithiol, namely glycol di(mercaptopropionate) (GDMP, scheme 11, top), was used. This way the reaction product would not be a polymer but mainly one DAP molecule connected to two GDMP molecules, one at each double bond.

A twelvefold molar excess of GDMP was added to a 10 wt% solution of DAP1000 or DAP2000 in THF. Then 0.1 wt% (relative to the amount of THF) camphorquinone were added. Under constant stirring the reaction mixture was subsequently subjected to irradiation of the LED-lamp (465 nm, power supply: 4 V) for two days, in a closed reaction vessel at room temperature. Afterwards, the product was precipitated by slowly adding the reaction mixture, dropwise, to iced diethyl ether in a ratio of 10:1 $\hat{=}$ v:v $\hat{=}$ ether:product-solution. Both products, the dithiol from DAP1000 (called DT1000, $M_n \cong 1560$ g/mol) and from DAP2000 (called DT2000, $M_n \cong 2560$ g/mol) (both scheme 11, bottom) were characterised by NMR and DT1000 additionally by MALDI-TOF.
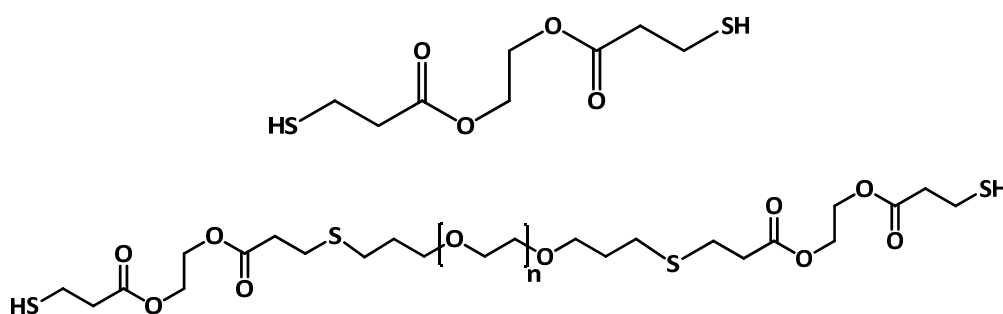
Scheme 11: GDMP (top) was used in combination with DAPX000 to form the water soluble difuctional thiols DTX000 (bottom), DT1000: n $\cong$ 23, DT2000: n $\cong$ 45

NMR-results:

^{1}H-NMR (400 MHz, CDCl$_3$): δ = 1.64-1.69 (t, 1.73 H (DT1000) or 1.69 H (DT2000), [S*H*]), 1.86 (q, 2.68 H or 3.53 H, [SCH$_2$C*H$_2$*CH$_2$O]), 2.60-2.82 (m, 19.46 H or 19.58 H, [HSC*H$_2$*C*H$_2$*C OO] and [OOC C*H$_2$*C*H$_2$*SC*H$_2$*]), 3.53-3.58 (m, 4.68 H or 4.68 H, [SCH$_2$CH$_2$C*H$_2$*O]), 3.57-3.74 (m, 77.96 H or 183.83 H, [OC*H$_2$*C*H$_2$*]$_n$), 4.33 (t, 8.00 H both, [C OOC*H$_2$*C*H$_2$*OOC]) ppm.

The NMR spectra of the two dithiols do not show any double bond peaks, which is not surprising since the thiol was applied in an excess amount thus reacting with all available enes. Hence, the end-groups are the GDMP molecules so that it was possible to form dithiols. For the NMR spectra see Appendix D, 2. Only the one of DT1000 is presented because both spectra are very similar.

MALDI-TOF result:
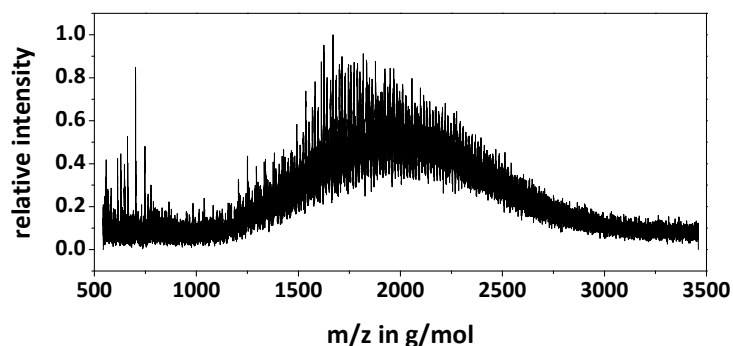
Fig. 26: MALDI-TOF spectrum of DT1000, compared to the spectrum of DAP1000 (Fig. 18, right hand side) it shows an increased molar mass as well as an increased polydispersity

The MALDI-TOF spectrum (Fig. 26) shows that the molar mass has increased compared to DAP1000, as has the polydispersity. The theoretical molar mass should be M$_n$ $\cong$ 1560 g/mol but in the spectrum the average molar mass seems to lie slightly above this value. This is no surprising result. Although a high excess of dithiol was used in the preparation, it is very well possible that the reaction does not stop at the point where two dithiols have added to the diene. After all the reaction mechanism is still the same as for a thiol-ene polymerisation. Hence, higher molecular weight products will be obtained as well, however to a much lower extent.

On the one hand, the dithiols were needed to prepare linear thiol-ene polymers in order to determine their dn/dc - values. On the other hand, they were used to form thiol-ene hydrogels that did not only consist of a diene and a trithiol but additionally a dithiol. This would take away the end-linking character of the polymerisation and enable the network chains to become longer and more polydisperse.

3.6.2   Preparation of Linear Thiol-Ene Polymers

The water soluble dithiols, DT1000 and DT2000, that were shown in the previous chapter were used for preparing linear, water soluble thiol-ene polymers, the composition of which would be similar to the thiol-ene hydrogels. These linear polymers could be used to indirectly determine the refractive-index increment of the hydrogels. The linear polymers were prepared from different, stoichiometric combinations of DAPs and DTs, as can be seen in table 8.

Table 8: Combinations of dienes (DAPX000) and dithiols (DTX000) that were used to prepare linear thiol-ene polymers, LN, with varying content of ethoxy-groups

| linear polymer	diene	dithiol
LN11	DAP1000	DT1000
LN12	DAP1000	DT2000
LN22	DAP2000	DT2000
LN32	DAP3000	DT2000

The linear polymers were prepared almost the same way as the hydrogels. The solvent was a mixture of 55 vol% ultrapurified water and 45 vol% ethanol. The concentration of the initiator remained the same at 0.4 g/L used in a stock solution.

The formulations that were used can be seen in table 9.

Table 9: Formulations for the preparation of linear thiol-ene polymers, $c_{DAPX000}$: concentration of DAPX000, c_{DTX000}: concentration of DTX000, c_{pol}: concentration of the polymer

	$c_{DAPX000}$ in wt%	c_{DTX000} in wt%	c_{pol} in wt%
LN11	4.1	5.9	10
LN12	3.0	7.0	10
LN22	4.5	5.5	10
LN32	5.5	4.5	10

The diene and dithiol were weighed into the reaction vessel, then the stock solution comprising the initiator was added. The vessel was sealed and under constant stirring subjected to irradiation of the LED-lamp (465 nm, power supply: 4 V) for two days at room temperature. In order to purify the product, the reaction mixture was dialysed against demineralised water for one week, renewing the water every day. The product was subsequently isolated by freeze-drying. Scheme 12 shows the structure of the resulting polymers.
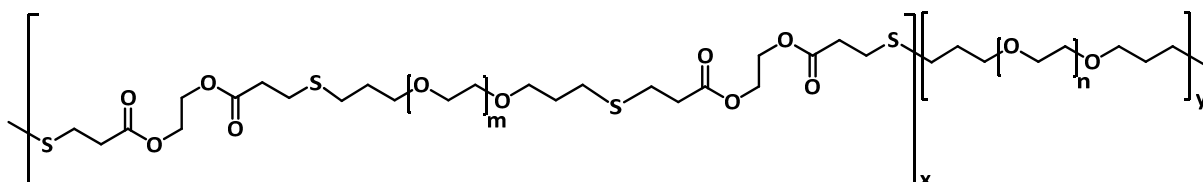
Scheme 12: Structure of the linear polymer formed from DAPX000 and DTX000; DT1000: m ≅ 23, DT2000: m ≅ 45; DAP1000: n ≅ 23, DAP2000: n ≅ 45, DAP3000: n ≅ 68

NMR-results:

^{1}H-NMR (600 MHz, CDCl$_3$): δ = 1.86 (q, 47.55 H (LN11), 147.55 H (LN12), 48.70 H (LN22) or 34.44 H (LN32), [SCH$_2$CH_2CH$_2$O]), 2.60-2.82 (m, 196.86 H, 484.92 H, 208.16 H or 118.25 H, [OOC CH_2CH_2SCH_2]), 3.52-3.55 (m, 61.12 H, 195.96 H, 82.21 H or 54.72 H, [SCH$_2$CH$_2$CH_2O]), 3.56-3.74 (m, 1527.42 H, 6568.56 H, 3889.77 H or 2903.95 H, [OCH_2CH_2]$_n$), 4.02 (d, 4.08 H, 3.38 H, 4.07 H or 3.97 H, [OCH_2CH=CH$_2$]), 4.31 (t, 95.50 H, 176.82 H, 100.79 H or 47.19 H, [C OOCH_2CH_2OOC]), 5.18 (d, 2.04 H, 1.98 H, 2.06 H or 1.98 H, [OCH$_2$CH=CH_2]), 5.28 (d, 2.09 H, 2.00 H, 2.05 H or 1.98 H, [OCH$_2$CH=CH_2]), 5.92 (q, 2.00 H all four, [OCH$_2$CH=CH$_2$]) ppm.

The NMR-spectra all show that there are no detectable thiol-groups left in the thiol-ene polymer. However, there are still double bonds in the molecules which, accordingly, have to be the end groups. Knowing the reactants and the fact that each polymer has DAP molecules at its chain-ends renders it possible to determine an average molar mass, M_{NMR}, from the NMR-spectra which serves as a good estimate (Table 10). For the NMR spectra see Appendix D, 3. Only the one of LN11 is presented because all four spectra are very similar.

Table 10: Average molar masses, M_{NMR}, of the linear thiol-ene polymers derived from their NMR-spectra

polymer	M_{NMR} in g/mol
LN11	21,500
LN12	86,000
LN22	50,200
LN32	37,500

3.6.3   Refractive Index Increment

The polymers described in chapter 3.6.2, PEG35,000 and an uncrosslinked PAAm were used to determine their refractive index increment (RII), dn/dc. It was measured with a Brice-Phoenix differential refractometer, Model BP-2000-V at 25 °C and a wavelength of 633 nm. First a calibration measurement with potassium chloride was carried out. For this purpose, pure water (ultrapurified) and six different concentrations of KCl in water were measured, seven times per concentration to receive a good average, and a calibration factor ($9.72 \cdot 10^{-4}$) for the instrument was obtained from the known RII of KCl in water (0.1318 mL/g [161]). The pure solvent and five different concentrations of the particular polymer in the solvent were measured afterwards, also seven times per concentration. By means of the calibration factor, the RIIs of the different systems could be determined (Table 11). The thiol-ene polymers (LN) and PEG35,000 were measured in the water-ethanol mixture (v:v ≙ 3:1) and PAAm in ultrapurified water.

Table 11: Comparison of the RII, (dn/dc), of different linear polymers measured at 25 °C and 633 nm; the molar mass, M_{NMR}, and the proportion of ethoxy groups within the polymer, c_{Etox}, were determined for the thiol-ene polymers and PEG35,000; (dn/dc)$_{Lit}$ are values derived from literature

	dn/dc in mL/g	M_{NMR} in g/mol	c_{Etox} in mol%	(dn/dc)$_{Lit}$ in mL/g
PEG35,000	0.129	35,000	100	0.132 (water, 25 °C, M_w = 6,700)[162]
LN11	0.177	21,500	82	-
LN12	0.128	86,000	87	-
LN22	0.137	50,200	90	-
LN32	0.166	37,500	92	-
PAAm	0.167	-	-	0.183 (water, 25 °C)[163] 0.146 (water, 23 °C)[163]

The gradual change of the structure of a copolymer, made up of 1,4- and 1,2-connected 1,3-butadiene units, towards the corresponding homopolymer with only 1,4-addition has been investigated by CHEN et al.[164]. Due to the modification of the polymer structure, the RII steadily increased, approaching the value of the polymer with almost complete 1,4-addition. The same behaviour cannot be observed for the thiol-ene polymers described in the previous chapter. The expectation was for the RII of the thiol-ene polymers to approach the value of PEG35,000 with increasing proportion of ethoxy groups, c_{Etox}. Nevertheless, no such connection between dn/dc and c_{Etox} was found (Fig. 27, left hand side).
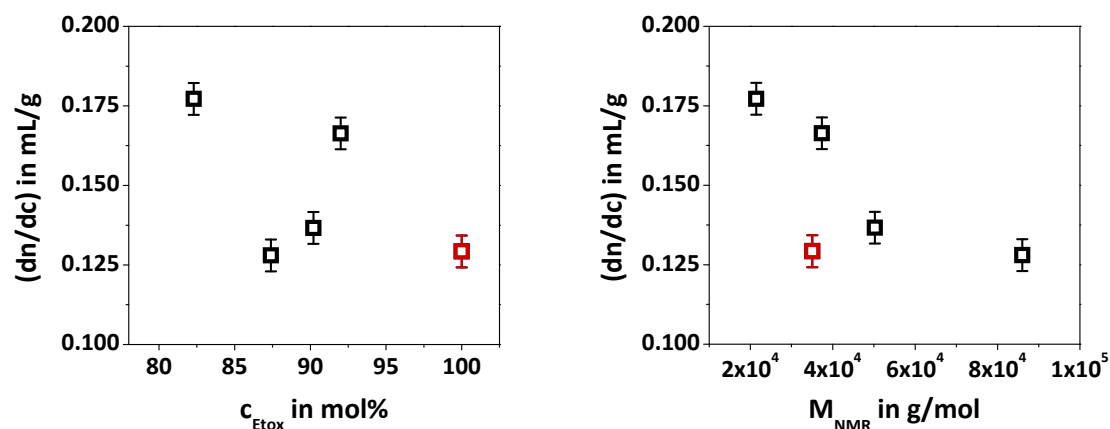

Fig. 27: The refractive index increment as a function of the proportion of ethoxy-groups, c_{Etox}, (left hand side) and the average molar mass, M_{NMR} (right hand side); the red markings denote the sample PEG35,000

Another variable that influences the RII of a polymer is its chain length. For homopolymers with a sufficiently high molar mass the RII is constant. However, below a certain threshold, depending on the polymer and the solvent, it changes with decreasing molar mass[165-169]. For PEG in water at 25 °C this threshold is about 4000 g/mol, below this value (dn/dc) declines[170]. This behaviour is attributed to a stronger impact of the end-groups in shorter polymer chains, influencing the RII. It can be observed, that with increasing molar mass of the thiol-ene polymers, M_{NMR}, the RII constantly decreases (Fig. 27, right hand side), approaching the value of PEG itself. LN12, which exhibits the longest polymer chains, has almost the lowest proportion of ethoxy-groups and is thus, structurally, comparatively dissimilar to PEG. Still, it has the lowest RII, essentially the same as that of pure PEG. In contrast, LN32, the polymer with the highest proportion of ethoxy groups, hence structurally most similar to PEG, possesses a RII rather different from PEG. It is concluded that the molar mass is the critical factor here, having a greater effect on the dn/dc - value than the polymer composition.

Since polymer gels have a quasi infinite molar mass and ideally no end-groups, the thiol-ene gels can be considered to have a RII similar to pure PEG although there may be deviations from this assumption at low proportions of ethoxy-groups.

Consequently, polyacrylamide in water has a higher dn/dc - value than the thiol-ene gels in water-ethanol and the scattering intensities of the two systems are not directly comparable. However, the literature values for PAAm (Table 11) make it clear that there are uncertainties concerning the measurement of RIIs.

3.6.4 Preparation of Modified Thiol-Ene Hydrogels

Usually the thiol-ene hydrogels just comprised a diene and a trithiol as monomers. For one reaction series, the dithiol DT2000 was included in the reaction mixture in varying amounts (Table 12). The three monomers, DAP2000, ETTMP1300 and DT2000, were combined in such a way that the number of double bonds was still the same as the number of thiol groups. Since the dithiol (2560 g/mol) had a higher molar mass than the trithiol (1274 g/mol), which was being replaced, the overall monomer concentration by weight increased, although the overall number of functional groups stayed the same.

The reaction mixtures were prepared as explained in chapter 3.2.1, additionally using DT2000 according to table 12. The basic reaction mixture that was used for the measurement without dithiol was DAP2000 17.5 wt%. The resulting samples were characterised by rheometry and DLS, as explained in chapters 3.3 and 3.4, respectively.

Table 12: Formulations for the formation of hydrogels comprising a trithiol (ETTMP1300) at the concentration c_{ETTMP}, a dithiol (DT2000) at the concentration c_{DT2000} and a diene (DAP2000) at the concentration $c_{DAP2000}$; c_{pol}: concentration of the polymer

percentage of thiol-groups from DT2000 in mol%	c_{ETTMP} in mmol/g	c_{DT2000} in mmol/g	$c_{DAP2000}$ in mmol/g	c_{pol} in wt%
0	0.0398	-	0.0598	17.5
2	0.0390	0.0012	0.0597	17.7
6	0.0372	0.0036	0.0594	18.0
10	0.0355	0.0059	0.0592	18.3
25	0.0291	0.0146	0.0583	19.6
50	0.0190	0.0284	0.0569	21.5
60	0.0150	0.0338	0.0563	22.3
75	0.0085	0.0684	0.0513	29.2

3.6.5   Differential Scanning Calorimetry (DSC)

The DSC-measurements were carried out on a Perkin Elmer DSC7 differential scanning calorimeter, equipped with a Perkin Elmer thermal analysis controller TAC 7/DX. The samples that were utilised for the DSC-measurements were PAAm- and thiol-ene hydrogels dried in an oven at 55 °C until they reached a constant weight (about one to two weeks). They are illustrated in table 13.

Table 13: DSC results of dried PAAm- and thiol-ene networks with T_g the glass transition temperature and T_{melt} the melting temperature

	c_{TEP} in wt%	T_g in °C	T_{melt} in °C		c_{PAAm} in wt%	T_g in °C
DAP1000	*10*	-54.6	16.0	**PAAm 1 % BIS**	*15*	140.5
	12.5	-55.3	14.9		*17*	140.3
	15	-55.9	15.7	**PAAm 0.35% BIS**	*15*	133.5
	17.5	-55.5	15.4		*17.5*	129.5
DAP2000	*15*	-54.0	34.4			
	17.5	-57.8	35.3			
DAP3000	*15*	-52.5	44.9			
	20	-55.8	45.6			

The dried thiol-ene hydrogels had to be measured with liquid nitrogen cooling since their glass transition temperature, T_g, was below room temperature (Table 13). The left diagram in fig. 28 shows a typical DSC-curve of a thiol-ene network (DAP1000 15 wt%) exhibiting a glass transition step at about -55 °C and a melting peak at 16 °C. The values of this and other thiol-ene networks are illustrated in table 13. Depending on the observation temperature, the dry thiol-ene networks were partially crystalline systems. While the DAP1000 networks were not crystalline at room temperature, the DAP2000 and DAP3000 networks were visibly white, indicating partial crystallisation.
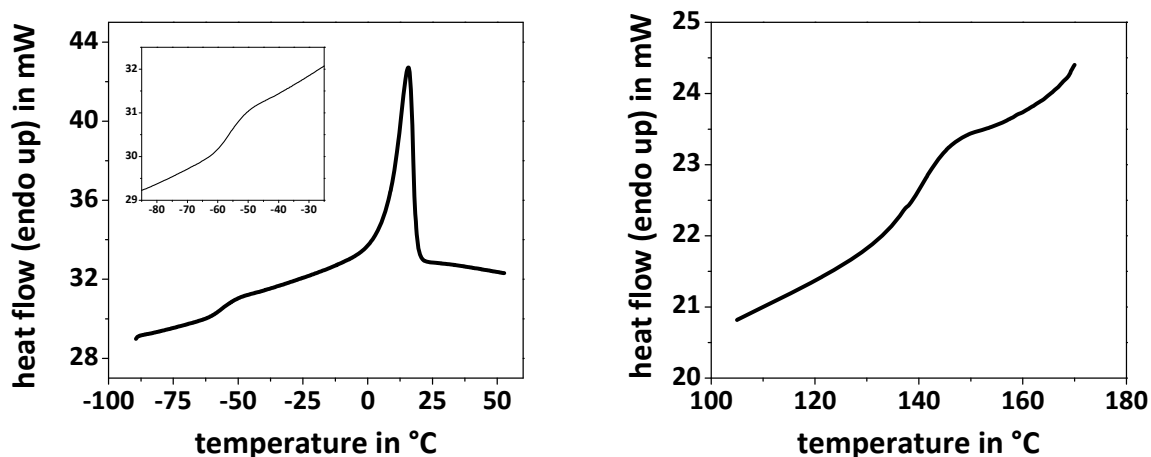
Fig. 28: DSC curves of DAP1000 at 15 wt% (left hand side) and PAAm at 15 wt% and 1 mol% BIS (right hand side); the graphs are plotted in the endo-up mode and they are heating curves; the thiol-ene networks show a pronounced melting peak apart from the glass transition step, the PAAm networks only exhibit the glass transition step

At room temperature the polyacrylamide networks were in a glassy state and only at around 140 °C they passed through their glass transition to become rubbery (Fig. 28, right hand side). At such high temperatures the organic molecules seemed to have started to decompose, perceptible by inflated measuring containers. The PAAm networks were visibly clear and the DSC-curves showed no indication of crystallisation. The glass transition temperature of the PAAm-networks was highly dependent on the degree of dryness. Samples that were first dried and then stored at room temperature and ambient humidity exhibited a glass transition temperature of only around 75 °C, thus indicating that the networks are hygroscopic, the water acting as a plasticiser. Pulverising the dried samples and then putting them in the oven again increased their T_g-values to around 149 °C, due to a higher dryness.

3.7   Variations in the Coherence Factor β

As explained in chapter 2.3.1 the intercept, σ^2, of the ICF should theoretically be unity in the homodyne case. However, it also depends on the detection optics. The employed instrument uses a three-mode fibre-optic detection unit.

Assuming single-mode fibre detection, the intercept of the ICF should be unity in the homodyne case. A single-mode fibre has a small diameter, comparable to the wavelength of the radiation source so that only the fundamental mode can propagate through to the actual detector. The describing quantity is the coherence factor, β, that can be expressed by eq. 60 where $\aleph$ is the number of modes[131]. In case of a single-mode fibre it is $\beta \le 1$. Thus, it does not appear in eqs. 32, 40 and 49.

$$\beta \le \frac{1}{\aleph} \qquad (60)$$

A multi-mode fibre has a higher diameter, so that not only the fundamental mode can propagate through it. A three-mode fibre also lets two additional higher order modes pass, gathering more light and increasing the average detected intensity, $\langle I(q,t) \rangle$. Since this does not affect the correlation, described by the numerator in eq. 61, the ICF and its intercept are shifted to lower values.

$$g^{(2)}(q,\tau) = \frac{\langle I(q,t) \cdot I(q,t+\tau) \rangle}{\langle I(q,t) \rangle^2} \qquad (61)$$

The coherence factor decreases and, in the homodyne case, it becomes $\beta \le 0.33$. Hence, the eqs. 32, 40 and 49 have to be rewritten to yield the eqs. 62, 63 and 64.

$$g^{(1)}(q,\tau) = \left(\frac{g^{(2)}(q,\tau) - 1}{\beta} \right)^{1/2} \qquad (62)$$

$$g^{(2)}(q,\tau) - 1 = \beta \cdot \left[\frac{2 \cdot \langle I_F \rangle \cdot \langle I_S \rangle}{\left(\langle I_F \rangle + \langle I_S \rangle \right)^2} \cdot g^{(1)}(q,\tau) + \left(\frac{\langle I_F \rangle}{\langle I_F \rangle + \langle I_S \rangle} \cdot g^{(1)}(q,\tau) \right)^2 \right] \qquad (63)$$

$$f(q,\tau) = 1 + \frac{\langle I \rangle_{T,p}}{\langle I \rangle_E} \left[\sqrt{\left(\frac{\left(g^{(2)}(q,\tau) - 1 \right) - \sigma_p^2}{\beta} + 1 \right)} - 1 \right] \qquad (\ 64\ )$$

The intercept of the ICF in the homodyne case had been measured to be $\beta = 0.358$ for the available instrument. However, different measurements of ergodic samples (polymer solutions, dispersions) have shown that it often differs from this value. This is probably due to incoherent background noise, like scattering from the solvent[171]. If the solvent scatters light significantly compared to the sample, a decrease of the intercept is observed. This can be attributed to the fact that the correlation decay of the solvent cannot be detected since it occurs at too short time scales. The correlation time of the sample does not change due to the scattering of the solvent.

For the partial-heterodyne method a varying intercept of the ICF is not a problem since this has no influence on the initial slope of the ICF, which is the crucial quantity of this analysis (eq. 45). The non-ergodic method is influenced by the intercept of the ICF (eq. 64) and thus the offset that gives information about the static part within a network. However, only the DAP1000 and the PAAm samples could be analysed with the non-ergodic method (chapter 2.3.1.2). Compared to the scattering of the solvent (around 9 kHz) these samples scatter light at least 15 times more strongly, rendering the solvent scattering negligible.

4 Results and Discussion

4.1 Necessary Monomer Concentration to Form a Perfect Network

The thiol-ene networks are built up in an end-linking process by a trithiol as crosslinker and a diene as the main part of the network chain. Since the dienes do not homopolymerise they always alternate with a trithiol. This implies that the formation of a perfect network requires a minimal concentration of reactants so the network can span the whole volume of the sample. Otherwise the probability of the diene molecules to be able to interconnect two different crosslinker molecules may be too low and the formation of loops is favoured[84]. Moreover, it can lead to dangling chains if there is no other thiol group in the proximity of a double bond (Fig. 29). Thus, the ability to form a network with a well-defined structure depends on the concentration of the reactants and the network chain length which is determined by the molar mass of the dienes. The longer the diene is, the lower the concentration can be, to theoretically form a perfect network, keeping in mind that in reality forming a perfect network is virtually impossible. The minimal, necessary concentration, c_{min}, of the three employed dienes should thus decrease from DAP1000 to DAP3000.

Fig. 29: Schematic representation of the network structure in an end-linking TEP comprising a trifunctional crosslinker (red) and a difunctional ene as the main part of the network chains (green); left hand side: homogeneous network formed at a sufficiently high monomer concentration and with sufficiently long diene chains, no topological defects are formed; right hand side: a network with topological imperfections like elastically ineffective loops and dangling chains, developed due to an insufficient monomer concentration and too short diene chains

In order to assess c_{min} it is necessary to ascertain the end-to-end distance of the network chains. It determines the minimal amount of chains that are necessary to form a continuous network within a certain volume. The network chains comprise not only a DAPX000 molecule but additionally two of the ethoxylated branches of the ETTMP1300 (Scheme 13). Thus, the molar mass of the network chains, M_{chain}, is the sum of the molar mass of a particular DAP, $M_{DAPX000}$, and of two of the branches of the trithiol, M_{branch}, one at each end of the DAP (Table 14).
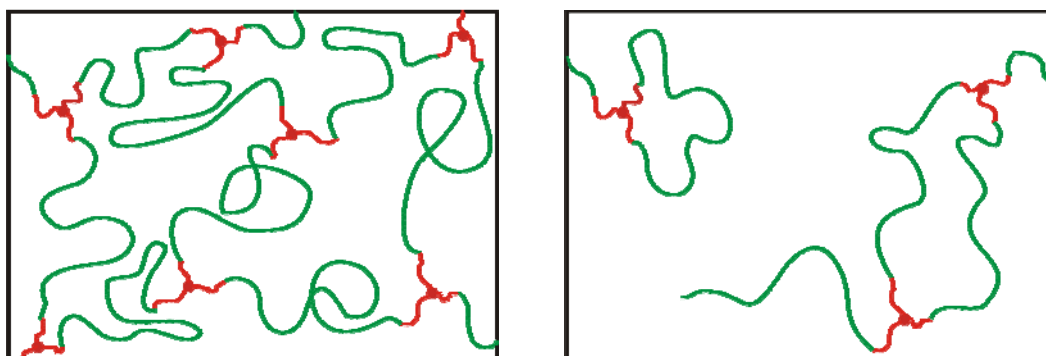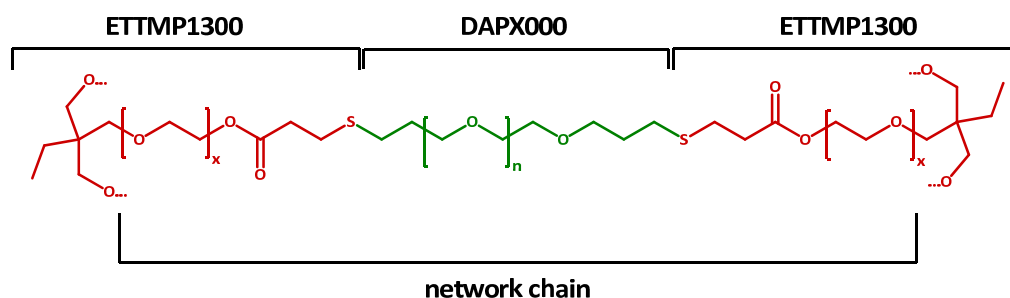

Scheme 13: Representation of one network strand in an end-linking TEP comprising a trifunctional crosslinker (red) and a difunctional ene (green); for this purpose the network chain is considered to be the diene and the two branches of the crosslinker that the ene is connected to; n $\cong$ 23 (DAP1000), 45 (DAP2000), 68 (DAP3000); x $\cong$ 7

Using M_{chain}, the root-mean-square end-to-end distance, r_0, of the network chains can be calculated by eq. 65 (r_0 is obtained in nm if M is given in g/mol)[172]. This equation describes the unperturbed dimensions of polyethylene oxide dissolved in water at 25 °C and thus does not exactly match the present situation. The proportion of ethoxy groups within a thiol-ene network is fairly high (Table 11) so that the deviations due to the slightly dissimilar molecular structure should be negligible. As for the solvent, the hydrogels were not prepared in pure water but in a water-ethanol mixture. Since the network chains that are supposed to be described actually are not freely diffusing coils but fixed at both ends by the crosslinks this calculation is merely an estimate. Hence, eq. 65 is considered to give a reasonably good assessment of r_0.

$$\sqrt{\langle r^2 \rangle_0} \equiv r_0 = 888 \cdot 10^{-4} \cdot M^{1/2} \qquad\qquad (65)$$

The yielded end-to-end distances are in the range of a few nanometres (Table 14) and as expected increase from the DAP1000 network to the DAP3000 network.

Table 14: Results for the determination of the end-to-end distance of the network chains; $M_{DAPX000}$: molar mass of the three dienes; M_{branch}: molar mass of both the branches of the crosslinkers a diene is connected to in a network; M_{chain}: molar mass of the actual network chains; r_0: root-mean-square end-to-end distance of the network chains at unperturbed dimensions

	$M_{DAPX000}$ in g/mol	M_{branch} in g/mol	M_{chain} in g/mol	r_0 in nm
DAP1000	1080	408	1900	3.9
DAP2000	2080	408	2900	4.8
DAP3000	3080	408	3900	5.5

The end-to-end distance can now be used to calculate c_{min} based on the determination of the volume of a network chain coil by eq. 66. Dividing the mass of a network chain, m_{chain}, by its volume yields the minimally required concentration (Table 15). The density of these solutions is assumed to be the same as for the reaction mixtures that were used to form the thiol-ene hydrogels, $\cong 0.98$ g/mL at room temperature.

$$V_{coil} = \frac{4}{3}\pi \cdot \left(\frac{r_0}{2}\right)^3 \qquad\qquad (66)$$

Table 15: Results for the determination of the minimally necessary monomer concentration in order to form a perfect network; r_0: root-mean-square end-to-end distance of the network chains at unperturbed dimensions; V_{coil}: volume of a network chain coil calculated by assuming spherical shape; m_{chain}: mass of a network chain; c_{min}: minimal monomer concentration needed to form a perfect network

	r_0 in nm	V_{coil} in nm^3	m_{chain} in 10^{-21} g	c_{min} in wt%
DAP1000	3.9	30.4	3.2	10.6
DAP2000	4.8	57.3	4.8	8.6
DAP3000	5.5	89.3	6.5	7.5

As expected, it is evident that the critical concentration, c_{min}, decreases from the DAP1000 to the DAP3000 samples. The minimal concentration that was used for the preparation of the three thiol-ene series was $c_{TEP,min}$ = 7.5 wt%. This signifies that, particularly for the DAP1000 samples, the concentrations were in some cases too low to enable the formation of a continuous, defectless network, which is in this case theoretically only possible from 10.6 wt% upwards. According to table 15 the DAP3000 samples should, regardless of the concentration, be capable of forming fairly homogeneous networks. This is due to the diene being long enough to not react within its surrounding area. Everywhere the double bonds can diffuse to, a sufficient number of reaction partners are available.

As this calculation is merely an estimation, the values are not to be taken as exact. In relative terms the results point out that it is more likely for the DAP3000 samples to form homogeneous networks without defects than for the DAP1000 samples. Especially at lower concentrations it is to be expected for the DAP1000 to form loops and dangling chains and to react with thiols within its closer vicinity more extensively yielding spatial inhomogeneity as well. Furthermore, since the DAP1000 chains are shorter than the DAP3000 ones it is inherently more likely for them to form loops and have both ends react with thiol-groups that are relatively close to each other, regardless of the concentration. This adds to the surmise that the hydrogels with the longer network chains probably exhibit a more homogeneous structure. Concerning network inhomogeneity the gels prepared from DAP2000 should consequently lie in between the other two.

4.2   Swelling Measurements

Swelling measurements were carried out according to chapter 3.5. The mass-related degree of swelling, Q_m, is illustrated in fig. 30 for all samples. The data of the TEP-gels is taken from swelling experiments in the water-ethanol mixture. The results in water were almost the same, only slightly smaller swelling was observed, so they are not additionally presented. It is evident that Q_m consistently decreases with increasing monomer concentration. This is reasonable, since an increasing monomer concentration in both systems, TEP and FCC, and thus an increasing amount of crosslinker, renders the networks stiffer. Accordingly, the hydrogels with a higher amount of crosslinker, DAP1000 and PAAm 1 mol% BIS, also swell to a lesser extent than the ones with less crosslinker. However, there is hardly a difference to be observed between the DAP2000 and DAP3000 samples although at the same weight concentration the DAP2000 samples comprise more crosslinker. The equilibrium degree of swelling will be further used to plot light scattering results of swollen gels against it.
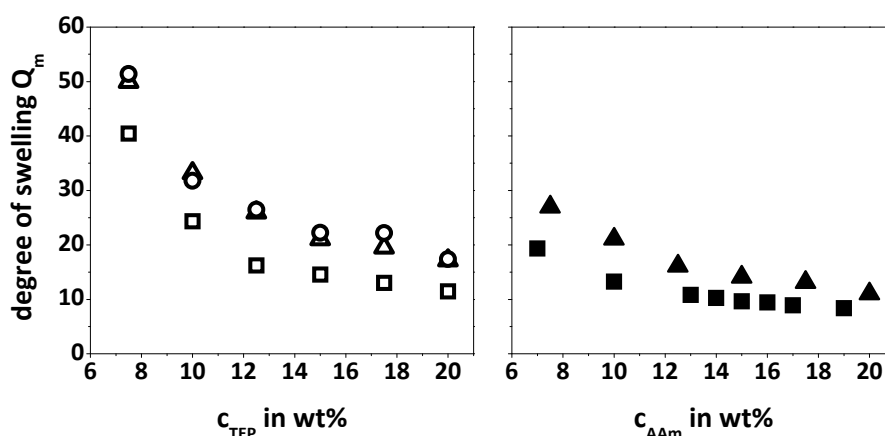

Fig. 30: Equilibrium degree of swelling, Q_m, plotted versus the overall monomer concentration, $c_{TEP/AAm}$; left hand side: TEP samples, open squares: DAP1000, open triangles: DAP2000, open circles: DAP3000; right hand side: PAAm samples, filled squares: PAAm 1 mol% BIS, filled triangles: PAAm 0.35 mol% BIS

The relative degree of swelling, $Q_{m,rel}$, is calculated by eq. 67 taking the ratio of the equilibrium degree of swelling, Q_m, and the reactor batch degree of swelling, $Q_{m,rb}$.

$$Q_{m,rel} = \frac{Q_m}{Q_{m,rb}} = \frac{m_{sw}}{m_{rb}} \qquad\qquad (\,67\,)$$

It is evident from fig. 31 that the relative solvent uptake is highest for the DAP2000 and DAP3000 gels. Compared to the reactor batch state they swell the most, yielding a threefold increase in mass. The PAAm 0.35 mol% BIS and DAP1000 gels have a relative degree of swelling of $Q_{m,rel} \cong 2$, so the increase in mass from the reactor batch to the equilibrium swollen state is smaller than for the DAP2000 and DAP3000 gels. The PAAm 1 mol% BIS gels swell the least when related to the reactor batch state, not even doubling their mass, due to the high amount of crosslinker.
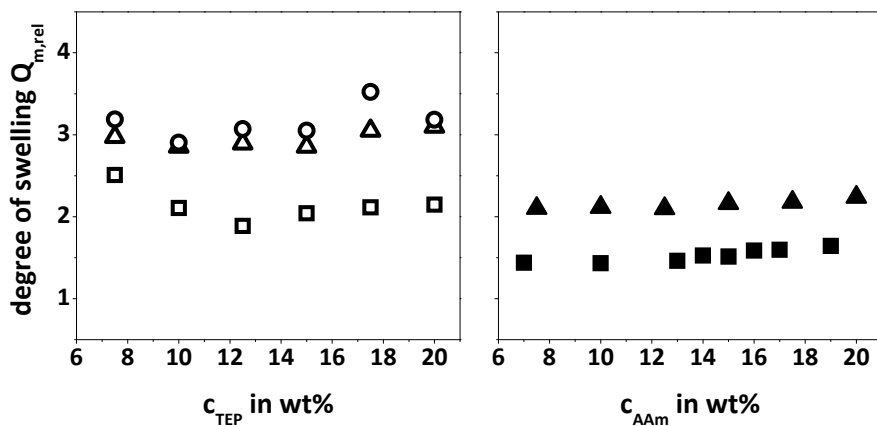
Fig. 31: Relative degree of swelling, $Q_{m,rel}$, plotted versus the overall monomer concentration, $c_{TEP/AAm}$; left hand side: TEP samples, open squares: DAP1000, open triangles: DAP2000, open circles: DAP3000; right hand side: PAAm samples, filled squares: PAAm 1 mol% BIS, filled triangles: PAAm 0.35 mol% BIS

Swelling measurements can be used to determine the conversion, p_{swell}, of the monomers that effectively contribute to network formation. After swelling all the material that may have reacted but is not attached to the network, is extracted from the hydrogel. Since it is dried afterwards the dry mass simply has to be compared to the originally utilised mass of monomers. The conversion, p_{swell}, will be used to plot light scattering results of swollen gels

against it. Fig. 32 shows p_{swell} for both the TEP- and FCC-systems. For the thiol-ene gels the two lowest concentrations exhibit lower conversions than the rest of the samples. This is due to network degradation that could be observed during swelling[99,100]. After about a week of swelling, especially the 7.5 wt% samples gradually started losing weight, thereby reducing the m_{dry} and thus p_{swell}. The other samples exhibit conversions of around 89 to 93 %. Such reduced values may be partly due to a system of functional groups that is not perfectly stoichiometrically balanced, e.g. owing to not completely pure reactants.

The PAAm samples show higher values, most of them even above 100 %. This is probably due to not fully dried samples. During drying the PAAm-hydrogels make a transition from rubbery to glassy. Thus, the drying speed goes down and the glassy state renders it difficult to get rid of residual traces of solvent. In chapter 3.6.5 it was reported that dried PAAm-networks that were pulverised and then further dried, contained less water, perceptible by a higher glass transition temperature. The networks that were used to determine the conversion were not pulverised and thus probably still enclosed some water, increasing the conversion to more than 100%.

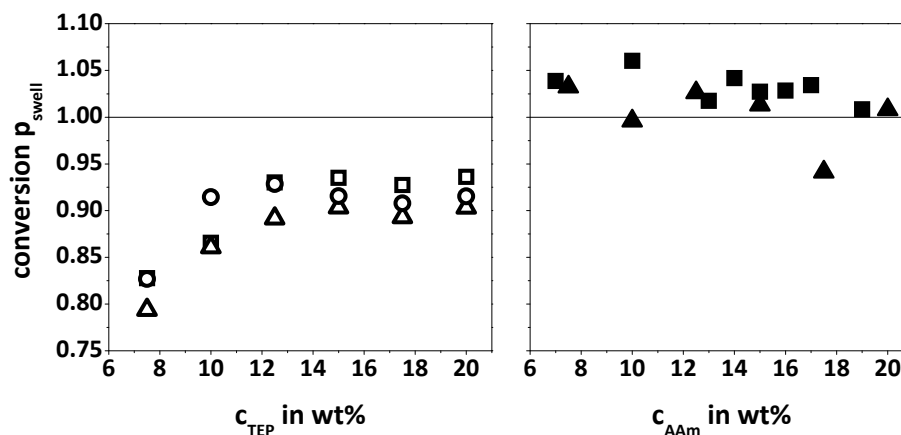Fig. 32: conversion of the unextractable part of the polymer network, p_{swell}, plotted versus the overall monomer concentration, $c_{TEP/AAm}$; left hand side: TEP samples, open squares: DAP1000, open triangles: DAP2000, open circles: DAP3000; right hand side: PAAm samples, filled squares: PAAm 1 mol% BIS, filled triangles: PAAm 0.35 mol% BIS

4.3 Mechanical Measurements

4.3.1 Preliminary Examinations

In order to characterise the hydrogels of both the TEP and the FCC macroscopically, rheological measurements were carried out to ensure that all of the investigated hydrogels had similar mechanical properties, thus providing the basis for reasonably comparing the otherwise essentially different systems.

As explained in chapter 3.3 the gels were prepared on the rheometer, so that the course of the relevant parameters, G' and G'', could be monitored (Fig. 33). It can clearly be seen that both the elastic and the viscous modulus increase with increasing reaction time and thus increasing conversion. In the beginning of the reaction the system is still in the sol state and G'' exhibits higher values than G'. After the gel point, which shall be considered as the point where the elastic modulus equals the viscous modulus, G' becomes significantly larger than G'' indicating a crosslinked system. With time they both level off to yield the plateau values G'_∞ and G''_∞.
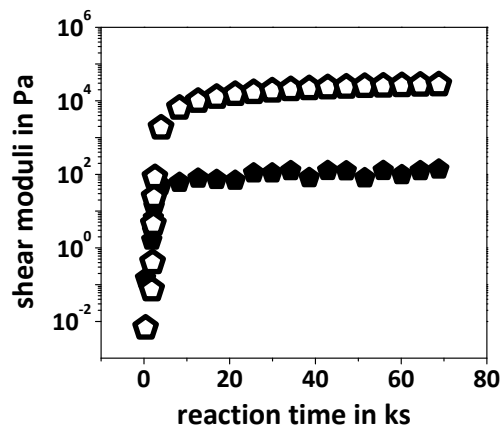
Fig. 33: Development of the shear moduli of the crosslinking reaction of DAP3000 20 wt% over the reaction time; open pentagons: elastic shear modulus, G'; filled pentagons: viscous shear modulus, G''; parameters: 1 % strain amplitude, oscillation frequency: 1 Hz

For a permanently crosslinked network the shear modulus is almost frequency independent towards low frequencies (Fig. 2, p. 8). It especially does not decrease with decreasing fequency. Thus the plateau value, G'_∞, should be equal to the equilibrium modulus, G_0, which is valid at $\omega \rightarrow 0$. Whether this is the case can be examined by

performing a frequency sweep of the fully developed network. This is illustrated in fig. 34 which is representative for all prepared hydrogels. The elastic modulus is constant over the chosen frequency range (eq. 68), demonstrating the existence of a permanent network. Towards higher frequencies the modulus will eventually increase, attaining the glassy state.

$$G'_\infty\left(\leq 100\,\text{Hz}\right) = G_0 \qquad\qquad\qquad (68)$$
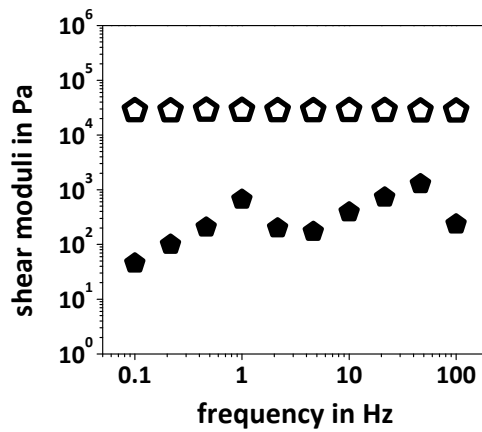
Fig. 34: Frequency sweep of a fully developed network of the sample DAP3000 20 wt%; open pentagons: plateau-value of elastic shear modulus, G'_∞; filled pentagons: plateau-value of viscous shear modulus, G''_∞; parameter: 1 % strain

4.3.2   Elastic and Viscous Modulus

The results gathered from all prepared hydrogels are shown in table 16 (TEP) and in table 17 (FCC). In all cases the loss tangent, $\tan\delta$, exhibits values well below unity, leading to the conclusion that the hydrogels are viscoelastic solids (Table 2, chapter 2.1.3.2). The significant difference between G'_∞ and G''_∞ further supports eq. 68[173].

Table 16: Results of the rheology measurements of the thiol-ene samples at 1 Hz; c_{TEP}: monomer concentration, G'_{∞}: plateau-value of elastic shear modulus, G''_{∞}: plateau-value of viscous shear modulus, $\tan\delta$: loss tangent (calculated by eq. 12)

c_{TEP} in wt%		7.5	10	12.5	15	17.5	20
DAP1000	G'_{∞} in Pa	1550	6460	16070	29640	35170	61640
	G''_{∞} in Pa	9	25	51	93	105	218
	$\tan\delta \cdot 10^3$	5.8	3.9	3.2	3.1	3.0	3.5
DAP2000	G'_{∞} in Pa	2450	4100	14700	19300	28300	40000
	G''_{∞} in Pa	10	18	45	69	97	145
	$\tan\delta \cdot 10^3$	4.1	4.4	3.1	3.6	3.4	3.6
DAP3000	G'_{∞} in Pa	2000	6180	9380	15600	25000	28050
	G''_{∞} in Pa	11	25	35	64	93	107
	$\tan\delta \cdot 10^3$	5.5	4.0	3.7	4.1	3.7	3.8

Table 17: Results of the rheology measurements of the PAAm samples at 1 Hz; c_{AAm}: monomer concentration, G'_{∞}: plateau-value of elastic shear modulus, G''_{∞}: plateau-value of viscous shear modulus, $\tan\delta$: loss tangent

c_{AAm} in wt%		7.5	10	12.5	15	17.5	20	
0.35 mol% BIS	G'_{∞} in Pa	3100	7200	12400	18100	30000	36000	
	G''_{∞} in Pa	39	508	213	201	321	397	
	$\tan\delta \cdot 10^3$	12.6	70.6	17.2	11.1	10.7	11.0	

c_{AAm} in wt%		7	10	13	14	15	16	19
1 mol% BIS	G'_{∞} in Pa	5600	15000	24000	27300	31800	42000	64000
	G''_{∞} in Pa	22	59	94	99	261	159	278
	$\tan\delta \cdot 10^3$	3.9	3.9	3.9	3.6	8.2	3.8	4.3

From the plot of the elastic modulus versus the monomer concentration (Fig. 35) it can be seen that with increasing monomer concentration both the TEP and the FCC hydrogels exhibit an increase in the value of G'_∞. For the TEP systems the amount of crosslinker, ETTMP1300, is directly related to the amount of diene, DAPX000. This is due to the precondition that the double bonds and thiol groups in the reaction mixture are to be used stoichiometrically. The same holds true for the FCC since the amount of crosslinker, BIS, is directly coupled to the amount of monomer, AAm. Thus, for both systems an increase in monomer concentration yields an increase in crosslinker concentration and, hence, an increase in the elastic modulus. As expected, the PAAm gels formed with 1 mol% BIS are elastically stronger than the ones with 0.35 mol% BIS which simply reflects that more crosslinker molecules are available in the 1 mol% case. For the TEP gels, a mixture of ETTMP1300 with DAP1000 (lower molar mass) has a higher amount of crosslinker than a mixture containing DAP3000, at the same concentration in wt%. So the elastic modulus of the DAP1000 mixture is higher than the modulus of the DAP3000 mixture at the same weight concentration, since it contains a higher amount of crosslinker. Consequently, G'_∞ of the DAP2000 samples lies in between the other two.
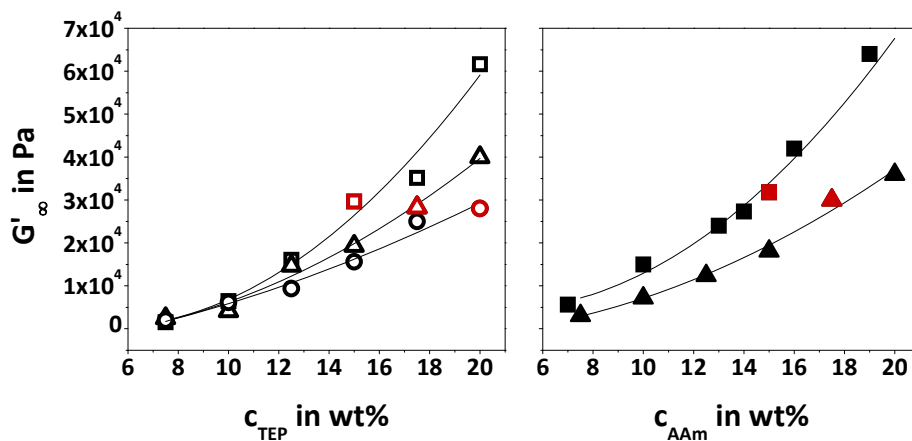

Fig. 35: Plateau-value of the elastic shear modulus, G'_∞, plotted versus the overall monomer concentration, $c_{TEP/AAm}$; left hand side: TEP samples, open squares: DAP1000, open triangles: DAP2000, open circles: DAP3000; right hand side: PAAm samples, filled squares: PAAm 1 mol% BIS, filled triangles: PAAm 0.35 mol% BIS; the red markings denote the samples illustrated in table 18

Another important fact evident in fig. 35 is the similarity of the elastic moduli of the TEP- and the FCC-samples, which was intended. One sample of each series, all of them exhibiting similar elastic moduli, is chosen for the purpose of comparison (Table 18). Those five specimen will in the next chapters be used to demonstrate the results because they have similar macroscopic properties.

Table 18: Rheology results of the samples that exhibit similar G'_{∞}-values and thus similar network chain densities as well, in the following these five samples will be used repeatedly to illustrate and compare results; $c_{TEP/AAm}$: monomer concentration, G'_{∞}: plateau-value of elastic shear modulus, $\tan\delta$: loss tangent

	DAP1000	DAP2000	DAP3000	PAAm 1 mol% BIS	PAAm 0.35 mol% BIS
$c_{TEP/AAm}$ **in wt%**	15	17.5	20	15	17.5
G'_{∞} **in Pa**	29,640	28,300	28,050	31,800	30,000
$\tan\delta \cdot 10^3$	3.1	3.4	3.8	8.2	10.7

4.3.3   Crosslinking efficiency

Applying the phantom network model to the prepared networks, the value of G'_{∞} can be used to calculate the effective network chain density, ν_{eff}, according to eq. 19.

$$\nu_{eff} = \frac{G_{ph,eff}}{RT \cdot \left(1 - \frac{2}{f}\right)} = \frac{G'_{\infty}}{RT \cdot \left(1 - \frac{2}{f}\right)} \qquad (19\,a)$$

The variable f is the functionality of the crosslinker which is three in the case of the TEP (ETTMP1300) and four in the case of the FCC (BIS). R is the universal gas constant and T the absolute temperature (295.15 K).

The crosslinking efficiency, ε (eq. 69), can be determined by the ratio of the effective network chain density, ν_{eff}, and the theoretical network chain density, ν_{th}. The latter relates to a perfect network in which each crosslinker has reacted according to its functionality.

There are no defects, trapped entanglements, undesired side reactions or elastically ineffective chains. In agreement with eq. 15 ν_{th} can be calculated by eq. 70.

$$\varepsilon = \frac{\nu_{eff}}{\nu_{th}} \qquad\qquad (\,69\,)$$

$$\nu_{th} = \mu \cdot \frac{f}{2} = c_{ETTMP/BIS} \cdot \frac{f}{2} \qquad\qquad (\,70\,)$$

The results are illustrated in tables 19 and 20.

Table 19: Results of the rheology measurements of the thiol-ene samples; c_{TEP}: monomer concentration, c_{ETTMP}: crosslinker concentration, G'_∞: plateau-value of elastic shear modulus, ν_{eff}: effective network chain density, ν_{th} theoretical network chain density, ε: crosslinking efficiency

	c_{TEP} in wt%	c_{ETTMP} in mol/L	G'_∞ in Pa	ν_{eff} in mol/L	ν_{th} in mol/L	ε
DAP1000	7.5	0.0254	1550	0.0019	0.0381	0.050
	10	0.0339	6460	0.0079	0.0508	0.156
	12.5	0.0423	16070	0.0196	0.0635	0.309
	15	0.0508	29640	0.0362	0.0762	0.475
	17.5	0.0593	35170	0.0430	0.0889	0.484
	20	0.0677	61640	0.0754	0.1016	0.742
DAP2000	7.5	0.0167	2450	0.0030	0.0251	0.120
	10	0.0223	4100	0.0050	0.0335	0.149
	12.5	0.0279	14700	0.0180	0.0418	0.431
	15	0.0334	19300	0.0236	0.0502	0.470
	17.5	0.0390	28300	0.0346	0.0585	0.591
	20	0.0446	40000	0.0489	0.0669	0.731
DAP3000	7.5	0.0125	2000	0.0024	0.0187	0.128
	10	0.0166	6180	0.0076	0.0250	0.304
	12.5	0.0208	9380	0.0115	0.0312	0.369
	15	0.0249	15600	0.0191	0.0374	0.511
	17.5	0.0291	25000	0.0306	0.0437	0.700
	20	0.0333	28050	0.0343	0.0499	0.687

Table 20: Results of the rheology measurements of the PAAm samples; c_{AAm}: monomer concentration, c_{BIS}: crosslinker concentration, G'_∞: plateau-value of elastic shear modulus, ν_{eff}: effective network chain density, ν_{th} theoretical network chain density, ε: crosslinking efficiency

	c_{AAm} in wt%	c_{BIS} in mol/L	G'_∞ in Pa	ν_{eff} in mol/L	ν_{th} in mol/L	ε
PAAm 0.35 mol% BIS	7.5	0.0037	3100	0.0025	0.0074	0.338
	10	0.0050	7200	0.0059	0.0099	0.596
	12.5	0.0062	12400	0.0101	0.0123	0.821
	15	0.0073	18100	0.0148	0.0146	1.014
	17.5	0.0086	30000	0.0245	0.0171	1.433
	20	0.0098	36000	0.0293	0.0196	1.495
PAAm 1 mol% BIS	7	0.010	5600	0.0046	0.0198	0.232
	10	0.014	15000	0.0122	0.0284	0.430
	13	0.018	24000	0.0196	0.0364	0.538
	14	0.020	27300	0.0223	0.0389	0.573
	15	0.021	31800	0.0259	0.0418	0.620
	16	0.022	42000	0.0342	0.0444	0.770
	19	0.026	64000	0.0522	0.0518	1.008

The crosslinking efficiency, ε, of both the thiol-ene gels and the PAAm-gels increases with concentration within each series (Fig. 36). This may be attributed to the reduced probability of loop and dangling chain formation with increasing monomer concentration, since the amount of crosslinker also rises. Thus, the possibility is higher for a network chain to connect two different or further apart crosslinkers. Especially for the thiol-ene samples at low concentrations the crosslinking efficiency is rather low for all three series. Only around 10 % or less of the theoretically expected, elastically active network chains are formed at 7.5 wt%. This clearly shows that the gels are far away from the perfect network structure, especially at higher dilution where the formation of loops is highly likely. The formation of dangling chains or incomplete conversion can also be reasons for the low efficiency. At the highest concentration, 20 wt%, the efficiency has increased up to 75 %, meaning that still 25 % of the overall possible network chains do not contribute to the network elasticity. Additionally, all three thiol-ene series exhibit the same ε-values at the same concentration. This is due to two effects that cancel each other. On the one hand the crosslinker concentration of the three series is not the same at the same overall monomer concentration. The lower molar mass of DAP1000 and the stoichiometric ratio between double bonds and thiol groups result in a higher crosslinker concentration than for DAP2000 and DAP3000 and thus, as explained

above, a higher crosslinking efficiency. On the other hand, the shorter chain length promotes the formation of loops and dangling chains, leading to a lower crosslinking efficiency.

The PAAm-gels show a comparatively high crosslinking efficiency at small concentrations already. In the system with 0.35 mol% BIS the efficiencies even increase to values above 100 % at the highest concentrations. This should theoretically be impossible but eq. 19 a does not account for some deficiencies of network formation.
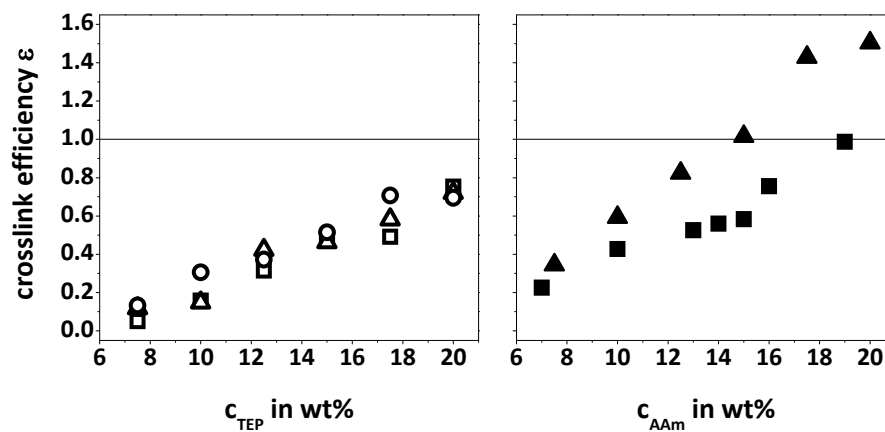

Fig. 36: crosslinking efficiency, ε, plotted versus the overall monomer concentration, $c_{TEP/AAm}$; left hand side: TEP samples, open squares: DAP1000, open triangles: DAP2000, open circles: DAP3000; right hand side: PAAm samples, filled squares: PAAm 1 mol% BIS, filled triangles: PAAm 0.35 mol% BIS

Firstly, in an acrylic system undesired crosslinking of network chains can occur. Under the usual reaction conditions of a free radical chain growth polymerisation, polyacrylamide is capable of reacting at the α-positions of the amide groups due to an acidic hydrogen atom (Scheme 14). A radical, $R^{\cdot}$, can abstract the acidic hydrogen, creating a carbon-centred radical function at the polymer backbone. Thus, branching or even additional crosslinking can take place, enabled by such chain transfer reactions, that occur especially at high concentrations. Consequently, this may increase the shear modulus, resulting in a higher crosslinking efficiency.
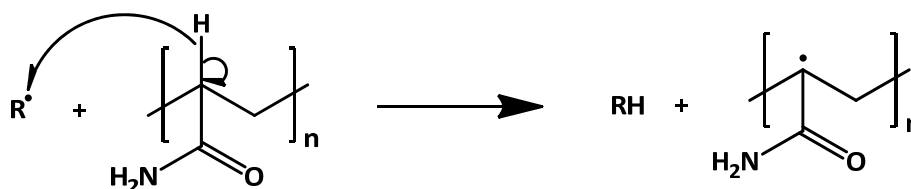
Scheme 14: Unwanted side-reaction in polymerisations using AAm as the monomer, the acidic hydrogen in α-position to the amide carbon atom can be abstracted by radicals in the reaction mixture, yielding a carbon centred radical at the polymer backbone which can lead to branching and additional crosslinking reactions

This additional crosslinking can be demonstrated by polymerising AAm without crosslinker. Two samples, one at 10 wt% and one at 20 wt% AAm were prepared under the same conditions as the hydrogels, only without BIS. Rheology experiments of the reactions showed that, at the measurement frequency of 1 Hz, the resulting PAAm behaved like a polymer gel, with G'_∞ being higher than G''_∞. By means of frequency sweeps the question was then cleared up whether or not permanently crosslinked networks were indeed formed. It was shown that for frequencies below 1 Hz G'_∞ and G''_∞ rapidly converge for the 10 wt% sample, even to the point where the moduli intersect (Fig. 37). The loss tangent determined from the two plateau values of the time-course measurement at 1 Hz is $\tan\delta = 0.48$ which, compared to the hydrogels formed with crosslinker, is a rather high value, close to the transition to a viscoelastic liquid. It can be concluded that, at this concentration, no permanent gel was formed although at 1 Hz pronounced entanglements due to very long and branched chains yield a transient, physical network. The loss tangent for the 20 wt% sample at 1 Hz is $\tan\delta = 0.096$, which is a significantly smaller value than for the first one. The frequency sweep does not show an intersection of G'_∞ and G''_∞ within the measured range, however they still seem to converge, possibly crossing at even lower frequencies (Fig. 38). These results suggest that at the present concentrations AAm does not permanently crosslink but, although the undesired additional crosslinking does not seem to be occuring completely, it probably develops chains that are capable of strongly entangling at the given concentrations. Accordingly, a high proportion of trapped entanglements should be present in the hydrogels, especially pronounced if the crosslinker concentration is smaller and the network chains should be longer, yielding remarkably high crosslink efficiencies.
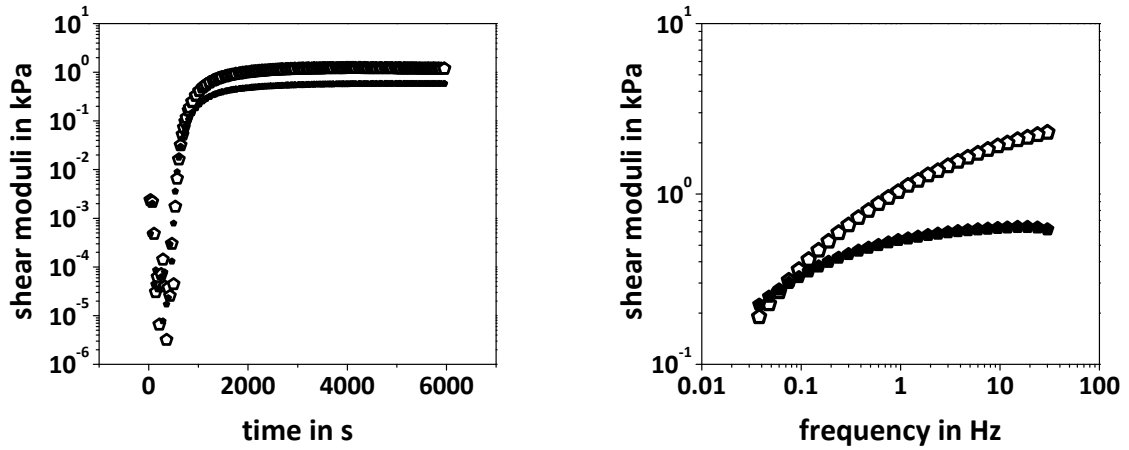
Fig. 37: Left hand side: Development of the shear moduli of the sample PAAm 10 wt% (without crosslinker) over the reaction time; open pentagons: elastic modulus, G′; filled pentagons: viscous modulus, G′′; parameters: 1 % strain, oscillation frequency: 1 Hz; right hand side: Frequency sweep of the sample PAAm 10 wt% (without crosslinker) subsequent to the time course measurement; open pentagons: elastic plateau modulus, G'_∞; filled pentagons: viscous plateau modulus, G''_∞; parameter: 1 % strain

Fig. 38: Left hand side: Development of the shear moduli of the sample PAAm 20 wt% (without crosslinker) over the reaction time; open pentagons: elastic modulus, G′; filled pentagons: viscous modulus, G′′; parameters: 1 % strain, oscillation frequency: 1 Hz; right hand side: Frequency sweep of the sample PAAm 20 wt% (without crosslinker) subsequent to the time course measurement; open pentagons: elastic plateau modulus, G'_∞; filled pentagons: viscous plateau modulus, G''_∞; parameter: 1 % strain
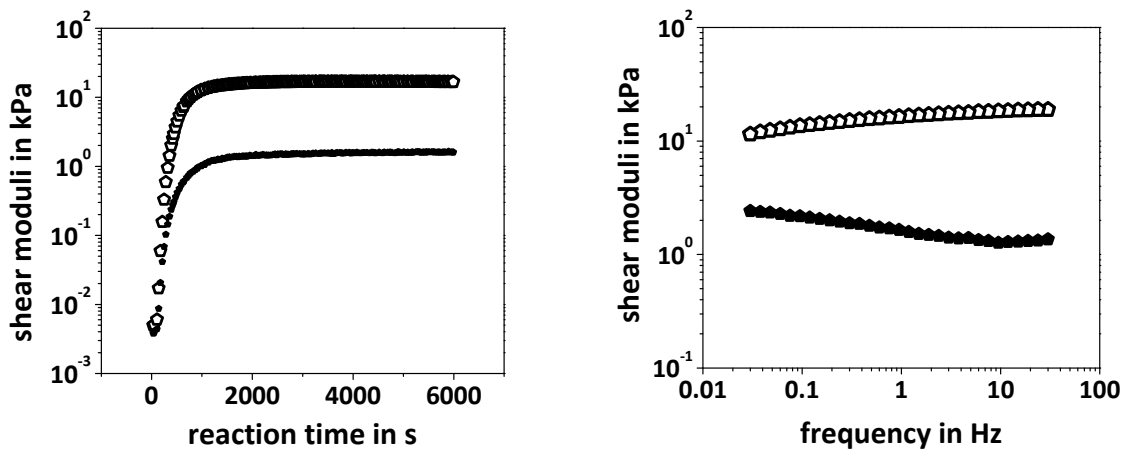
Secondly, the assumption that the hydrogels are describable by the phantom network model may not be valid. Usually, it is a good approximation for swollen polymer networks but as already mentioned it is only a limiting case and often the true values lie between the phantom and the affine network. The affine model leads to ν_{eff} - values that are 1-2/f times lower than for the phantom model. Assuming an affine network thus decreases the effective network chain density and thereby the efficiency, ε. For the TEP-hydrogels this leads to a drastic decrease of ε by a factor of three whereas the values of the PAAm-hydrogels are divided by two (Fig. 39). The highest crosslinking efficiency for the thiol-ene crosslinking polymerisation is 25.3 % if the affine network model is applied. This seems fairly low, implying that 75 % or more of the theoretically possible network chains do not contribute to the network elasticity. This could either be due to a very low conversion, which, as was shown in chapter 4.2, is not the case, or to extensive loop and dangling chain formation as well as highly crosslinked domains.
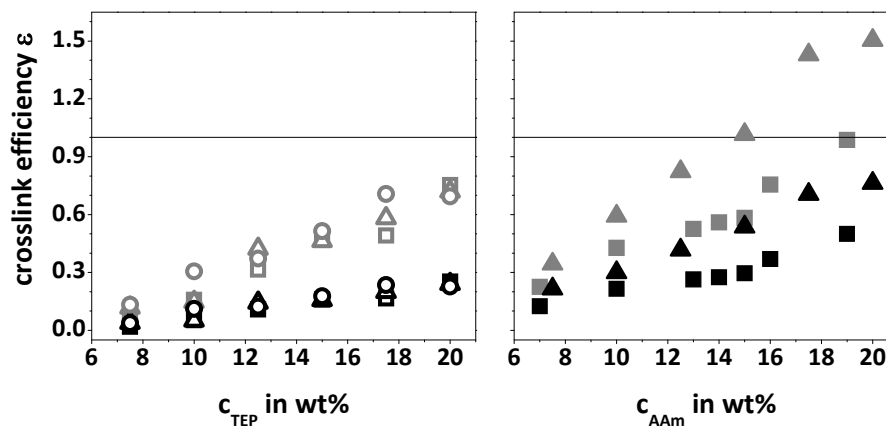
Fig. 39: Crosslinking efficiency, ε, plotted versus the overall monomer concentration, $c_{TEP/AAm}$; left hand side: TEP samples, open squares: DAP1000, open triangles: DAP2000, open circles: DAP3000; right hand side: PAAm samples, filled squares: PAAm 1 mol% BIS, filled triangles: PAAm 0.35 mol% BIS; black symbols denote the values calculated according to the affine network model, grey symbols denote the values calculated according to the phantom network model

At any rate, with none of the two models do the thiol-ene gels approach a crosslinking efficiency of 100 %. This means that a certain amount of loop and dangling chain formation, leading to ineffective network chains, is inevitable, a non-quantitative conversion adding to it. Moreover, it is probable that the contribution of entanglements among the network chains is rather low. The values for the PAAm gels, especially the ones with 0.35 mol% BIS, seem more reasonable when applying the affine network model, however this may simply conceal the strong entangling among the network chains. Probably, neither of the two models describes the hydrogels perfectly accurate, nevertheless they work well at roughly assessing the samples, whereas it shall be assumed that the phantom network model is still more realistic due to the rather low ε - values for the thiol-ene gels when applying the affine model.

4.3.4 Comparison at the Theoretical Network Chain Density

The hitherto carried out examinations show that the elastic modulus, G'_∞, and the crosslinking efficiency, ε, of both TEP- and PAAm-hydrogels increase with increasing concentration. The increase in G'_∞ is attributed to the rising crosslinker concentration and the increase in ε is explained with the decreasing probability for loop and dangling chain formation. Since the same monomer concentration of the different samples does not imply the same amount of crosslinker or theoretically expected network chain density, ν_{th} is also an interesting parameter by which to compare the different hydrogels.

Basically, ν_{th} is nothing other than the crosslinker concentration multiplied with a constant factor (eq. 70). Plots of G'_∞ versus ν_{th} for the TEP- and FCC-hydrogels are shown in fig. 40. It is evident that the crosslinker concentration of the PAAm samples, particularly the one with 0.35 mol% BIS, is generally lower than that of the comparable thiol-ene samples. Still they adopt elastic moduli that are just as high or even higher than for the thiol-ene samples, due to the higher crosslinking efficiency. Another important aspect is that within one system, TEP or PAAm, the elastic moduli vary strongly at the same crosslinker concentration. For the thiol-ene samples it can be said that G'_∞ approaches the theoretically possible modulus (dashed line) more and more, if the network chains grow longer.
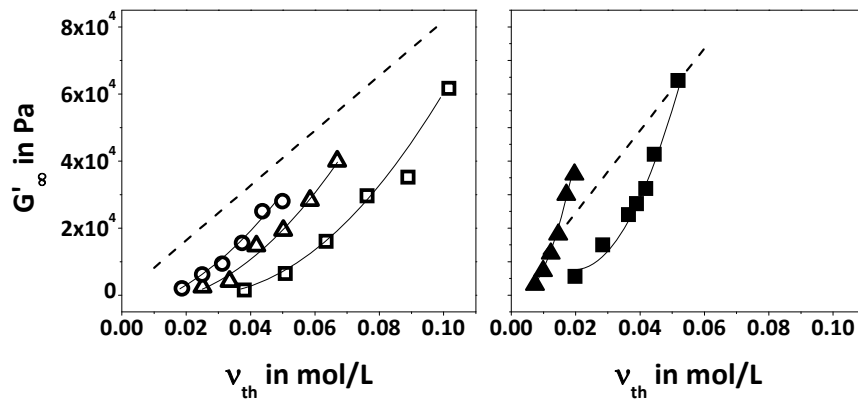
Fig. 40: Elastic plateau modulus, G'_∞, plotted versus the theoretical network chain density, ν_{th}; left hand side: TEP samples, open squares: DAP1000, open triangles: DAP2000, open circles: DAP3000; right hand side: PAAm samples, filled squares: PAAm 1 mol% BIS, filled triangles: PAAm 0.35 mol% BIS; the dashed line denotes the theoretically possible maximal elastic modulus for a phantom network

The same behaviour can be observed in the plot of ε versus ν_{th} (Fig. 41) for both the TEP- and FCC-hydrogels. The crosslinking efficiency within one system clearly varies at the same theoretical network chain density.
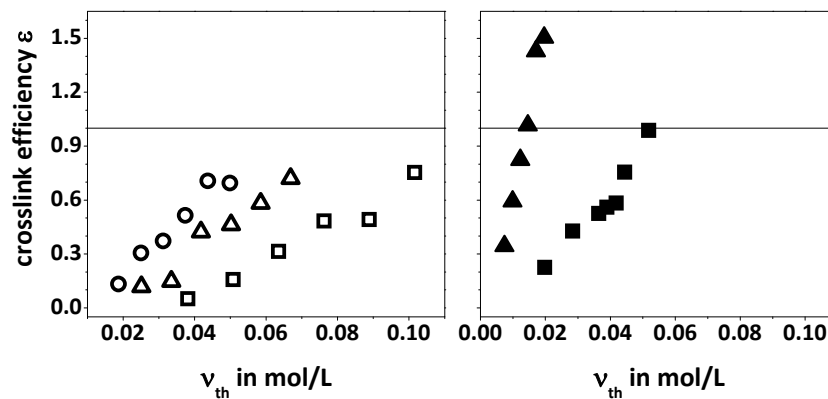

Fig. 41: Crosslinking efficiency, ε, plotted versus the theoretical network chain density, ν_{th}; left hand side: TEP samples, open squares: DAP1000, open triangles: DAP2000, open circles: DAP3000; right hand side: PAAm samples, filled squares: PAAm 1 mol% BIS, filled triangles: PAAm 0.35 mol% BIS

Table 21 summarises values of G'_∞ and ε at approximately the same theoretical network chain density, ν_{th}. Comparing the different DAP-samples it becomes obvious that the elastic modulus and the crosslinking efficiency increase from the DAP1000 to the DAP3000 samples. The same holds true when passing from PAAm 1 mol% to 0.35 mol% BIS. This indicates that the samples that exhibit the longer network chains (for the PAAm samples determined by ν_{th}) exploit the amount of crosslinker much more efficiently by forming a higher amount of elastically active network chains. Those samples are less prone to loop[84] and dangling chain formation as well as highly crosslinked regions (spatial inhomogeneities) which are reasons for a decreased modulus and thus reduced crosslinking efficiency. Longer network chains possess chain ends that are farther apart, thus decreasing the probability of them both reacting in a close vicinity. This fact yields the implication that within the TEP series the samples comprising DAP3000 form structures with the lowest degree of defects and imperfections, as assumed earlier in chapter 4.1. The same holds true for the PAAm samples consisting of 0.35 mol% BIS compared to the ones containing 1 mol% BIS, as well.

Table 21: Rheology results of samples with similar theoretical network chain density, ν_{th}; G'_∞: plateau-value of elastic shear modulus, ε: crosslinking efficiency

	ν_{th} in mol/L	G'_∞ in Pa	ε
DAP1000 10 wt%	0.050	6460	0.160
DAP2000 15 wt%	0.051	19300	0.471
DAP3000 20 wt%	0.050	28050	0.680
PAAm 1% 7 wt%	0.020	5600	0.250
PAAm 0.35% 20 wt%	0.019	36000	1.526

4.3.5   Summary of the Mechanical Measurements

In summary, the measurements show that essentially none of the prepared samples exhibited a perfect network structure. The elastic modulus and thus the crosslinking efficiency of the thiol-ene gels remain, often significantly, below the theoretically possible values. The PAAm gels exhibit the opposite behaviour by partly even exceeding those values. Consequently, to a certain degree all the gels possess defects or inhomogeneities rendering them imperfect.

For the thiol-ene gels, fig. 36 shows that with rising crosslinker concentration the network formation becomes more and more efficient, reducing the degree of looping and other structural defects. In fig. 41 it can be seen that at the same crosslinker concentration the amount of those defects in the network structure decreases with increasing network chain length from DAP1000 to DAP3000. These findings lead to the conclusion, that the DAP3000 gels exhibit the most homogeneous network structure, compared to the two other thiol-ene series, especially because of the reduced probability of looping, due to the longer network chains. Consequently, dynamic light scattering should show that the DAP3000 20 wt% gel is the most homogeneous thiol-ene gel overall.

These interpretations of fig. 36 and 41 basically also hold for the PAAm gels. However, particularly the ones containing 0.35 mol% BIS, seem to exhibit a high amount of trapped entanglements and maybe even additional crosslinks, due to side reactions.

4.4   Dynamic Light Scattering

4.4.1   Introduction

Rheological measurements yield macroscopic properties averaged over the whole sample. However, since we want to find out about the inhomogeneity of our gels, we need to get information on the structure of the underlying network. For the analysis of this microstructure we used dynamic light scattering. This way the fluctuating part of the network stemming from the network chains carrying out diffusive motion, although restricted by being tethered to the crosslinks, can be separated from the frozen part, mainly resulting from spatial inhomogeneities. In the following, the DLS measurements that were conducted with reactor-batch and equilibrium swollen hydrogels will be elucidated. The partial-heterodyne method as well as the non-ergodic method have been employed to analyse the DLS data. A third way of analysing DLS-data has been utilised which is based on the statistical distribution of scattering intensities at different sample positions due to the non-ergodicity of polymer gels.

4.4.2   Reactor-Batch Hydrogels

4.4.2.1   Partial-Heterodyne Method

For the partial-heterodyne method the hydrogels were measured at a high number of different positions. Plotting the resulting scattering intensities, $\langle I \rangle_{T,p}$, versus the measured sample positions yields the so-called speckle patterns (Fig 43 & 44). Each of the sample positions yields an autocorrelation function that is analysed according to chapter 2.3.1.1. A graph of $\langle I \rangle_{T,p}/D_A$ versus $\langle I \rangle_{T,p}$ then leads to the straight lines (eq. 47), illustrated in fig. 42, that are characteristic of this method. In this figure all lines, except for the sample DAP3000, are shifted to higher intensities along the x-axis by a constant value for the sake of clarity. The slope of the straight lines yields the diffusion coefficient, D, of the fluctuating network chains. The scattering intensity of the fluctuating part of the sample, $\langle I_F \rangle$, is determined from the y-axis intercept of these lines. In the speckle patterns $\langle I_F \rangle$ is generally denoted by a red line and the ensemble average scattering intensity, $\langle I \rangle_E$, by a green line. $\langle I \rangle_E$ is determined by averaging all $\langle I \rangle_{T,p}$ - values of a speckle pattern.
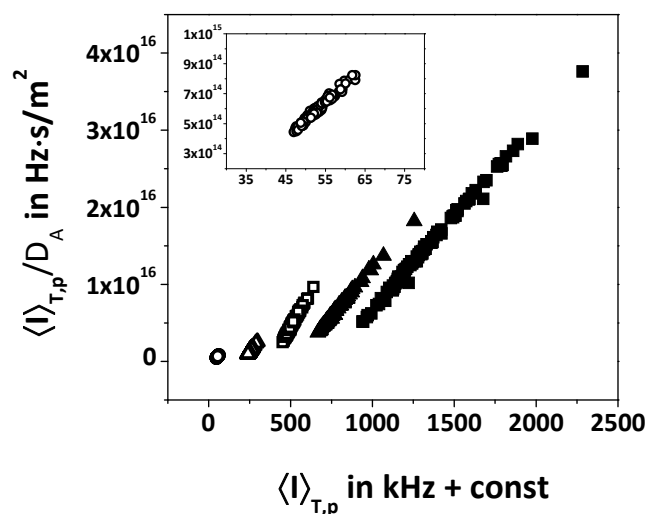
Fig. 42: Straight lines acquired from the partial-heterodyne evaluation method; $\langle I \rangle_{T,p}$: time average, position dependent scattering intensity, D_A: apparent diffusion coefficient; TEP samples: open squares: DAP1000 15 wt%, open triangles: DAP2000 17.5 wt%, open circles: DAP3000 20 wt%; PAAm samples, filled squares: PAAm 1 mol% BIS 15 wt%, filled triangles: PAAm 0.35 mol% BIS 17.5 wt%; all lines, apart from DAP3000, were shifted along the x-axis by constant values in order for them not to overlap; the inset shows the DAP3000 series in more detail

The speckle patterns demonstrate that the scattering intensity and the distribution of the data points vary strongly with the sample type. Fig. 43 shows the speckle patterns of the three thiol-ene samples mentioned in table 18. It is evident that with increasing network chain length the scattering intensity becomes lower. Furthermore, the scatter of the data reduces significantly. The same behaviour can be seen for the PAAm samples in fig. 44. Decreasing the amount of crosslinker, thus generating longer network chains, diminishes $\langle I \rangle_{T,p}$ and the noise of the data points. Generally, comparing two systems of the same chemical composition but with different structure, the one exhibiting the higher homogeneity scatters light less than the more inhomogeneous one. This can be transferred to each of the two systems used in this thesis. The only basic difference between the two PAAm-systems is the crosslinker concentration. Thus, it can be concluded that, as expected, the PAAm-hydrogels form spatially more homogeneous networks if they comprise a smaller amount of crosslinker since, in that case, they scatter light to a lesser extent. The three TEP-series differ more strongly from each other than the two PAAm-series, since with increasing DAP-chain length their proportion of ethoxy groups increases as well. However, as shown in chapter 3.6.3, the difference in the RIIs of the three series is considered negligible in the high molecular weight

108

network state. Hence, the decrease in scattering intensity from the DAP1000, over the DAP2000 to the DAP3000 sample is probably due to decreasing static concentration fluctuations (spatial inhomogeneities). The two more homogeneous samples even seem to have no real speckle pattern, at all. All the different positions appear to possess almost the same scattering intensity.
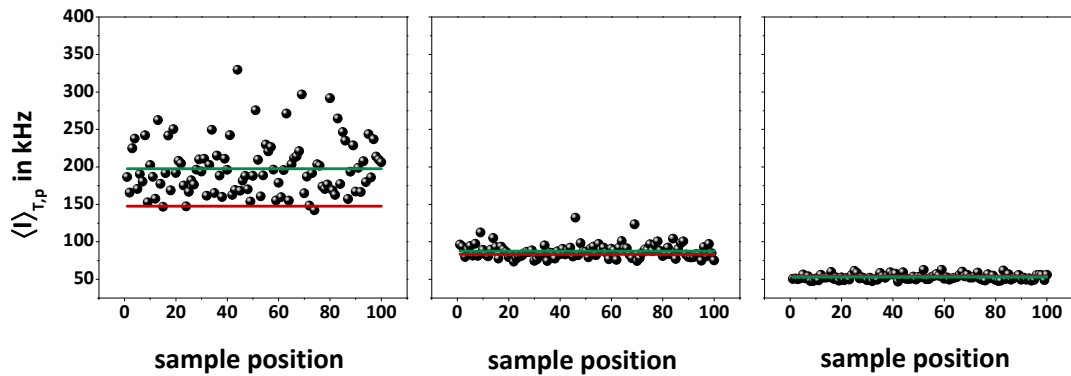

Fig. 43: Speckle patterns of the three thiol-ene samples DAP1000 15 wt% (left hand side), DAP2000 17.5 wt% (middle) and DAP3000 20 wt% (right hand side), see table 18, the black dots denote the scattering intensities, $\langle I \rangle_{T,p}$, at the different positions that were measured; the red lines denote the scattering intensity of the fluctuating part, $\langle I_F \rangle$; the green lines denote the overall ensemble average scattering intensity, $\langle I \rangle_E$

Fig. 44: Speckle patterns of the two PAAm samples PAAm 1 mol% BIS 15 wt% (left hand side) and PAAm 0.35 mol% BIS 17.5 wt% (right hand side), see table 18, the black dots denote the scattering intensities, $\langle I \rangle_{T,p}$, at the different positions that were measured; the red lines denote the scattering intensity of the fluctuating part, $\langle I_F \rangle$; the green lines denote the overall ensemble average scattering intensity, $\langle I \rangle_E$;
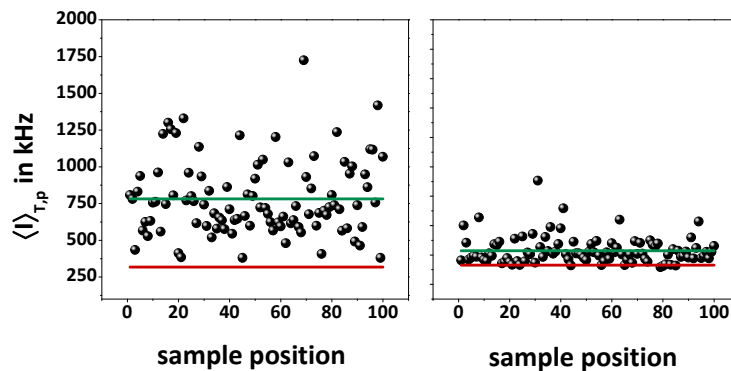
Making a statement about network homogeneity by directly comparing the light scattering intensities of the TEP- and the PAAm-systems is not reasonable. The RII of the thiol-ene-samples (0.129, like pure PEG35,000, chapter 3.6.3) is smaller than that of the PAAm-samples (0.167), meaning that the latter inherently scatter the employed light more strongly. Hence, the higher scattering intensity of the PAAm-samples cannot be entirely attributed to a more inhomogeneous network structure.

To avoid this problem, an approach can be used in which relative terms are compared. Certainly, the fluctuating component of the intensity $\langle I_F \rangle$ and the corresponding static component $\langle I_S \rangle_E$ have something to do with the homogeneity of the observed samples, however the absolute values are of no use if different systems are to be compared. Thus, it is better to express the homogeneity as a percentage of $\langle I_F \rangle$ or $\langle I_S \rangle_E$ of the overall intensity $\langle I \rangle_E$. Since it is more easily compared to the results of the non-ergodic analysis method the relation that shall be used in the following as a measure of network homogeneity is $\langle I_S \rangle_E / \langle I \rangle_E$. The highest value it can adopt is one, with the network being completely frozen-in. The lowest value is zero, describing a fully fluctuating, ergodic system without any static components, hence an absolutely homogeneous concentration distribution throughout the network (eq. 71).

$$0 \leq \frac{\langle I_S \rangle_E}{\langle I \rangle_E} \leq 1 \qquad\qquad (\,71\,)$$

The obtained results are illustrated in table 22. For the selected samples, it shows the diffusion coefficient, D, (cooperative diffusion) determined from the slopes of the straight lines in fig. 42 and the dynamic correlation length, ξ_D, calculated from eq. 48. Furthermore, $\langle I \rangle_E$, $\langle I_F \rangle$, $\langle I_S \rangle_E$ and $\langle I_S \rangle_E / \langle I \rangle_E$ are presented.

Table 22: Results of the partial-heterodyne DLS method of the samples illustrated in table 18; D: diffusion coefficient, ξ_D: dynamic correlation length, $\langle I \rangle_E$: ensemble average scattering intensity, $\langle I_F \rangle$: scattering intensity of the thermally fluctuating component within a network, $\langle I_S \rangle_E$: scattering intensity of the static component within a network, $\langle I_S \rangle_E / \langle I \rangle_E$: measure for network homogeneity

	D in $\mu m^2/s$	ξ_D in nm	$\langle I \rangle_E$ in kHz	$\langle I_F \rangle$ in kHz	$\langle I_S \rangle_E$ in kHz	$\langle I_S \rangle_E / \langle I \rangle_E$
DAP1000 15 wt%	52.6	2.24	197.7	147.4	50.3	0.25
DAP2000 17.5 wt%	67.2	1.76	87.5	83.4	4.1	0.05
DAP3000 20 wt%	82.8	1.43	52.9	54.3	-1.4	-0.03
PAAm 1 mol% BIS 15 wt%	84.1	2.92	781.9	317.6	464.3	0.59
PAAm 0.35 mol% BIS 17.5 wt%	82.3	2.99	428.5	330.8	97.7	0.23

The diffusion coefficient of the TEP samples increases with precursor chain length and concentration, for both the gels with a similar elastic modulus (Table 22) and the gels with a similar theoretical network chain density (Fig. 45, left hand side). The correlation length accordingly decreases (eq. 48). At the same G'_∞ and ν_{th}, the DAP3000 gels always have the highest overall concentration. Thus, they also have the highest polymer density and consequently the highest diffusion coefficient, because the correlation of the network chain segments decays faster in a dense state where they are more strongly entangled.

The diffusion coefficient for the PAAm samples with similar G'_∞ adopts essentially the same values (Table 22). Comparing D using ν_{th} (Fig. 45, right hand side), it shows the same behaviour as for the TEP samples. The PAAm gel with 0.35 mol% BIS has a higher polymer concentration than the one with 1 mol% BIS yielding a higher diffusion coefficient.
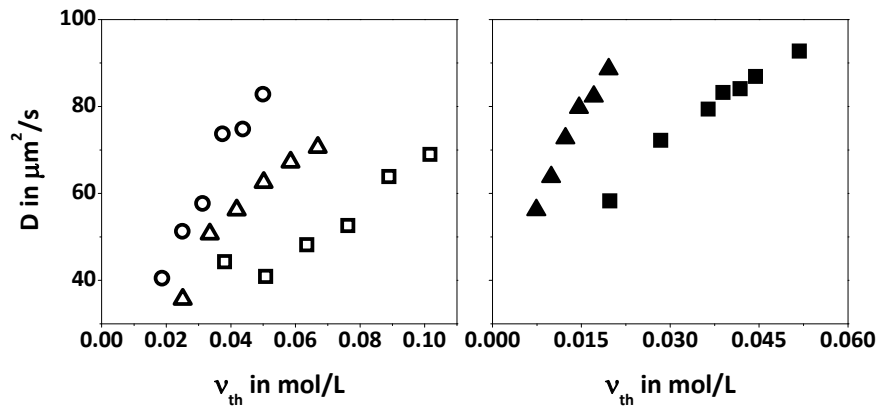
Fig. 45: Diffusion coefficient, D, plotted versus the theoretical network chain density, ν_{th}; left hand side: TEP samples, open squares: DAP1000, open triangles: DAP2000, open circles: DAP3000; right hand side: PAAm samples, filled squares: PAAm 1 mol% BIS, filled triangles: PAAm 0.35 mol% BIS

With rising monomer concentration the diffusion coefficient increases for all series (Fig. 46). Correspondingly, the dynamic correlation length decreases as expected (Fig. 47), since with increasing monomer concentration the concentration of the crosslinker increases, as well. Thus, the correlation length, which is related to the distance throughout which the segmental cooperative diffusion is correlated, becomes smaller.

A somewhat unexpexted behaviour of the diffusion coefficient is displayed in fig. 46. At the same concentration the DAP1000 gels always possess the highest amount of crosslinker. Still, they exhibit slightly lower diffusion coefficients and thus higher correlation lengths than the other two series. The opposite is true for the PAAm gels. The sample with the higher amount of crosslinker at the same overall concentration (PAAm 1 mol% BIS), exhibits slightly higher diffusion coefficients.

112
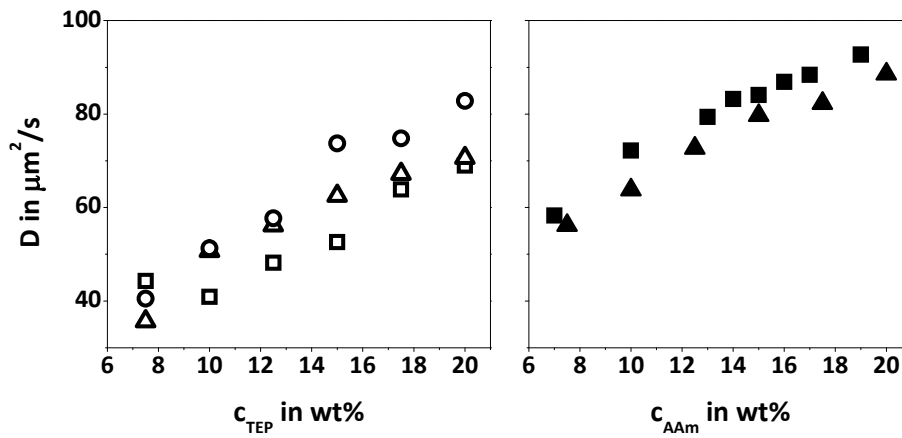
Fig. 46: Diffusion coefficient, D, plotted versus the monomer concentration, $c_{TEP/AAm}$; left hand side: TEP samples, open squares: DAP1000, open triangles: DAP2000, open circles: DAP3000; right hand side: PAAm samples, filled squares: PAAm 1 mol% BIS, filled triangles: PAAm 0.35 mol% BIS
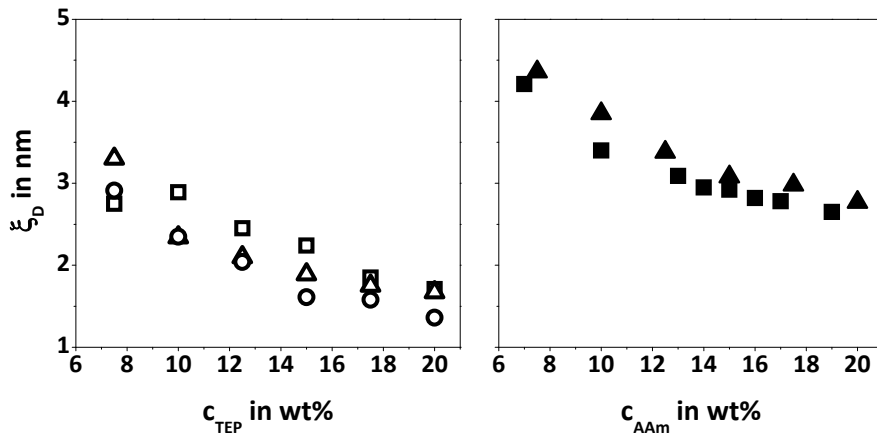
Fig. 47: Dynamic correlation length, ξ_D, plotted versus the monomer concentration, $c_{TEP/AAm}$; left hand side: TEP samples, open squares: DAP1000, open triangles: DAP2000, open circles: DAP3000; right hand side: PAAm samples, filled squares: PAAm 1 mol% BIS, filled triangles: PAAm 0.35 mol% BIS

Fig. 48 shows all the $\langle I_S \rangle_E / \langle I \rangle_E$ - values taken from the different concentrations of the TEP (left hand side) and the PAAm samples (right hand side).

Fig. 48: $\langle I_S \rangle_E / \langle I \rangle_E$ plotted versus the monomer concentration, $c_{TEP/AAm}$; left hand side: TEP samples, open squares: DAP1000, open triangles: DAP2000, open circles: DAP3000; right hand side: PAAm samples, filled squares: PAAm 1 mol% BIS, filled triangles: PAAm 0.35 mol% BIS
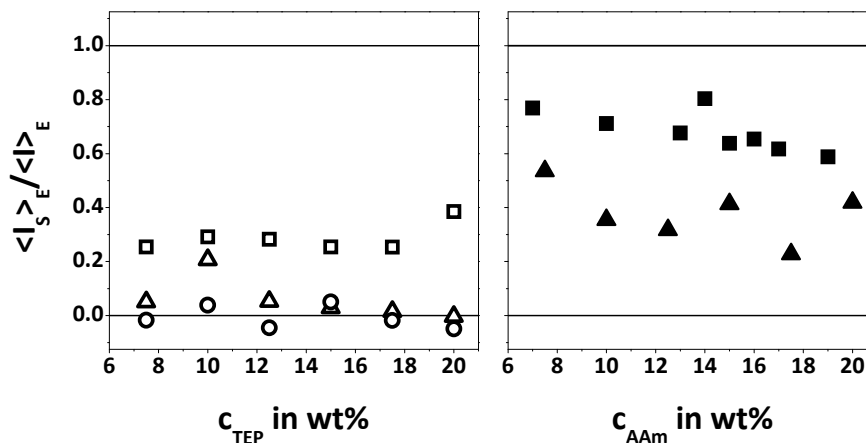
The thiol-ene systems with DAP2000 and DAP3000, seem to exhibit virtually no inhomogeneity at all, since the $\langle I_S \rangle_E / \langle I \rangle_E$ - values are very close to zero. There should be hardly any static inhomogeneities within those samples. Still, a slight difference between DAP2000 and DAP3000 can be observed in that the latter seems to be a little more homogeneous due to even lower values. The DAP1000 samples have a visibly higher inhomogeneity with values around 0.3. This behaviour is in accord with the results taken from the rheological measurements which also showed that the DAP1000 gels possess a higher degree of imperfections or defects than the DAP3000 gels. As for the PAAm samples, the ones with 1 mol% BIS are clearly more inhomogeneous than all the other samples, PAAm or TEP. The static component accounts for 60 to 80 % of the overall scattering intensity. A decrease in inhomogeneity from low to high monomer concentration can be detected. However, this tendency can hardly be verified by the four other series. The series PAAm 0.35 mol% BIS exhibits values that are in the same range as DAP1000.

114

Generally, opposed to the crosslinking efficiency in fig. 36 (chapter 4.3.3) the DLS results show no significant dependence of the homogeneity on the network concentration. However, the rheological data point out that especially at low concentrations the networks exhibit a considerable degree of defects attributed to strong loop formation at low polymer content or for short network chains, particularly for the TEP. The DAP2000 and DAP3000 samples appear perfectly homogeneous in DLS. Obviously, the topological defects detected by rheology do not affect the light scattering properties of those samples. There are no static concentration fluctuations observable by DLS for the DAP2000 and DAP3000 samples, but there certainly are defects, which simply seem to be homogeneously distributed across the network.

Investigating the samples DAP2000 17.5 wt% and DAP3000 20 wt% (Fig. 49) more closely, it is evident that the $\langle I_F \rangle$ - values determined according to chapter 2.3.1.1 show some inconsistence. For the DAP2000 sample $\langle I_F \rangle$ is visibly larger than many of the $\langle I \rangle_{T,p}$-values and for the DAP3000 sample it is even larger than $\langle I \rangle_E$. Both cases are theoretically impossible. This only occurs with the two most homogeneous series, DAP2000 and DAP3000, at every concentration that was used. A similar case of a rather homogeneous gel with a theoretically irrational $\langle I_F \rangle$ - value has been observed earlier by SUSOFF and OPPERMANN[82] for a polystyrene network prepared by random crosslinking. This implies that the partial-heterodyne evaluation method has difficulties describing samples that are highly homogeneous.
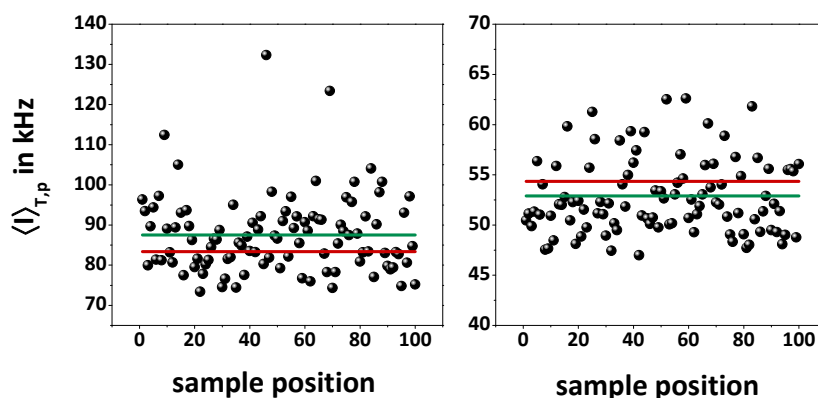
Fig. 49: Speckle patterns of the thiol-ene samples DAP2000 17.5 wt% (left hand side) and DAP3000 20 wt% (right hand side); the black dots denote the scattering intensities, $\langle I \rangle_{T,p}$, at the different positions that were measured; the red lines denote the scattering intensity of the fluctuating part, $\langle I_F \rangle$; the green lines denote the overall ensemble average scattering intensity, $\langle I \rangle_E$; note the different scales of the y-axes

Having another look at fig. 42 it is evident that the spatial variations of scattering intensities strongly decrease with increasing homogeneity. Compared to the PAAm samples the data points of the DAP3000 gel appear to be all almost the same. This leads to an increased uncertainty in the extrapolation of the data to the y-axis in order to determine intercept and thus the fluctuating component $\langle I_F \rangle$, which primarily affects the two very homogeneous systems comprising DAP2000 and DAP3000. The slope and the y-axis intercept are obtained by fitting a straight line to the data points. Adjusting the intercept of this fitted line so as for it to yield reasonable $\langle I_F \rangle$ - values by simply replacing it with the lowest $\langle I \rangle_{T,p}$ - value of the particular sample, the resulting fits (Fig. 50) still show good coefficients of determination, R^2 (Table 23).
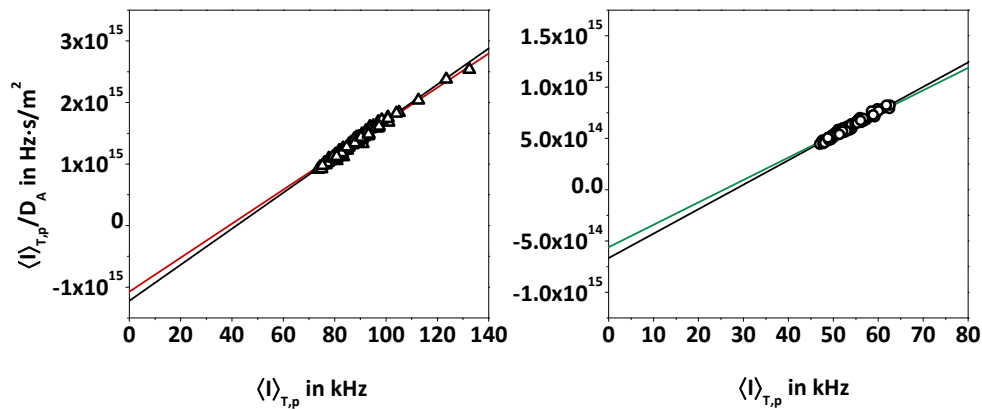

Fig. 50: Graph of the straight lines of the thiol-ene samples DAP2000 17.5 wt% (left hand side, open triangles) and DAP3000 20 wt% (right hand side, open circles), acquired from the partial-heterodyne evaluation method; $\langle I \rangle_{T,p}$: time average, position dependent scattering intensity, D_A: apparent diffusion coefficient; the black lines are the normal linear fits, the coloured lines are the linear fits with an adjusted intercept so that $\langle I_F \rangle$ exhibits the same value as the lowest $\langle I \rangle_{T,p}$ datapoint; note the different scales of the y-axes

Table 23: Values of the scattering intensities of the thermally fluctuating component for the case of the normal partial-heterodyne analysis, $\langle I_F \rangle$, as well as the (according to fig. 50) adjusted value, $\langle I_F \rangle_{adjusted}$, and the corresponding coefficients of determination, R^2 and $R^2_{adjusted}$

	$\langle I_F \rangle$ in kHz	R^2	$\langle I_F \rangle_{adjusted} = \langle I \rangle_{T,p,min}$ in kHz	$R^2_{adjusted}$
DAP2000 17.5 wt%	83.4	0.9802	73.5	0.9771
DAP3000 20 wt%	54.3	0.9691	47.0	0.9622

Hence, it is assumed that choosing the lowest $\langle I \rangle_{T,p}$-value as $\langle I_F \rangle$ for the DAP2000 and DAP3000 systems is a sensible way of generating reasonable values which account for the fact that those systems still have a speckle pattern, owing to minor inhomogeneities that still render the very homogeneous samples slightly non-ergodic (Fig. 51). The order of decreasing inhomogeneity, from DAP1000 to DAP3000, is still the same. However the values are no longer too small or even negative (Fig. 52).
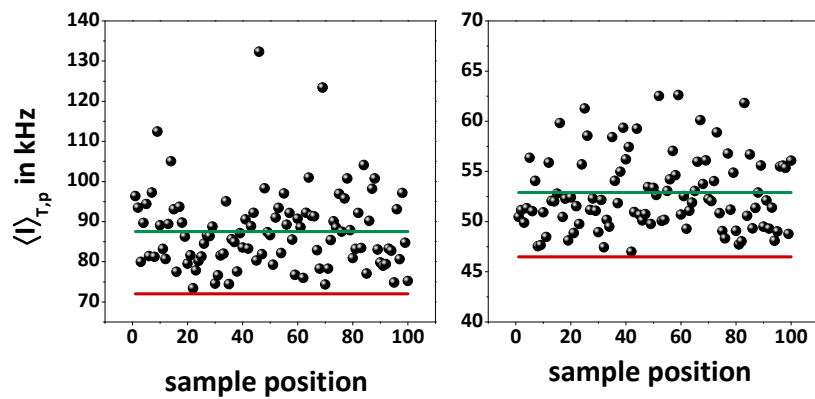
Fig. 51: Speckle patterns of the thiol-ene samples DAP2000 17.5 wt% (left hand side) and DAP3000 20 wt% (right hand side); the black dots denote the scattering intensities, $\langle I \rangle_{T,p}$, at the different positions that were measured; the red lines denote the scattering intensity of the fluctuating part, $\langle I_F \rangle$; the green lines denote the overall ensemble average scattering intensity, $\langle I \rangle_E$; $\langle I_F \rangle$ is not determined by the partial-heterodyne method, but replaced by the lowest $\langle I \rangle_{T,p}$-value, according to table 23
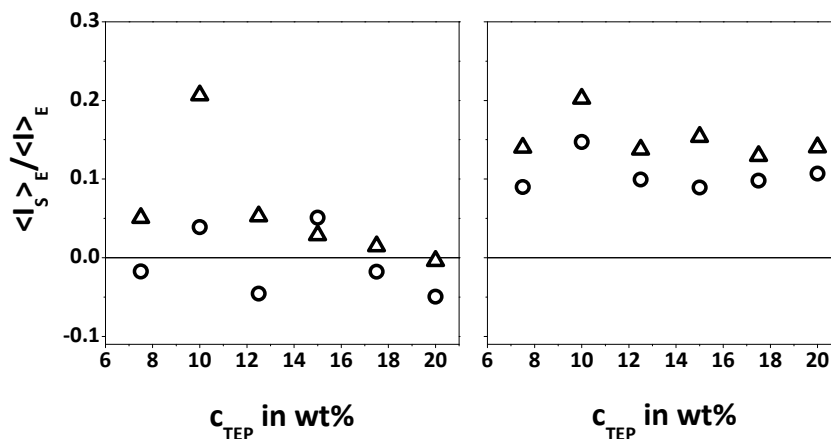
Fig. 52: $\langle I_S \rangle_E / \langle I \rangle_E$ plotted versus the monomer concentration, c_{TEP}; open triangles: DAP2000, open circles: DAP3000; the left hand side shows the unadjusted $\langle I_S \rangle_E / \langle I \rangle_E$-values determined by the partial-heterodyne method, the right hand side shows the adjusted values according to table 23

In conclusion, it can be said that DLS measurements of the used polymer hydrogels analysed by the partial-heterodyne method work fairly well determining their network homogeneity. The basic result is that, as expected, the thiol-ene hydrogels are generally more homogeneous than the comparable PAAm hydrogels, however depending on the crosslinker concentration of the FCC and the chain length of the diene. The PAAm 1 mol% BIS samples evidently have the highest inhomogeneity of all samples. Decreasing the crosslinker concentration to 0.35 mol% BIS yields a significant reduction of network inhomogeneity, a behaviour that has often been observed. The TEP samples with the shortest diene chain length, DAP1000, are in terms of inhomogeneity in the same range as the PAAm 0.35 mol% BIS samples, possibly exhibiting a somewhat higher homogeneity. However, within experimental error, both systems are rather similar. The two TEP series comprising higher molecular weight dienes, DAP2000 and DAP3000, obviously are markedly more homogeneous than all the other examined gels. According to the analysis, both systems seem to exhibit extremely low proportions of inhomogeneity down to virtually none, whereas the DAP3000 gels in general seem to be still a little bit more homogeneous. This is also true if the $\langle I_S \rangle_E / \langle I \rangle_E$ - values are adjusted according to the lowest $\langle I \rangle_{T,P}$ - values. The reason for this order of homogeneity are the fundamentally different crosslinking mechanisms. The FCC is known to carry out pronounced intramolecular crosslinking at low conversions leading to a high extent of static spatial inhomogeneities. However, with decreasing amount of crosslinker the intramolecular crosslinking becomes less significant. The end-linking process, that the TEP is based on, is noted for forming rather homogeneous networks if the boundary conditions are appropriate. Shorter network chain precusors lead to a higher probability for loop formation[84]. The same holds true for low concentrations. If the chain is not long enough to reach another crosslinker molecule that it can add to, it will either not react at all or form circular structures that do not take part in building up an elastic network. Hence, the networks comprising DAP1000 are relatively inhomogeneous compared to the other two series. With increasing network chain length the homogeneity increases due to a lesser extent of topological imperfections. Furthermore, the thiol-ene polymerisation does not only have the advantage of being an end-linking process but additionally exhibiting the mechanism of a step growth polymerisation with a delayed gel point. This gives rise to a relatively low viscosity for a comparatively long time, thus rendering the system capable of chain relaxations to adopt a more random structure with lesser clustering. The results

concerning the order of the degree of homogeneity within one system (TEP or PAAm) are supported by what was found by the rheological measurements, also pointing to an increasing homogeneity at a higher chain length of the network chain precursors (TEP) or at a lower crosslinker concentration (PAAm).

4.4.2.2   Non-Ergodic Medium Method

Another possibility to analyse the DLS data concerning static and fluctuating components of a polymer network is the so-called non-ergodic medium method developed by PUSEY and VAN MEGEN described in chapter 2.3.1.2. As explained there, the ICFs, $g^{(2)}(q,\tau)$ - 1, determined from the DLS instrument, are converted into the FCFs, $f(q,\tau)$, by eq. 49, yielding offset values that describe the static proportion of the observed samples. An example of the obtained ICF for the sample DAP1000 15 wt% is shown in fig. 53 on the left hand side. The curves all decay to zero but the intercept varies over a certain range, illustrating the non-ergodicity of the investigated sample. As mentioned in chapter 3.7, the coherence factor of the instrument was taken to be $\beta = 0.358$. The resulting FCF all decay from the initial value one to different plateau values (Fig. 53, right hand side).
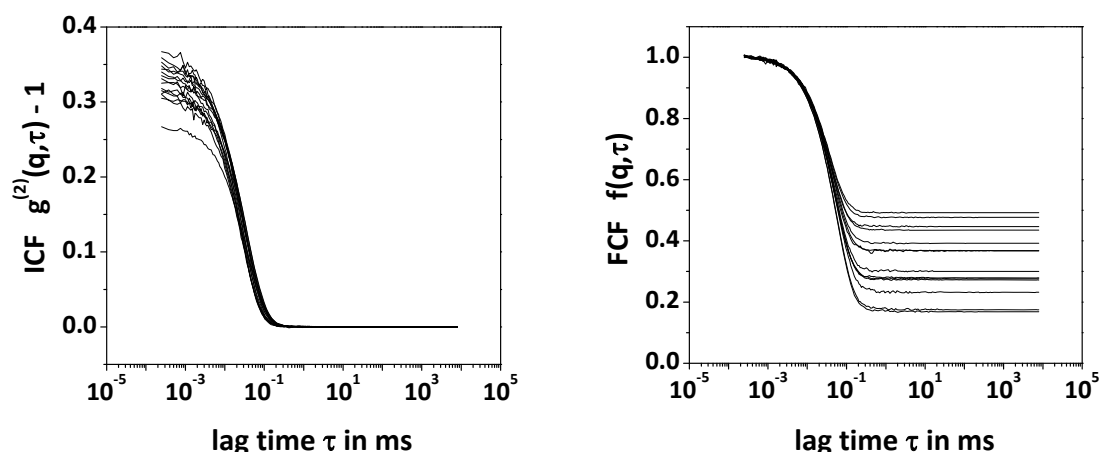

Fig. 53: Typical correlation curves in the non-ergodic method for the sample DAP1000 15 wt%; left hand side: ICF measured at different positions within the same sample, right hand side: FCF calculated from the ICF by eq. 49; note the logarithmic scale of the x-axes and the different scales of the y-axes

Theoretically, all those plateau values should be the same, so that only one measurement at one position of the sample would suffice to describe it, in combination with a rotation measurement yielding the ensemble average scattering intensity, $\langle I \rangle_E$. However, this was never the case for any examined system. Thus, the average of all plateau values of one sample was taken to determine the static proportion.

Unfortunately, this method did not work out for all the examined gels, since the required FCF could not be calculated in many cases, especially for the very homogeneous gels prepared with DAP2000 and DAP3000 due to the term in the square root (eq. 49) becoming negative. Hence, only the more inhomogeneous samples, DAP1000, PAAm 1 mol% BIS and 0.35 mol% BIS were analysed this way in the reactor batch state. In the following chapter the results of the non-ergodic medium method will be compared with the results of the partial-heterodyne method.

4.4.2.3   Comparison of the Partial-Heterodyne and the Non-Ergodic Medium Method

As can be seen in Fig. 54, 55 and 56 the non-ergodic method gives essentially the same results as the partial-heterodyne method. This is not surprising, since the same data was used for the analyses and it shows that both approaches work reasonably well. Only, the difficulties with very homogeneous samples are more problematic for the non-ergodic method, since the unswollen samples comprising DAP2000 and DAP3000 could not be analysed with it, at all. In contrast, the partial-heterodyne technique produces results for those samples, and although they show some inconsistence they can easily be adjusted to meet the theoretical requirements. Consequently, in this chapter only the samples to which the non-ergodic method is applicable are compared, DAP1000, PAAm 1 mol% BIS and 0.35 mol% BIS.

Fig. 54: Diffusion coefficient, D, plotted versus the monomer concentration; left hand side: results yielded by the non-ergodic method, right hand side: results yielded by the partial-heterodyne method; open squares: DAP1000, filled squares: PAAm 1 mol% BIS, filled triangles: PAAm 0.35 mol% BIS
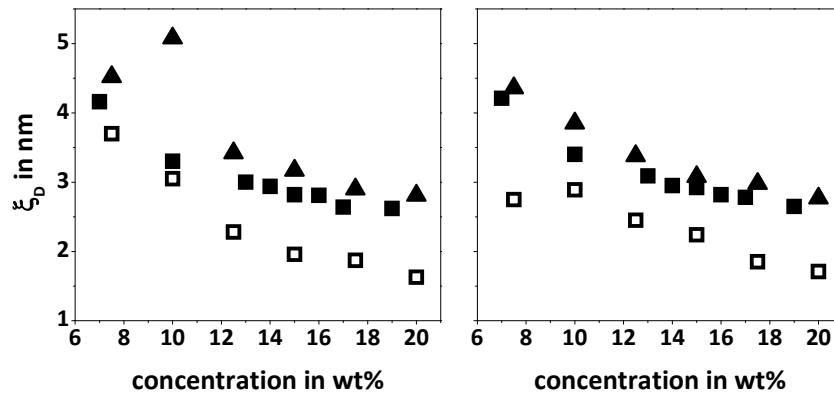
Fig. 55: Dynamic correlation length, ξ_D, plotted versus the monomer concentration; left hand side: results yielded by the non-ergodic method, right hand side: results yielded by the partial-heterodyne method; open squares: DAP1000, filled squares: PAAm 1 mol% BIS, filled triangles: PAAm 0.35 mol% BIS

The plateau value, $f(q,\infty)$, to which a FCF levels off in the non-ergodic method is directly comparable to the $\langle I_S \rangle_E / \langle I \rangle_E$ - value used in the partial-heterodyne method as a measure for network homogeneity. Both values describe the percentage of the intensity scattered from the static, non-fluctuating component within the observed network. For the most inhomogeneous series, PAAm 1 mol% BIS, a decrease of the inhomogeneity from low to high monomer concentration can be observed. The other samples are on average concentration independent (Fig. 56).
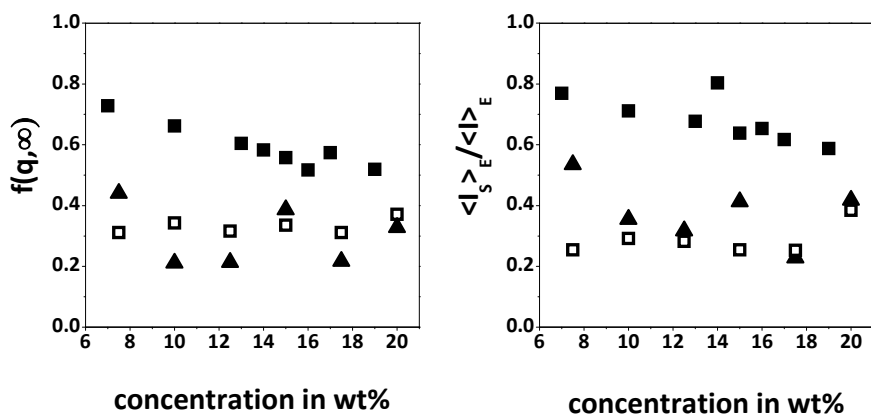
Fig. 56: Percentage of the scattered light stemming from the static part of the gel, $f(q,\infty)$ and $\langle I_S \rangle_E / \langle I \rangle_E$ (both measures for the network homo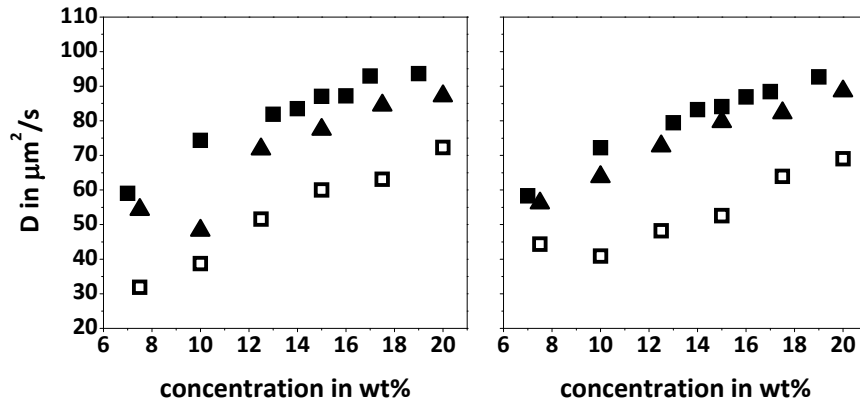geneity), plotted versus the monomer concentration; left hand side: results yielded by the non-ergodic method, right hand side: results yielded by the partial-heterodyne method; open squares: DAP1000, filled squares: PAAm 1 mol% BIS, filled triangles: PAAm 0.35 mol% BIS

In summary, the non-ergodic medium method and the partial-heterodyne method give very similar results. However both techniques have advantages and drawbacks that have to be considered when deciding which method to use. The non-ergodic method seems to fail when it comes to very homogeneous networks. It works reasonably well for more inhomogeneous samples, though, and it is not necessary to perform a very high number of measurements. The partial-heterodyne method copes much better with very homogeneous networks, even if the results are not entirely consistent with the theory in these cases. The number of measurements, however, has to be relatively high in order to obtain meaningful data, thus taking up much more time.

4.4.2.4 Determination of $\langle I_F \rangle$ by the Intensity Distribution in Speckle Patterns

In chapter 4.4.2.1 the $\langle I_F \rangle$ - values of the samples comprising DAP2000 and DAP3000, which seem unreasonably high, were adjusted by choosing the lowest value of $\langle I \rangle_{T,p}$ to be the actual $\langle I_F \rangle$, since it is theoretically the highest value that it should be able to adopt. The approach that is applied in this chapter[58,132,138,143,145] is similar. The examined polymer gels were measured at a very high number of positions (mostly 2000), whereas the method presented here does not involve the analysis of the ACF of all those measurements. Thus, it is not possible to make statements about diffusion coefficients or correlation lengths. The chief point is the determination of the network homogeneity by ascertaining $\langle I_F \rangle$. Executing such a very high number of measurements, the distribution of the yielded $\langle I \rangle_{T,p}$ - values in the resulting speckle pattern (Fig. 57) should be statistically significant.
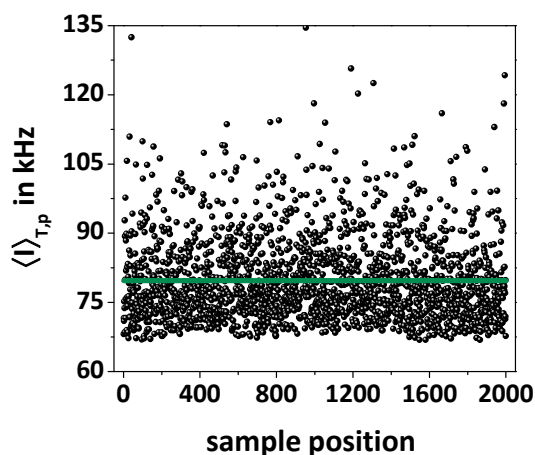
Fig. 57: Speckle pattern of the thiol-ene sample DAP2000 17.5 wt% from a measurement at 2000 positions; the black dots denote the scattering intensities, $\langle I \rangle_{T,p}$, at the different positions that were measured; the green line denotes the overall ensemble average scattering intensity, $\langle I \rangle_E$

In a plot of the intensity distribution, $P(\langle I \rangle_{T,p})$ (Fig. 58), of a speckle pattern, the frequency of the data points is zero at very low intensities. At a certain intensity it sharply increases, which can also be observed in fig. 57. This increase stems from the fluctuating part of the scattering intensity, $\langle I_F \rangle$, which, in an ergodic system, would also be the ensemble average scattering intensity, $\langle I \rangle_E$. At intensities higher than $\langle I_F \rangle$, which are caused by additional static

components within the observed network, and which raise $\langle I \rangle_E$ towards higher values, the data frequency decays exponentially.
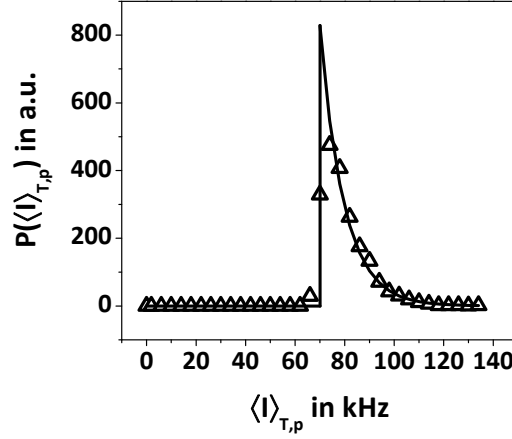
Fig. 58: Plot of the intensity distribution, $P(\langle I \rangle_{T,p})$, versus the time-average scattering intensity, $\langle I \rangle_{T,p}$, of the sample DAP2000 17.5 wt%; open triangles: experimental data, black curve: fit according to eq. 74; interval size: 4 kHz

The intensity distribution, $P(\langle I \rangle_{T,p})$, is proportional to the product of the HEAVISIDE step function and an exponential factor that decays with increasing intensity of the static component, $\langle I_S \rangle_{T,p} = \langle I \rangle_{T,p} - \langle I_F \rangle$ (eq. 72). Fitting this equation to the experimental data yields $\langle I_F \rangle$ and consequently $\langle I_S \rangle_E / \langle I \rangle_E$.

$$P\left(\langle I \rangle_{T,p}\right) \propto H\left(\langle I \rangle_{T,p} - \langle I_F \rangle\right) \cdot \exp\left[-\frac{\langle I \rangle_{T,p} - \langle I_F \rangle}{\langle I \rangle_E - \langle I_F \rangle}\right] \qquad (\,72\,)$$

The so-called HEAVISIDE step function, $H(x)$, in this case simply describes the fact that at low intensities (below $\langle I_F \rangle$) the only value the intensity distribution curve adopts is zero, and at $\langle I_F \rangle$ it increases in an instant up to its maximum (eq. 73).

$$H(x) = \begin{cases} 0 & \text{if } x < 0 \\ 1 & \text{if } x > 0 \end{cases} \qquad (\,73\,)$$

124

Each of the samples displayed in table 18 was measured at 2000 different positions (except for DAP1000 15 wt% for which one of the usual measurements was employed) and afterwards the data were grouped into intervals of different size, depending on the broadness of the intensity distribution (from 40 kHz intervals for PAAm 1 mol% BIS 15 wt% to 2 kHz intervals for DAP3000 20 wt%). The fitting function that was used, is eq. 74. The HEAVISIDE step function was indirectly incorporated in the equation by the amplitude A of the exponential decay. The cutoff value yielding $\langle I_F \rangle$ is determined from the exponential factor, with the ensemble average scattering intensity, $\langle I \rangle_E$, being determined from the average of the $\langle I \rangle_{T,p}$ - values.

$$P\left(\langle I \rangle_{T,p}\right) = A \cdot \exp\left[-\frac{\langle I \rangle_{T,p} - \langle I_F \rangle}{\langle I \rangle_E - \langle I_F \rangle}\right] \qquad (74)$$

The results that were obtained for the five samples are displayed in table 24. Compared to the partial-heterodyne method, $\langle I_S \rangle_E / \langle I \rangle_{E,p-h}$, both methods have a very similar outcome, whereas the deviation is higher for the PAAm samples than for the TEP samples, if the corrected values for DAP2000 and DAP3000 are considered. The order of homogeneity is the same, only the inhomogeneity of the PAAm 1 mol% BIS samples is underrated compared to the partial-heterodyne method.

Table 24: Results of the statistical method used on samples that were measured at 2000 positions (except for DAP1000 15 wt% with 100 positions); $\langle I \rangle_E$: ensemble average scattering intensity, A: amplitude of the exponential decay (eq. 74), $\langle I_F \rangle$: scattering intensity of the thermally fluctuating component, $\langle I_S \rangle_E / \langle I \rangle_E$: measure for network homogenety determined from the statistical method, $\langle I_S \rangle_E / \langle I \rangle_{E,p-h}$: measure for network homogenety determined by the patial-heterodyne method; the $\langle I_S \rangle_E / \langle I \rangle_{E,p-h}$-values for the DAP2000 and DAP3000 samples are either ascertained by the partial-heterodyne method (left) or by using the lowest $\langle I \rangle_{T,p}$-value as $\langle I \rangle_F$ (right)

	$\langle I \rangle_E$ in kHz	A	$\langle I_F \rangle$ in kHz	$\langle I_S \rangle_E / \langle I \rangle_E$	$\langle I_S \rangle_E / \langle I \rangle_{E,p-h}$
DAP1000 15 wt%	196	19	153	0.22	0.25
DAP2000 17.5 wt%	80	822	70	0.13	0.05 / 0.13
DAP3000 20 wt%	53	693	48	0.09	-0.03 / 0.11
PAAm 1 mol% BIS 15 wt%	747	227	395	0.47	0.59
PAAm 0.35 mol% BIS 17.5 wt%	426	233	302	0.29	0.23

In conclusion, this method shows that for very homogeneous networks, which pose certain problems to the partial-heterodyne analysis, the estimation concerning the fluctuating part of the scattering intensity being in the range of the lowest intensity speckle is a reasonable approach. The strategy used here is essentially the same and gives comparable results.

4.4.2.5 Influence of the Ambient Temperature on the Homogeneity of the TEP-Samples

The thiol-ene networks largely consist of ethoxy groups and can thus reasonably well be compared to pure PEG or polyethylene oxide (PEO, M > 35,000 g/mol). Dissolved in water, PEO is known to have a lower critical solution temperature (LCST) leading to phase separation at elevated temperatures[157]. The LCST depends on the composition of the solution and the molar mass of the PEO. The higher the molar mass is, the lower becomes the LCST, down to around 100 °C at M $\cong 1 \cdot 10^6$ g/mol. The usual measurement temperature for the DLS measurements was 25 °C. Raising the measurement temperature of a PEO/water solution should have an effect on the detected data, since with increasing temperature the quality of the solvent deteriorates yielding gradual reduction of the excluded volume and thus contraction of the polymer coils. In the case of this thesis the network is not swollen in pure water but in a mixture with ethanol. However, due to the high percentage of water, an effect is still expected if the measurement temperature is increased.

The measurements at different temperatures were carried out with the three thiol-ene samples displayed in table 18. Fig. 59 shows an example of the effect of the varying temperature on the speckle pattern of a TEP hydrogel with the DAP2000 17.5 wt% sample. It is evident that the overall scattering intensity increases with rising temperature, the scatter of the data does, however, not seem to become more pronounced. The same behaviour can be observed for the two other samples, DAP1000 15 wt% and DAP3000 20 wt%. The increase in scattering intensity can be explained by stronger concentration fluctuations due to the gradual worsening of the solvent quality.
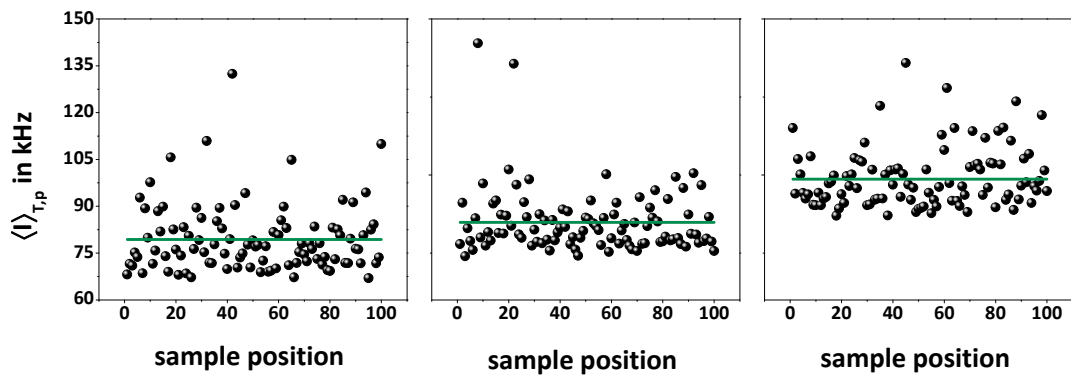
Fig. 59: Speckle patterns of the thiol-ene sample DAP2000 17.5 wt% measured at 25 °C (left hand side), 35 °C (middle) and 45 °C (right hand side); the black dots denote the scattering intensities, $\langle I \rangle_{T,p}$, at the different positions that were measured; the green lines denote the ensemble average scattering intensity, $\langle I \rangle_E$

Although the temperature increase has an easily perceivable effect on the scattering intensity of the samples, the $\langle I_S \rangle_E / \langle I \rangle_E$ - values hardly change at all, at least there is no noticeable, consistent tendency (Fig. 60). This means, within the range that was examined the homogeneity of the samples was not affected by the measurement temperature. The diffusion coefficient increased with rising temperature causing the correlation length, ξ_D, to decrease (Fig. 61).
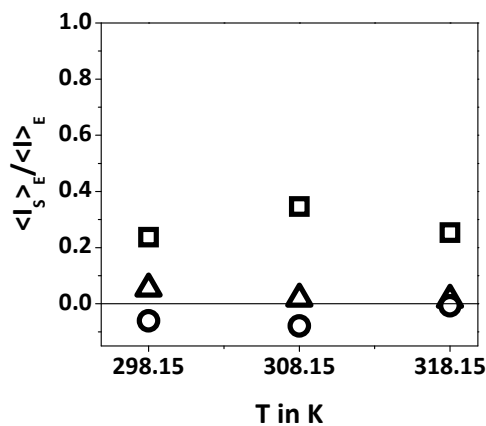
Fig. 60: $\langle I_S \rangle_E / \langle I \rangle_E$ plotted versus the measurement temperature, T; open squares: DAP1000 15 wt%, open triangles: DAP2000 17.5 wt%, open circles: DAP3000 20 wt%
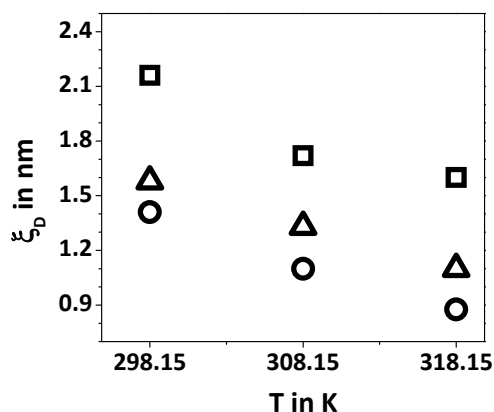
Fig. 61: ξ_D plotted versus the measurement temperature, T; open squares: DAP1000 15 wt%, open triangles: DAP2000 17.5 wt%, open circles: DAP3000 20 wt%

4.4.2.6   Additional Dithiol

The reactants usually used for a thiol-ene crosslinking polymerisation were a trifunctional thiol and an difunctional ene. Ruling out homopolymerisation, this approach leads to an end-linking reaction. In order to proceed to a mechanism that allows to build up network chains that do not only comprise the diene and thus always have the same chain length, a difunctional thiol was added to the reaction mixture in different proportions (see chapter 3.6.4). The mechanism is then no longer determined by pure end-linking but with increasing amount of dithiol the focus is more and more on the step-growth nature of the reaction. The basic reaction mixture that was used for the measurement without dithiol was DAP2000 17.5 wt%. The formulations were prepared in such a way that always the same number of functional groups was present. Fig. 62 shows the results of the rheological measurements of these systems. With increasing amount of dithiol replacing the trithiol, the elastic modulus decreased since the crosslinker concentration reduced, as well. At a concentration of around 60 mol% of the thiol groups being contributed by the dithiol, the viscous modulus became higher than the elastic modulus, since the amount of crosslinker no longer sufficed to form a continuous network.

Fig. 62: Shear moduli of the samples in table 12 plotted versus the percentage of thiol groups in the reaction mixture, stemming from the dithiol; open pentagons: plateau-values of the elastic modulus, G'_∞; filled pentagons: plateau-values of the viscous modulus, G''_∞; parameters: 1 % strain, oscillation frequency: 1 Hz; the dashed line illustrates the highest value of G'_∞ that can theoretically be obtained for a phantom network

The dashed line in fig. 62 shows the theoretically possible elastic modulus, G'_{th}. The increasing gap between the values of G' and G'_{th} is a sign of the crosslinking efficiency decreasing with increasing dithiol concentration. This observation is illustrated in fig. 63. The crosslinking efficiency decreases significantly even when only a small amount of dithiol is added. This is an indication of the formation of more and more elastically inactive chains owing to network defects, like loops, dangling chains and highly crosslinked clusters, with rising dithiol concentration.

Fig. 63: Crosslinking efficiency, ε, of the samples in table 12 plotted versus the percentage of thiol groups in the reaction mixture, stemming from the dithiol

The course of the fluctuating component of the scattering intensity, $\langle I_F \rangle$, and the overall scattering intensity, $\langle I \rangle_E$, can be seen in fig. 64. While, up to 50 mol%, $\langle I \rangle_E$ increases with increasing dithiol concentration, $\langle I_F \rangle$ decreases. This signifies that the percentage of light scattered from thermally fluctuating chains is getting lower, the more the polymerisation mechanism deviates from the end-linking process and, simultaneously, the more the monomer concentration rises with increasing substitution.

At high dithiol concentrations, that no longer allow the formation of a continuous network (60 and 75 mol% of the thiol groups stemming from the dithiol) $\langle I_F \rangle$ and $\langle I \rangle_E$ approach each other again, the proportion of the fluctuating intensity becoming very high again. Uncrosslinked polymer solutions are ergodic systems in which there is no difference between the fluctuating part of the scattering intensity and the overall scattering intensity.
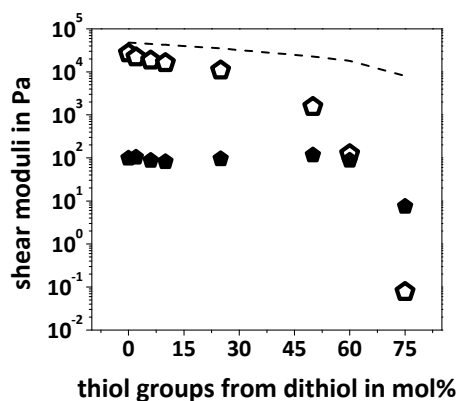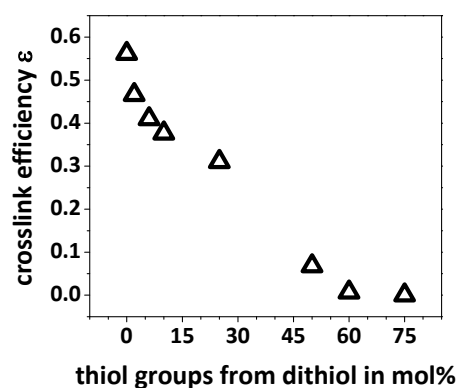

Fig. 64: Scattering intensity of the samples in table 12 plotted versus the percentage of thiol groups in the reaction mixture, stemming from the dithiol; hexagons: scattering intensity of the thermally fluctuating component, $\langle I_F \rangle$; rhombuses: ensemble-average scattering intensity, $\langle I \rangle_E$

Fig. 65 illustrates the same circumstances from another point of view. The ratio $\langle I_S \rangle_E / \langle I \rangle_E$ shows that the inhomogeneity of the samples increased with increasing dithiol concentration although the crosslinker concentration decreased simultaneously which usually leads to an improved *homogeneity*. At the highest dithiol concentration that still yielded a sufficiently crosslinked network, 50 mol%, the inhomogeneity even rose to a value that is in the same range as for the rather inhomogeneous PAAm 1 mol% BIS samples. The two following samples with an even higher dithiol concentration exhibited a decreased inhomogeneity again, since the samples were not crosslinked anymore. Polymer solutions do not show such spatial inhomogeneity. The well-defined, uniform network structure achieved by the end-linking process of the system only comprising a trithiol and a diene could obviously not be maintained.
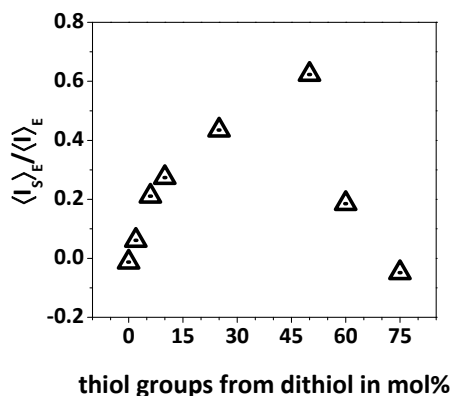
Fig. 65: $\langle I_S \rangle_E / \langle I \rangle_E$ of the samples in table 12 plotted versus the percentage of thiol groups in the reaction mixture, stemming from the dithiol

As the amount of crosslinker decreases the amount of dithiol rises, altering the reaction mechanism. Since the diene cannot only react with the trithiol (crosslinker) anymore but also with the dithiol, it is no longer merely one diene chain alternating with the crosslinker but the network chains are theoretically capable of growing longer. In fig. 66 it can be seen that the diffusion coefficient increases and the dynamic correlation length, ξ_D, accordingly decreases as more dithiol is added. At the point where there is no efficient crosslinking anymore, ξ_D strongly rises again. The probability for the formation of entanglements among the network chains should grow with their molar mass, introducing additional physical crosslinks. This could be an explanation for the decreasing correlation length at the lower

dithiol concentrations. However, the strong decrease in the crosslinking efficiency with rising dithiol content (Fig. 63) does not support this theory.

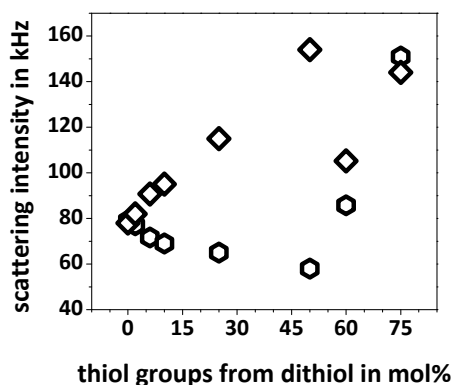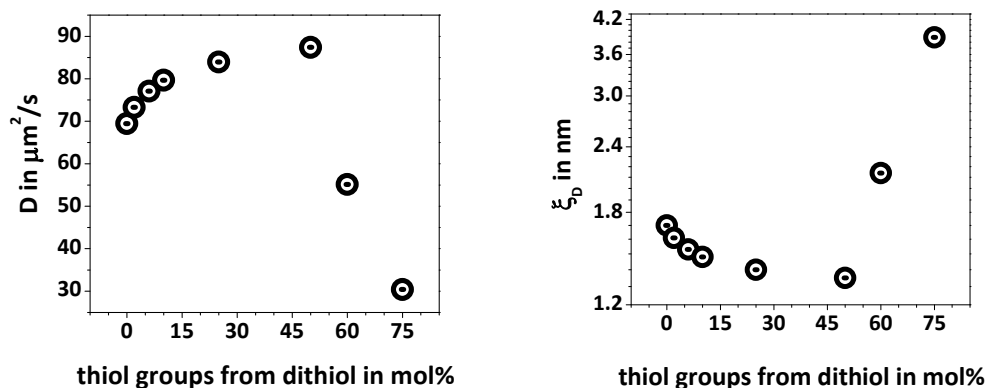Fig. 66: Left hand side: Diffusion coefficient, D, of the samples in table 12 plotted versus the percentage of thiol groups in the reaction mixture, stemming from the dithiol; Right hand side: Dynamic correlation length, ξ_D, of the samples in table 12 plotted versus the percentage of thiol groups in the reaction mixture, stemming from the dithiol

4.4.2.7   Summary of Reactor Batch Hydrogels

The experiments performed on the two systems, TEP and FCC, clearly show that the thiol-ene polymerisation is capable of forming much more homogeneous networks than the free radical crosslinking copolymerisation. Depending on the way they are analysed, it even seems as if the networks are completely homogeneous with respect to their concentration distribution. The DAP2000 and DAP3000 gels appear to have no significant spatial concentration fluctuations. However, not all networks prepared with TEP are this homogeneous. The resulting structure strongly depends on the reactants. In a system of a trithiol as the crosslinker and a diene forming the network chains it is e.g. necessary for the diene to have a sufficiently high molar mass and concentration, so that the tendency to form loops or dangling chains is suppressed[84].

The experiment in chapter 4.4.2.6 shows that the most vital characteristic of the thiol-ene polymerisation presented in this thesis is its end-linking fashion. Exhibiting sufficiently long network chains and suppressing homopolymerisation of the ene, this mechanism is predestined to yield homogeneous networks. As soon as the pure end-linking process is

132

disturbed by adding a dithiol, the inhomogeneity strongly increases although the crosslinker concentration decreases, which usually promotes the formation of more homogeneous networks.

A fundamental problem of very homogeneous gels seems to be the characterisation with DLS analysis methods. The non-ergodic medium method appears to be incapable of describing very homogeneous gels, since it is impossible to generate results for them. Utilising the partial-heterodyne method, it is possible to obtain data for the very homogeneous gels, however they are not entirely consistent with the underlying theory.

4.4.3   Equilibrium Swollen Hydrogels

It is a commonly known fact that polymer gels that are swollen to the equilibrium degree of swelling scatter light stronger than the corresponding reactor batch gels and are more inhomogeneous in their structure[58,78]. In the reactor batch state there are always regions within the gel that are more strongly crosslinked as well as regions that exhibit a lower crosslink density. However, owing to a still rather evenly distributed polymer concentration it may not have a strong impact on the scattering intensity. Subjecting the gel to equilibrium swelling, however, brings out the non-uniformity in the crosslink concentration, since the zones that are more highly crosslinked do not swell as much as the less crosslinked ones. This yields a system with much greater concentration differences than before leading to stronger scattering.

This effect can be very well seen in the speckle patterns of the swollen hydrogels (TEP: Fig. 67 & PAAm: Fig. 68). For the equilibrium swollen hydrogels the ensemble average scattering intensity increased by a factor of three to six compared to the reactor batch swollen hydrogels, depending on the sample (Table 25). The scattering intensity of the more homogeneous samples increases more strongly than that of the more inhomogeneous ones. Compared to the increase in $\langle I \rangle_E$ the fluctuating component $\langle I_F \rangle$ only becomes slightly larger due to swelling.
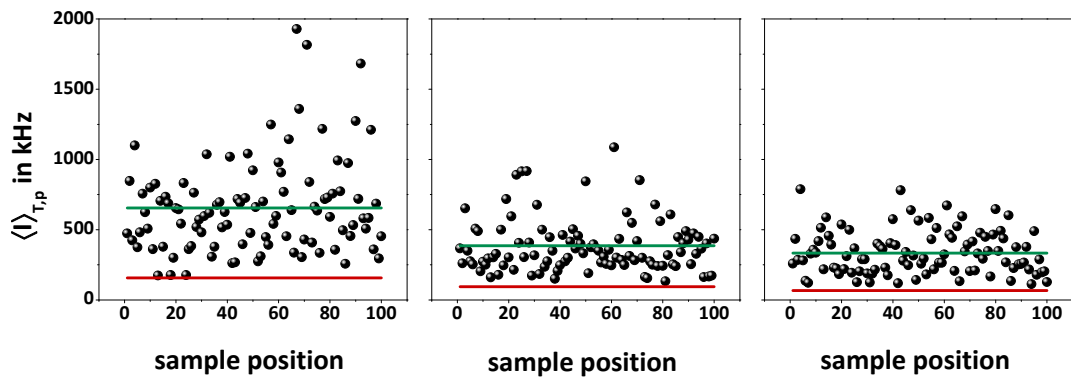
Fig. 67: Speckle patterns of the equilibrium swollen thiol-ene samples DAP1000 15 wt% (left hand side), DAP2000 17.5 wt% (middle) and DAP3000 20 wt% (right hand side), see table 18; the black dots denote the scattering intensities, $\langle I \rangle_{T,p}$, at the different positions that were measured; the red lines denote the scattering intensity of the fluctuating part, $\langle I_F \rangle$; the green lines denote the overall ensemble average scattering intensity, $\langle I \rangle_E$; (compare to reactor-batch gels: Fig. 43, p. 109)
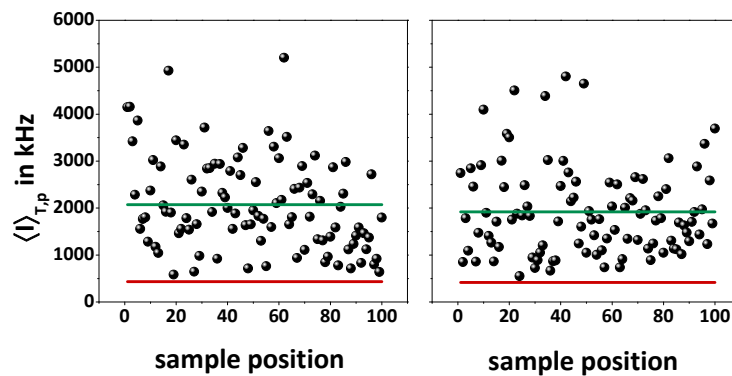
Fig. 68: Speckle patterns of the equilibrium swollen PAAm samples PAAm 1 mol% BIS 15 wt% (left hand side) and PAAm 0.35 mol% BIS 17.5 wt% (right hand side), see table 18; the black dots denote the scattering intensities, $\langle I \rangle_{T,p}$, at the different positions that were measured; the red lines denote the scattering intensity of the fluctuating part, $\langle I_F \rangle$; the green lines denote the overall ensemble average scattering intensity, $\langle I \rangle_E$; (compare to reactor-batch gels: Fig. 44, p. 109)

Table 25: Comparison of the results of the partial-heterodyne DLS method of reactor batch (rb) and equilibrium swollen (sw) gels; $\langle I_F \rangle$: scattering intensity of the thermally fluctuating component within a network, $\langle I \rangle_E$: ensemble average scattering intensity, $\langle I_S \rangle_E$: scattering intensity of the static component within a network, $\langle I_S \rangle_E / \langle I \rangle_E$: measure for network homogeneity

	DAP1000 15 wt%	DAP2000 17.5 wt%	DAP3000 20 wt%	PAAm 1 mol% BIS 15 wt%	PAAm 0.35 mol% BIS 17.5 wt%
$\langle I_F \rangle_{rb}$ in kHz	147.4	83.4	54.3	317.6	330.8
$\langle I_F \rangle_{sw}$ in kHz	155.9	93.8	68.0	436.3	415.0
$\langle I \rangle_{E,rb}$ in kHz	197.7	87.5	52.9	781.9	428.5
$\langle I \rangle_{E,sw}$ in kHz	654.9	386.2	334.1	2076.2	1919.1
$\langle I_S \rangle_{E,rb}$ in kHz	50.3	4.1	- 1.4	464.3	97.7
$\langle I_S \rangle_{E,sw}$ in kHz	499.0	292.4	266.1	1639.9	1504.1
$(\langle I_S \rangle_E / \langle I \rangle_E)_{rb}$	0.25	0.05	- 0.03	0.59	0.23
$(\langle I_S \rangle_E / \langle I \rangle_E)_{sw}$	0.76	0.76	0.80	0.79	0.78

The higher inhomogeneity of the equilibrium swollen gels can also be observed in the ICF measured at different positions within the sample (Fig. 69).
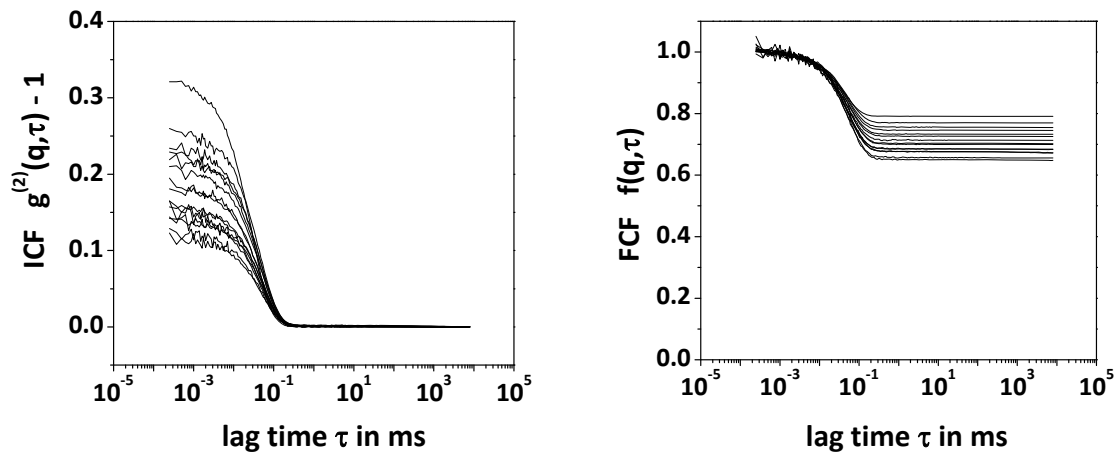
Fig. 69: : Typical correlation curves in the non-ergodic method for the equilibrium swollen sample DAP1000 15 wt%; left hand side: ICF measured at different positions within the same sample, right hand side: FCF calculated from the ICF by eq. 49; note the logarithmic scale of the x-axes and the different scales of the y-axes; (compare to reactor-batch gels: Fig. 53, p. 119)

On average, their y-axis intercept decreased by a factor of around three, dependent on the sample and the particular position within it. Using the non-ergodic medium method on the ICF, the resulting offset values increase visibly, thus indicating a considerably higher frozen-in fraction in the samples.

The inhomogeneity of both the TEP and PAAm samples, described by the $\langle I_S \rangle_E / \langle I \rangle_E$ - values, is illustrated in fig. 70. Both methods, partial-heterodyne and non-ergodic, give similar results, thus only the ones determined from the partial-heterodyne method are shown.
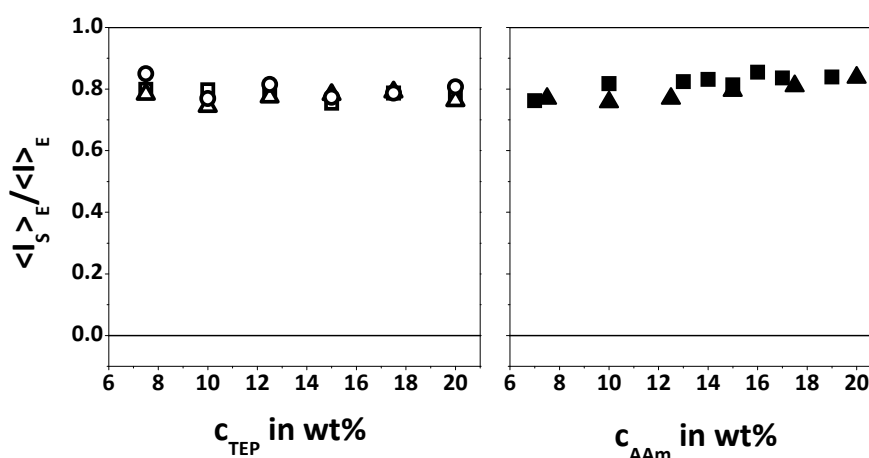
Fig. 70: $\langle I_S \rangle_E / \langle I \rangle_E$ of the equilibrium swollen samples plotted versus the monomer concentration, $c_{TEP/AAm}$; left hand side: TEP samples, open squares: DAP1000, open triangles: DAP2000, open circles: DAP3000; right hand side: PAAm samples, filled squares: PAAm 1 mol% BIS, filled triangles: PAAm 0.35 mol% BIS; (compare to reactor-batch gels: Fig. 48, p. 114)

The static part of the networks increased up to about 80 %, basically the same proportion for all the measured samples. Thus, the relative increase in inhomogeneity was significantly higher for the hydrogels that had originally been more homogeneous, whereas for the lowly concentrated PAAm 1 mol% BIS samples there is almost no increase in inhomogeneity, at all (Table 25). On the one hand this means that the last-named PAAm samples are already so inhomogeneous in the state of preparation, that not much further difference in concentration can be caused by swelling. Additionally, they also have the lowest degree of swelling, Q_m, of all the five series (Fig. 30, p. 89) and, particularly the PAAm 1 mol% BIS, also the lowest relative degree of swelling, $Q_{m,rel}$, (Fig. 31, p. 90). The increase in inhomogeneity

by swelling is certainly more pronounced the stronger a sample swells. On the other hand it has to be concluded that even the most homogeneous samples in the reactor batch state (DAP3000) have the potential to swell rather non-uniformly. This signifies for those reactor batch gels to have a rather homogeneous concentration distribution of the polymer chains but also inhomogeneities, like loops and domains of higher crosslinker density, that do not become visible until the network is swollen. They are not detectable in the state of preparation because they do not affect the homogeneous polymer concentration distribution.

As with the reactor batch gels, the diffusion coefficient increases with increasing monomer concentration (Fig. 71). For the TEP hydrogels all three series exhibit lower values for the diffusion coefficient than in the state of preparation. The same holds true for the PAAm 0.35 mol% BIS samples. This is an expected result since swelling should essentially lead to an expansion of the network chain coils and an increased distance of the network junctions. Consequently, those coils are partially disentangled so that the chain segments which move correlatedly become longer, decreasing the diffusion coefficient.
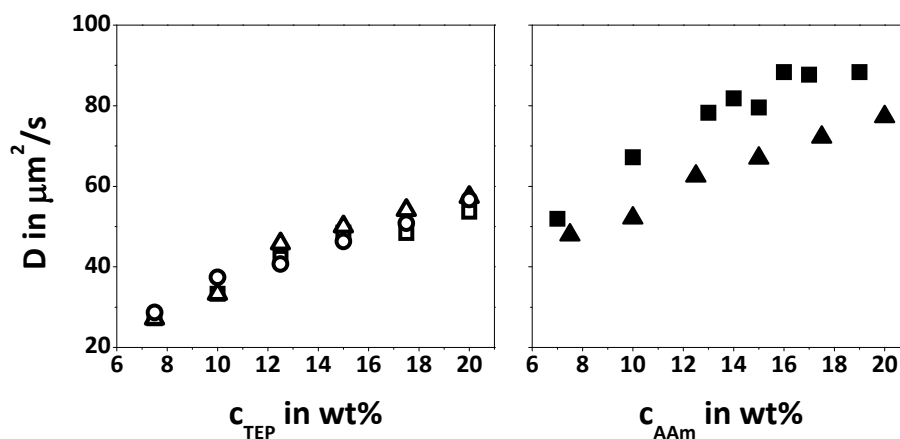
Fig. 71: Diffusion coefficient, D, of the equilibrium swollen samples determined by the partial-heterodyne method plotted versus the overall monomer concentration; left hand side: TEP samples, open squares: DAP1000, open triangles: DAP2000, open circles: DAP3000; right hand side: PAAm samples, filled squares: PAAm 1 mol% BIS, filled triangles: PAAm 0.35 mol% BIS; (compare to reactor-batch gels: Fig. 46, p. 113)

The correlation length, which describes the distance between neighbouring network junctions, becomes higher when the networks are swollen (Fig. 72), suiting the image of the crosslinks moving apart with rising degree of swelling. The PAAm 1 mol% BIS series exhibits almost the same values for the diffusion coefficient as in the reactor batch state. As already mentioned, the degree of sweeling, Q_m, of these samples is the lowest compared to the other samples at the same concentration (chapter 4.2). Thus, the volume of the network chains and the distance between the network junctions do not increase as significantly as for the other series, yielding a less pronounced difference in the diffusion coefficient.
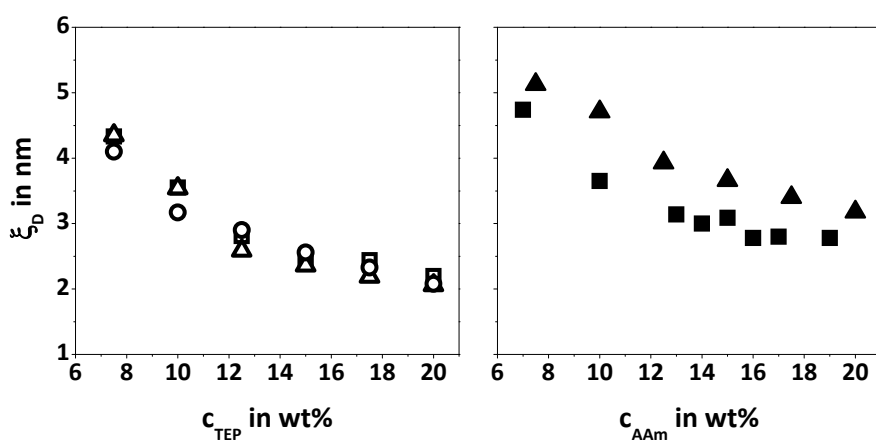
Fig. 72: Dynamic correlation length, ξ_D, of the equilibrium swollen samples determined by the partial-heterodyne method plotted versus the overall monomer concentration; left hand side: TEP samples, open squares: DAP1000, open triangles: DAP2000, open circles: DAP3000; right hand side: PAAm samples, filled squares: PAAm 1 mol% BIS, filled triangles: PAAm 0.35 mol% BIS; (compare to reactor-batch gels: Fig. 47, p. 113)

In fig. 73 the correlation lengths, ξ_D, are plotted versus the equilibrium degree of swelling, Q_m. An evidently positive slope signifies that the average distance between the network junctions is higher if a sample exhibits a higher degree of swelling. Since that involves a smaller amount of crosslinker molecules, this was to be expected. For the PAAm samples, a smaller increase in Q_m results in a considerably stronger rise of ξ_D than for the TEP samples.
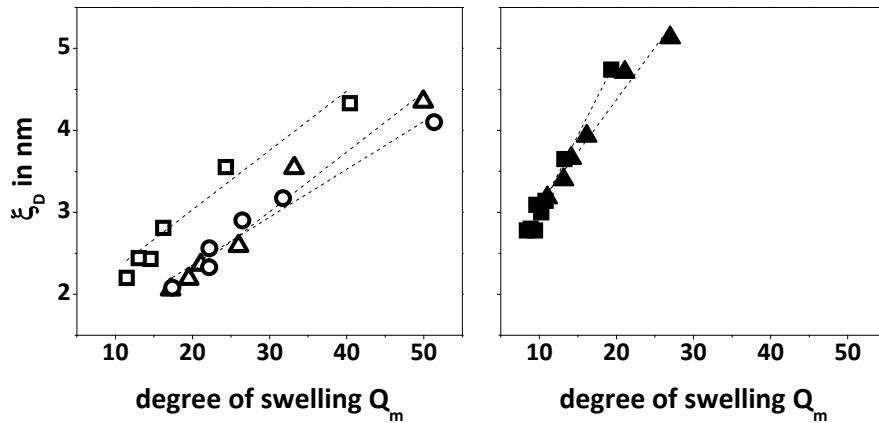
Fig. 73: Dynamic correlation length, ξ_D, of the equilibrium swollen samples determined by the partial-heterodyne method plotted versus the equilibrium degree of swelling, Q_m; left hand side: TEP samples, open squares: DAP1000, open triangles: DAP2000, open circles: DAP3000; right hand side: PAAm samples, filled squares: PAAm 1 mol% BIS, filled triangles: PAAm 0.35 mol% BIS

4.5 Static Light Scattering

The static light scattering measurements were analysed by the DEBYE-BUECHE approach (chapter 2.3.2). This method is based on comparing the RAYLEIGH-ratio of a polymer gel to the one of a corresponding polymer solution. The resulting excess scattering that is induced by gels usually scattering light stronger than solutions because of spatial inhomogeneity, is a measure for the inhomogeneity of the observed gel. However, the more highly concentrated PAAm hydrogels behaved the opposite way, the polymer solution scattering the incident light stronger than the corresponding gel. This results in a negative excess scattering, implying the PAAm-solutions to be more inhomogeneous than the gels. Consequently, only the reactor-batch TEP hydrogels were analysed by SLS. In chapter 3.6.3 it was concluded that the thiol-ene gels have essentially the same refractive-index increment as pure PEG35,000, $dn/dc \cong 0.13$. Thus, due to a lack of a sufficiently high amount of linear TEP-polymer, PEG35,000 solutions in the water-ethanol mixture were used for acquiring the data of the polymer solutions.

Fig. 74 demonstrates the excess RAYLEIGH-ratio, $R_{ex}(q)$, of the three TEP series. Dynamic light scattering measurements demonstrated that among the three series the inhomogeneity decreases from DAP1000 over DAP2000 to DAP3000 (chapter 4.4.2.7).

Fig. 74: Excess RAYLEIGH-ratio, $R_{ex}(q)$, plotted versus the square of the scattering vector, q; left hand side: DAP1000, middle: DAP2000, right hand side: DAP3000

As can be seen here, the same statement holds true for static light scattering. On average, the DAP1000 samples show the highest excess scattering, meaning that the gels scatter the incident light considerably stronger than the solution. This can be equated with DAP1000 exhibiting the spatially most inhomogeneous samples. For DAP2000 the excess scattering reduces and it decreases even more for DAP3000, except for the 7.5 wt% sample which is considered to be an outlier.

Another look at fig. 74 shows that there is hardly any angle dependence of the excess RAYLEIGH-ratio. Almost all of the datasets are rather close to being horizontal lines. Usually, for comparatively large structures within a measured sample (larger than 1/20 of the wavelength of the incident light) the scattering intensity, and with it the RAYLEIGH-ratio, become angle dependent due to intramolecular interference effects[127]. The scattering centres in such structures are relatively far apart from one another so that the light scattered from them exhibits a distinct path difference, which becomes more and more pronounced while the scattering angle or the scattering vector, q, increases. Consequently, the RAYLEIGH-ratio decreases noticeably moving from lower onto higher scattering vectors. At q = 0 the path difference disappears. Accordingly, the q-independent RAYLEIGH-ratios in fig. 74 show that there are no scattering domains within the observed gels that are large enough to provoke intramolecular interference.

The independence of the results on the scattering vector lead to difficulties in the DEBYE-BUECHE evaluation. The typical graph of this analysis is the inverse of the square root of $R_{ex}(q)$ plotted versus q^2 as illustrated in fig. 75. This plot should theoretically show data that can reasonably well be fitted by straight lines exhibiting a positive slope. In the present cases the slopes were mainly positive but very small. Some of the samples, however, had slightly negative slopes and could thus not be evaluated. This happened especially often for the DAP3000 samples.

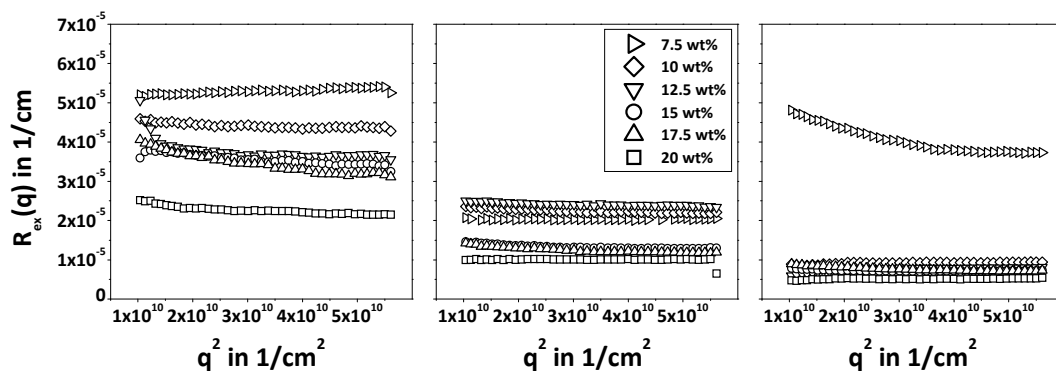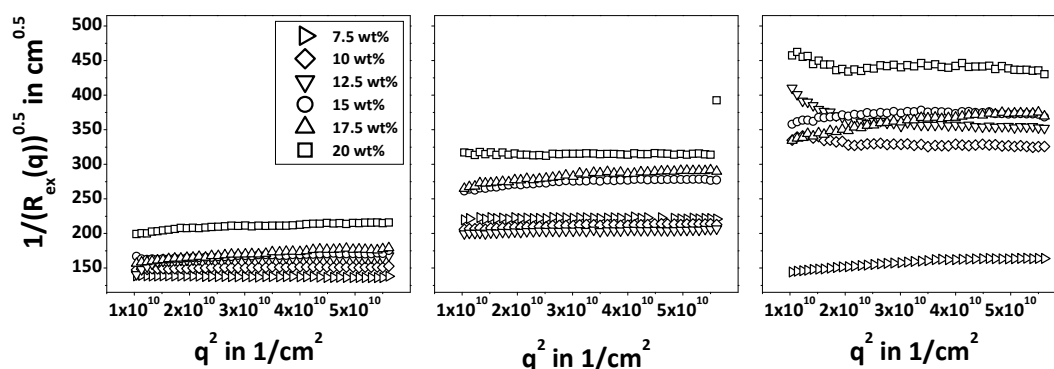Fig. 75: Typical DEBYE-BUECHE plots with the inverse of the square root of the excess RAYLEIGH-ratio, R_{ex}, plotted versus the square of the scattering vector, q; left hand side: DAP1000, middle: DAP2000, right hand side: DAP3000

In the following the results that could be determined will be shown. It has to be kept in mind that due to the angle indpendence of the data the SLS results are not as meaningful as the DLS results, especially for the DAP3000 series.

In fig. 76 the mean square refractive index fluctuation, $\langle \delta n^2 \rangle$, is shown, acquired from the straight line fits of the data in fig. 75 according to eq. 58. For the DAP1000 and DAP2000 series the 7.5 wt% samples could not be evaluated and for the DAP3000 series the concentrations 10 wt%, 12.5 wt% and 20 wt% could not be calculated, all due to negative slopes in the DEBYE-BUECHE plot. The mean square refractive index fluctuation is a measure for the magnitude of the spatial network inhomogeneities. The higher $\langle \delta n^2 \rangle$ is, the more pronounced are the differences in refractive index within the sample and thus the more uneven is the polymer concentration distribution yielding a higher light scattering intensity. Accordingly, the lowly concentrated DAP1000 samples that exhibit the highest excess RAYLEIGH-ratio also possess the strongest refractive index fluctuations due to a comparatively inhomogeneous concentration distribution.
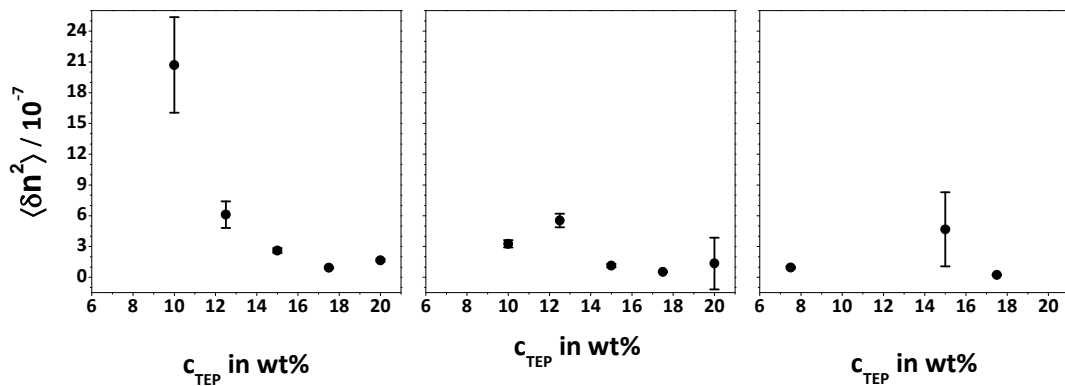
Fig. 76: Mean square refractive index fluctuation, $\langle \delta n^2 \rangle$, plotted versus the monomer concentration, c_{TEP}; left hand side: DAP1000, middle: DAP2000, right hand side: DAP3000

Fig. 77 illustrates the static correlation length, ξ_S, of the three different TEP series. The range of the static correlation lengths lies between 6 and 18 nm and is thus noticeably smaller than 1/20 of the wavelength of the incident laser light ($\cong$ 32 nm), consistent with the q-independent scattered light intensity. Compared to the dynamic correlation length, ξ_D, which exhibits values of 1.5 to 3.5 nm, ξ_S is considerably larger. ξ_D is interpreted to be a measure for the average distance between neighbouring network junctions. ξ_S, however, describes the average dimension of the refractive index[174]. Although there does not seem to be a strict order of ξ_S with regard to the monomer concentration, a general increase can be observed from low to high concentrations (disregarding the DAP3000 7.5 wt% sample which was considered to be an outlier before).
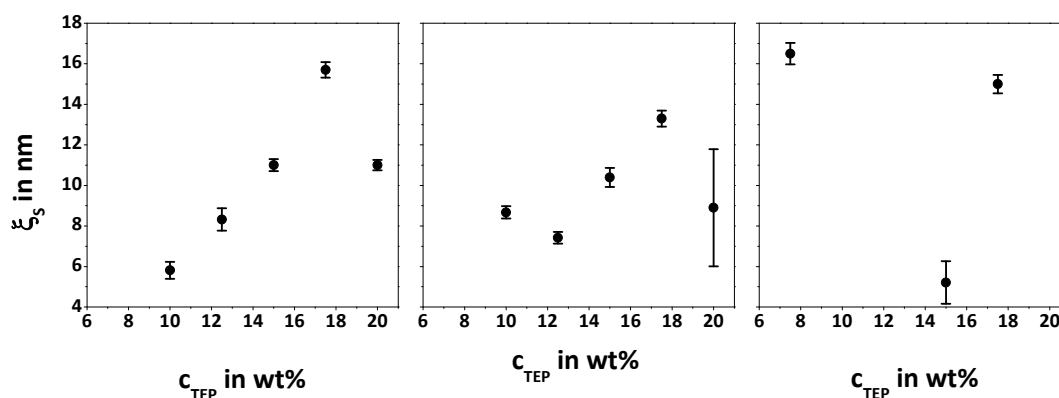
Fig. 77: Static correlation length, ξ_S, plotted versus the monomer concentration, c_{TEP}; left hand side: DAP1000, middle: DAP2000, right hand side: DAP3000

The fluctuation in refractive index can be recalculated to a fluctuation in concentration, $\langle\delta c^2\rangle$, according to eq. 59. Those fluctuations can then be compared to the overall monomer concentration, which is a measure for the average, macroscopic concentration of the observed gels. Fig. 78 demonstrates the concentration fluctuations as error bars of c_{TEP}. Especially for the lower concentrated samples of the DAP1000 series the deviations from the actual concentration of the systems are quite significant, the highest being 11 % for the DAP1000 10 wt% sample. The concentration varies by 11 mg/L in a sample of a macroscopic concentration of 98 mg/L. Although this seems to be a rather substantial discrepancy, it means that the lowest concentration in the system is still not close to zero, signifying that there are probably very few gaps in the polymer network and accordingly also few very highly concentrated microgel-like domains.
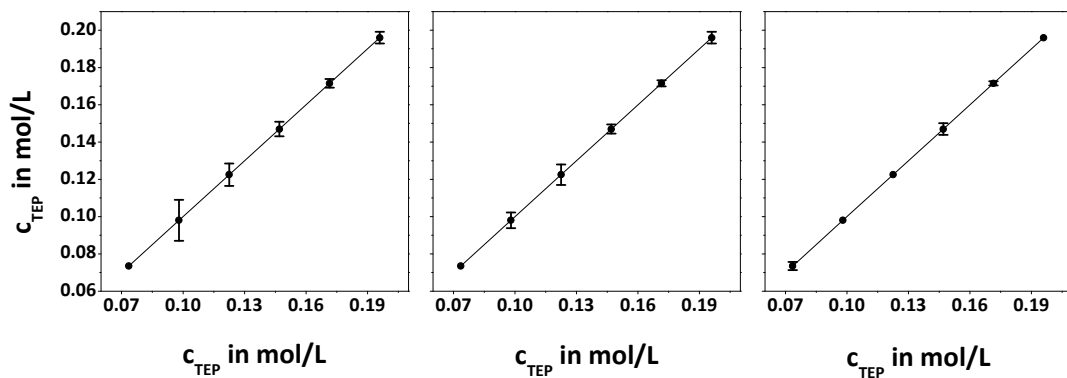
Fig. 78: Monomer concentration, c_{TEP}, plotted versus itself; left hand side: DAP1000, middle: DAP2000, right hand side: DAP3000; the error bars describe the deviation of the local concentration from the overall, macroscopic concentration of the system

All the other samples exhibit a lower concentration deviation (table 26), consistent with the fact that the sample DAP1000 10 wt% is the most spatially inhomogeneously sample of all the ones that could be analysed.

Table 26: Deviation of the local concentration ($c_{TEP} \pm \langle \delta c^2 \rangle^{0.5}$) from the overall monomer concentration c_{TEP}, for the samples of the three TEP series that could be evaluated by the DEBYE-BUECHE analysis

	c_{TEP} in wt%	7.5	10	12.5	15	17.5	20
DAP1000	$\langle \delta c^2 \rangle^{0.5}/c_{TEP}$	--	0.112	0.049	0.027	0.014	0.016
DAP2000	$\langle \delta c^2 \rangle^{0.5}/c_{TEP}$	--	0.044	0.047	0.018	0.010	0.014
DAP3000	$\langle \delta c^2 \rangle^{0.5}/c_{TEP}$	0.032	--	--	0.036	0.007	--

Unfortunately, for the DAP3000 series three samples could be evaluated and one of them seems to be an outlier. Again, light scattering measurements do not seem to be completely suitable to investigate very homogeneous network structures. In summary, it can be stated that the SLS measurements yielded results very similar to the ones obtained from DLS. The network homogeneity seems to improve from the DAP1000 to the DAP3000 series.

5   Summary and Conclusion

For this thesis thiol-ene hydrogels were characterised by rheology and by light scattering measurements. The aim was to find out about the homogeneity of those gels and to synthesise comparatively homogeneous network structures. As a reference polyacrylamide hydrogels, that were prepared by common free radical crosslinking copolymerisation (FCC), were used since they are well known for possessing rather inhomogeneous network structures. An important difference between those two systems is the polymerisation mechanism. The thiol-ene gels were formed by an end-linking polymerisation which is able to form very homogeneous networks if the network chain precursors (in this case the dienes) are sufficiently long. In contrast, the FCC often yields strong frozen-in concentration fluctuations due to the formation of highly crosslinked clusters in the beginning of the reaction.

The gels were examined in reactor batch state, i.e. directly after preparation, and in equilibrium swollen state. To be able to compare systems with macroscopically similar network structures, the reactor batch gels that were used possessed similar shear moduli as determined by rheological measurements.

The most important evaluation method for the network homogeneity was dynamic light scattering. The partial-heterodyne method and the non-ergodic medium method were employed, both with a very similar outcome. The results for the reactor batch state gels clearly demonstrated that the thiol-ene gels were more homogeneous than the polyacrylamide gels. Especially the thiol-ene gels with the longer diene chains (DAP2000 and DAP3000) showed virtually no inhomogeneity at all, according to dynamic light scattering.

Swelling the hydrogels to equilibrium led to an increase in inhomogeneity, especially pronounced for the very homogeneous reactor-batch gels. All the gels, thiol-ene and polyacrylamide, exhibited the same, rather high inhomogeneity, according to the dynamic light scattering measurements. In the state of preparation those gels exhibited an evenly distributed polymer concentration and potential defects did not have a strong impact on the scattering intensity. However, subjecting the gels to equilibrium swelling brought out the non-uniformity of the network concentration. Zones that were more highly crosslinked did not swell as much as the less crosslinked ones which yielded systems with much greater concentration differences than before, leading to stronger scattering.

147

This discrepancy between the reactor batch and the equilibrium swollen state gels is surprising. It seems as if the homogeneity combined with a very low scattering intensity in the state of preparation describes a very homogeneous....

A fundamental problem of the very homogeneous gels was the characterisation with DLS analysis methods. The non-ergodic medium method appeared to be incapable of describing very homogeneous gels. Utilising the partial-heterodyne method, it was possible to obtain data for the DAP2000 and DAP3000 gels, however they were not entirely consistent with the underlying theory.

In conclusion it can be said that in the state of preparation the thiol-ene hydrogels certainly had a more homogeneous network structure than the usually inhomogeneous PAAm samples. However, particularly at lower concentrations the thiol-ene gels certainly possessed no perfect network structure. Still, the DLS measurements showed that the reactor-batch gels containing DAP2000 and DAP3000 had an almost perfectly homogeneously distibuted polymer concentration. At equilibrium swelling the "hidden" inhomogeneities appeared. In this state all of the gels, thiol-ene or PAAm, showed the same high network inhomogeneity.

References

[1]   *Hydrogele: Verwendungsmöglichkeiten und thermodynamische Eigenschaften*
         Thiel, J.; Maurer, G.; Prausnitz, M. *Chem. Ing. Tech.* **1995**, *67*, 1567-1583

[2]   *Superabsorbent Hydrogel Composites and Nanocomposites: A Review*
         Kabiri, K.; Omidian, H.; Zohuriaan-Mehr, M.J.; Doroudiani, S. *Polym. Comp.* **2011**, *32*, 277-289

[3]   *Microrobotics and MEMS-Based Fabrication Techniques for Scaffold-Based Tissue Engineering*
         Zhang, H.; Hutmacher, D.W.; Chollet,F.; Poo,A.N.; Burdet, E.
         Macromol. Biosci. **2005**, *5*, 477-489

[4]   *Hydrogels in Regenerative Medicine*
         Slaughter, B.V.; Khurshid, S.S.; Fisher, O.Z.; Khademhosseini, A.; Peppas, N.A.
         Adv. Mater. **2009**, *21*, 3307-3329

[5]   *Polymeric Materials for Contact Lenses*
         Singh, J.; Agrawal, K.K. *J.M.S.-Rev. Macromol . Chem . Phys*. **1992**, *C32*, 521-534

[6]   *Advances in non-hygienic applications of superabsorbent hydrogel materials*
         Zohuriaan-Mehr, M.J.; Omidian, H.; Doroudiani, S.; Kabiri, K. *J. Mater. Sci.* **2010**, *45*, 5711-5735

[7]   *Controlled Release of Proteins from Poly (L-lactic acid) Coated Polyisobutylcyanoacrylate
         Microcapsules*
         Park, T.C.; Alonso, M.J.; Laner, R. *J. Appl. Polym. Sci.* **1994**, *52*, 1797-1807

[8]   *Hydrogels for biomedical applications*
         Hoffman, A.S. *Advanced Drug Delivery Reviews* **2002**, *43*, 3-12

[9]   *PVA–clay nanocomposite hydrogels for wound dressing*
         Kokabi, M.; Sirousazar, M.; Muhammad Hassan, Z. *Eur. Polym. J.* **2007**, *43*, 773-781

[10]   *Hydrogel Sensors and Actuators*
         Gerlach, G.; Arndt, K.F. Eds. *Springer* **2010**, *XI*

[11]   *'Smart' polymers and what they could do in biotechnology and medicine*
         Galaev, I.Y.; Mattiasson, B. *Tibtech* **1999**, *17*, 335-340

[12]   *Hydrogel Nanocomposite as a Synthetic Intra-Ocular Lens Capable of Accomodation*
         Ravi, N.; Aliyar, H.A.; Hamilton, P.D. *Macromol. Symp.* **2005**, *227*, 191-201

[13]   *First successful design of semi-IPN hydrogel–silver nanocomposites: A facile approach for
         antibacterial application*
         Murthy, P.S.K.; Mohan, Y.M.; Varaprasad, K.; Sreedhar, B; Mohana Raju, K.
         J. Coll. Int. Sci. **2008**, *318*, 217-224

[14]   *Polymer-Coated Adsorbents for the Separation of Biopolymers and Particles*
         Ivanov, A.E.; Saburov, V.V.; Zubov, V.P. *Adv. Polym. Sci.* **1992**, *104*, 135-175

[15]   *Chemistry and Physics of "Agricultural" Hydrogels*
         Kazanskii, K.S.; Dubrovskii, S.A. *Adv. Polym. Sci.* **1992**, *104*, 97-133

[16]   *Rubberlike Elasticity - A Molecular Primer*
         Mark, J.E.; Erman, B. *John Wiley & Sons Inc.* **1988**

[17]   *Physical chemistry of supramolecular polymer networks*
         Seiffert, S.; Sprakel, J. *Chem. Soc. Rev.* **2012**, Advance Article (DOI: 10.1039/c1cs15191f)

[18] *Superabsorbent Polymer Materials: A Review*
Zohuriaan-Mehr, M.J.; Kabiri, K. *Iran. Polym. J.* **2008**, *17*, 451-477

[19] *Formation of double helical and filamentous structures in models of physical and chemical gels*
Kröger, M.; Peleg, O.; Ding, Y.; Rabin, Y. *Soft Matter* **2008**, *4*, 1-180

[20] *Polymer Physics*
Rubinstein, M.; Colby, R.H. *Oxford University Press* **2003**, pp. 199

[21] *Introductory Lecture – Aspects of Polymer Gels*
Keller, A. *Faraday Discuss.,* **1995**, *101*, 1-49

[22] *Dynamic Mechanical Measurement of Crystallization-Induced Gelation in Thermoplastic Elastomeric Poly(propylene)*
Lin, Y.G.; Mallin, D.T.; Chien, J.C.W.; Winter, H.H. *Macromolecules* **1991**,*24*, 850-854

[23] *Crystallinity in Poly(Vinyl Chloride)*
Gilbert, M. *J.M.S-Rev. Macromol. Chem. Phys.* **1994**, *C34*, 77-135

[24] *Physical Gelation in a Triblock Copolymer Solution: In Situ Study of Stress-Strain Behavior and Structural Development*
Kleppinger, R.; van Es, M.; Mischenko, N.; Koch, M.H.J.; Reynaers, H.
Macromolecules **1998**, *31,* 5805-5809

[25] *Thermoreversible Physical Gelation of Block Copolymers in a Selective Solvent*
Sato, T.; Watanabe, H.; Osaki, K. *Macromolecules* **2000**, *33,* 1686-1691

[26] *Electrospinning Physical Gels: The Case of Stereocomplex PMMA*
Crne, M.; Park, J.O.; Srinivasarao, M. *Macromolecules* **2009**, *42*, 4353-4355

[27] *Helix-Coil Transition and Physical Gelation of Isotactic Polystyrene in cis- and trans-Decalin Monitored by Fluorescence Measurements*
Itagaki, H.; Takahashi, I. *Macromolecules* **1995**,*28*, 5477-5486

[28] *Equilibrium statistical distributions for subchains in an entangled polymer melt*
Greco, F. *Eur. Phys. J.* **2008**, *E 25*, 175-180

[29] *Self-healing polymeric materials: A review of recent developments*
Wu, D.Y.; Meure, S.; Solomon, D. *Prog. Polym. Sci.* **2008**, *33* 479-522

[30] *The world of smart healable materials*
Murphy, E.B.; Wudl, F. *Progr. Polym. Sci.* **2010**, *35*, 223-251

[31] *Physical crosslinking effects in α,ω-dihydroxy terminated polybutadienes*
Krakovsky, I.; Hanykova, L.; Trchova, M.; Baldrian, J.; Wübbenhorst, M.
Polymer **2007**, *48*, 2079-2086

[32] *Stress-relaxation behavior in gels with ionic and covalent crosslinks*
Zhao, X.; Huebsch, N.; Mooney, D.J.; Suo, Z. *J. Appl. Phys.* **2010**, *107*, 063509

[33] *Transient network topology of interconnected polyelectrolyte complex micelles*
Lemmers, M.; Voets, I.K.; Cohen Stuart, M.A.; van der Gucht, J. *Soft Matter* **2011**, *7*, 1378-1389

[34] *Dendritic Physical Gel: A Liquid Crystalline Gel for Application in Light Scattering Displays*
Heo, J.; Jang, W.-D. *Macromolecular Research* **2008**, 16, 586-589

[35] *Structural Studies of a New Low Molecular Mass Organic Gelator for Organic Liquids Based on Simple Salt*
Ballabh, A.; Trivedi, D.R.; Dastidar, P. *Chem. Mater.* **2003**, *15,* 2136-2140

References

[36] *Physikalische Chemie*
      Atkins, P.W. *Wiley VCH Verlag GmbH Weinheim* **2001**, 3. korrigierte Auflage, p. 722

[37] *Very Strong Hydrogen Bonding*
      Emsley, J. *Chem. Soc. Rev.* **1980**, *9*, 91-124

[38] *Physikalische Chemie*
      Atkins, P.W. *Wiley VCH Verlag GmbH Weinheim* 2**001**, 3. korrigierte Auflage, p. 1033

[39] *Definition of the Concept of Polymer Gel*
      Rogovina, L.Z.; Vasilev, V.G.; Braudo, E.E. *Polymer Science, Ser. C* **2008***, 50,* 85-92

[40] *The Physics of Rubber Elasticity*
      Treloar, L.R.G. *Clarendon Press Oxford* **1975**, 3rd edition, pp. 128

[41] *Principles of Polymer Chemistry*
      Flory, P.J. *Cornell University Press* **1953**, pp. 576

[42] *Rubberlike Elasticity - A Molecular Primer*
      Mark, J.E.; Erman, B. *John Wiley & Sons Inc.* **1988**, p. 49

[43] *Structures and Properties of Rubberlike Networks*
      Erman, B; Mark, J.E. *Oxford University Press* **1997**, p. 56

[44] *Gel formation in free-radical crosslinking copolymerization*
      Naghash, H. J.; Okay, O.; Yildrim, H. *J. Appl. Polym. Sci..* **1995**, *56*, 477

[45] *Structures and Properties of Rubberlike Networks*
      Erman, B; Mark, J.E. *Oxford University Press* **1997**, pp. 4

[46] *Polymer Physics*
      Rubinstein, M.; Colby, R.H. *Oxford University Press* **2003**, pp. 282

[47] *Das Rheologie Handbuch: Für Anwender von Rotations- und Oszillations-Rheometern*
      Mezger, T.G. *Vincentz Network,* **2006,** 2. Auflage

[48] *Can the Gel Point of a Cross-linking Polymer Be Detected by the G' - G" Crossover?*
      Winter, H.H. *Polym Eng. Sci.* **1987**, *27*,1698-1702

[49] *Stopping of Crosslinking Reaction in a PDMS Polymer at the Gelpoint*
      Chambon, F.; Winter, H.H. *Pol. Bull.* **1985**, *13*, 499-503

[50] *Composition Dependence of the Viscoelasticity of End-Linked Poly(dimethylsi1oxane) at the Gel Point*
      Scanlan, J.C.; Winter, H.H. *Macromolecules* **1991**,*24*, 47-54

[51] *Stoichiometry Effects on Rheology of Model Polyurethanes at the Gel Point*
      Winter,H.H.; Morganelli, P.; Chambon, F. *Macromolecules* **1988**,*21*, 535-537

[52] *Rheological Analysis of the Gelation Behavior of Tetraethylorthosilane/Vinyltriethoxysilane Hybrid Solutions*
      Kim, S.-Y.; Choi, D.-G.; Yang, S.-M. *Korean J. Chem. Eng*. **2002**, *19*, 190-196

[53] *Model Networks Based on 'Endlinking' Processes: Synthesis, Structure and Properties*
      Hild, G. *Prog. Polym. Sci.* **1998**, *23*, 1019-1149

[54] *Rubberlike Elasticity - A Molecular Primer*
      Mark, J.E.; Erman, B. *John Wiley & Sons Inc.* **1988**, p. 26

[55] *Rubber-Like Elasticity*
      Erman, B.; Mark, J.E. *Annu. Rev. Phys. Chem.* **1989**, *40*, 351-374

[56] *Polymer Physics*
      Rubinstein, M.; Colby, R.H. *Oxford University Press* **2003**, pp. 255

[57] *Some experimental results for the end-linked polydimethylsiloxane network system*
      Ladegaard Larsen, A.; Sommer-Larsen, P.; Hassager, O. *e-Polymers* **2004**, *050*, 1-18

[58] *Spatial inhomogeneity and dynamic fluctuations of polymer gels*
      Shibayama, M. *Macromol. Chem. Phys*. **1998**, *199*, 1-30

[59] *Light Scattering from Swollen Gels*
      Bueche, F. J. *Coll. Int. Sci.* **1970**, *33*, 61-66

[60] *Suppression of inhomogeneities in hydrogels formed by free-radical crosslinking copolymerization*
      Orakdogen, N.; Kizilay, M.Y.; Okay, O. *Polymer* **2005**, *46*, 11407-11415

[61] *Inhomogeneities in poly(acrylamide) gels: position-dependent elastic modulus measurements*
      Durmaz, S.; Okay, O. *Polym. Bull.* **2001**, *46*, 409-418

[62] *Application of Thiol-Ene Photopolymerization for Injectable Intraocular Lenses: A Preliminary Study*
      Niu, G.; Song, L.; Zhang, H.; Cui, X.; Kashima, M.; Yang, Z.; Cao, H.; Wang, G.; Zheng, Y.; Zhu,S.;

      Yang, H. *Polym. Eng. Sci.* **2010**, *50*, 174-182

[63] *Permeability of Heterogeneous Gels*
      Weiss, N.; van Vliet, T.; Silberberg, A. *J. Polym. Sci. Polym. Phys. Ed.* **1979**, *17*,2229-2240

[64] *Structural Inhomogeneities in the Range 2.5-2500 Å in Polyacrylamide Gels*
      Hecht, A.-M.; Duplessix, R.; Geissler, E. *Macromolecules* **1985**, *18*, 2167-2173

[65] *Characterization of Inhomogeneous Polyacrylamide Hydrogels*
      Cohen, Y.; Ramon, O.; Kopelman, I.J.; Mizrahi, S.
      J. Polym. Sci. B: Polym. Phys. **1992**, *30*, 1055-1067

[66] *Inhomogeneities in poly(acrylamide) gels: position-dependent elastic modulus measurements*
      Durmaz, S.; Okay, O. *Polym. Bull.* **2001**, *46*, 409-418

[67] *Minimization of spatial inhomogeneity in polystyrene gels formed by free-radical mechanism*
      Cerid, H.; Okay, O. *Eu. Polym. J.* **2004**, *40*, 579-587

[68] *Inhomogeneity Control in Polymer Gels*
      Ikkai, F.; Shibayama, M. *J. Polym. Sci. B: Polym. Phys.* **2005**, *43*, 617-628

[69] *Nitroxide-Controlled Free-Radical Copolymerization of Vinyl and Divinyl Monomers. 2. Gelation*
      Ide, N.; Fukuda, T. *Macromolecules* **1999**, *32*, 95-99

[70] *Comparison of the gelation dynamics for polystyrenes prepared by conventional and living radical polymerizations: a time-resolved dynamic light scattering study*
      Norisuye, T.; Morinaga, T.; Tran-Cong-Miyata, Q.; Goto, A.; Fukuda, T.; Shibayama, M.
      Polymer **2005**, *46*, 1982-1994

[71] *Influence of the Cross-Linker Reactivity on the Formation of Inhomogeneities in Hydrogels*
      Lindemann, B.; Schröder, U.P.; Oppermann, W. *Macromolecules* **1997**, *30*, 4073-4077

[72] *Homogeneous Poly(acrylamide) Hydrogels Made by Large Size, Flexible Dimethacrylate Cross-Linkers*
      Abdurrahmanoglu, S.; Okay, O. *Macromolecules* **2008**, *41*, 7759-7761

[73] *Influence of Formation Conditions on Spatial Inhomogeneities in Poly(N-isopropylacrylamide) Hydrogels*
Nie, J.; Du, B.; Oppermann, W. *Macromolecules* **2004**, *37*, 6558-6564

[74] *Effect of degree of cross-linking on spatial inhomogeneity in charged gels. I. Theoretical predictions and light scattering study*
Shibayama M., Ikkai F., Shiwa Y., Rabin Y. *J. Chem. Phys.* **1997**, *107*, 5227-5235

[75] *Preparation of homogeneous polyacrylamide hydrogels by free-radical crosslinking copolymerization*
Kuru, E.A.; Orakdogen, N.; Okay, O. *Eu. Polym. J.* **2007**, *43*, 2913-2921

[76] *Effect of Initial Monomer Concentration on Spatial Inhomogeneity in Poly(acrylamide) Gels*
Kizilay, M.Y.; Okay, O. *Macromolecules* **2003**, *36*, 6856-6862

[77] *Minimization of spatial inhomogeneity in polystyrene gels formed by free-radical mechanism*
Cerid, H.; Okay, O. *Eu. Polym. J.* **2004**, *40*, 579-587

[78] *Large-Scale Heterogeneities in Randomly Cross-Linked Networks*
Bastide, J.; Leibler, L. *Macromolecules* **1988**, *21*, 2647-2649

[79] *Development of networks in atom transfer radical polymerization of dimethacrylates*
Yu, Q.; Zhou, M.; Ding, Y.; Jiang, B.; Zhu, S. *Polymer* **2007**, *48*, 7058-7064

[80] *Controlled/living radical polymerization: Features, developments, and perspectives*
Braunecker, W.A.; Matyjaszewski, K. *Prog. Polym. Sci.* **2007**, *32*, 93-146

[81] *Spatial Inhomogeneities of Polystrene Gels Prepared from Semidilute Solutions*
Liu, R.; Oppermann, W. *Macromolecules* **2006**, *39*, 4159-4167

[82] *A New Method To Generate Polystyrene Gels*
Susoff, M.; Oppermann, W. *Macromolecules* **2009**, *42*, 9195-9198

[83] *Design and Fabrication of a High-Strength Hydrogel with Ideally Homogeneous Network Structure from Tetrahedron-like Macromonomers*
Sakai, T.; Matsunaga, T.; Yamamoto, Y.; Ito, C.; Yoshida, R.; Suzuki, S.; Sasaki, N.; Shibayama, M.; Chung, U. *Macromolecules*, **2008**, *41*, 5379-5384

[84] *Effect of Dilution on Structure and Properties of Polyurethane Networks. Pregel and Postgel Cyclization and Phase Separation*
Dušková-Smrčková, M.; Valentová, H.; Ďuračková, A.; Dušek, K. *Macromolecules* **2010**, *43*, 6450-6462

[85] *Thiol–Enes: Chemistry of the Past with Promise for the Future*
Hoyle, C.E.; Lee, T.Y.; Roper, T. *J. Polym. Sci. A: Polym. Chem.* **2004**, *42*, 5301-5338

[86] *Synthesis and Thiol–Ene Photopolymerization of Allyl-Ether Functionalized Dendrimers*
Nilsson, C.; Simpson, N.; Malkoch, M.; Johansson, M.; Malmström, E. *J. Polym. Sci. A: Polym. Chem.* **2008**, *46*, 1339-1348

[87] *Thiol-Yne Photopolymerizations: Novel Mechanism, Kinetics, and Step-Growth Formation of Highly Cross-Linked Networks*
Fairbanks, B.D.; Scott, T.F.; Kloxin, C.J.; Anseth, K.S.; Bowman, C.N. *Macromolecules* **2009**, *42*, 211-217

[88] *Beitrage zur Kenntniss der ungesattigten Verbindungen. II. Ueber die Addition von Mercaptanen an ungesättigte Kohlenwasserstoffe*
Posner, T. *Berichte der deutschen chemischen Gesellschaft* **1905**, *38*, 646-657

[89]   *The Peroxide Effect in the Addition of Reagents to Unsaturated Compounds. XVI. The Addition of Thiogylcolic Acid to Styrene and Isobutylene*
Kharasch, M. S.; Mayo, F. R. *Chem. Ind.* **1938**, *57*, 752

[90]   *Application of Thiol-Ene Photopolymerization for Injectable Intraocular Lenses: A Preliminary Study*
Niu, G.; Song, L.; Zhang, H.; Cui,X.; Kashima, M.; Yang, Z.; Cao,H.; Wang, G.; Zheng, Y.; Zhu, S.; Yang, H. *Polym. Eng. Sci.* **2010**, *50*, 174-182

[91]   *Recent Advances and Developments in Composite Dental Restorative Materials*
Cramer, N.B.; Stansbury, J.W.; Bowman, C.N. *J. Dent. Res.* **2011**, *90*, 402-416

[92]   *Poly(ethylene glycol)-Based Thiol-ene Hydrogel Coatings-Curing Chemistry, Aqueous Stability and Potential Marine Antifouling Applications*
Lundberg,P.; Bruin, A.; Klijnstra, J.W.; Nyström, A.M.; Johansson, M.; Malkoch, M.; Hult, A. *ACS Appl. Mat. Int.* **2010**, *2*, 903-912

[93]   *A versatile approach to high-throughput microarrays using thiol-ene chemistry*
Gupta, N.; Lin, B.F.; Campos, L.M.; Dimitriou, M.D.; Hikita, S.T.; Treat, N.D.; Tirrell, M.V.; Clegg, D.O.; Kramer, E.J.; Hawker, C.J. *Nature Chemistry* **2010**, *2*, 138-145

[94]   *Tailorable low modulus, reversibly deformable elastomeric thiol–ene materials for microfluidic applications*
Good, B.T.; Reddy, S.;Davis, R.H.; Bowman, C.N. *Sens. Act. B* **2007**, *120*, 473-480

[95]   *A water-activated pump for portable microfluidic applications*
Good, B.T.; Bowman, C.N.; Davis, R.H*. J. Coll. Int. Sci.* **2007**, *305*, 239-249

[96]   *The Power of Thiol-ene Chemistry*
Kade, M.J.; Burke, D.J.; Hawker, C.J. *J. Polym. Sci. A: Polym. Chem.* **2010**, *48*, 743-750

[97]   *Thiol/Ene Photocurable Polymers*
Margan, C.R.; Magnotta, F.; Ketley, A.D. *J. Polym. Sci.: Polym. Chem. Ed.* **1977**, *15*, 627-645

[98]   *Chemie und Physik der synthetischen Polymeren: Ein Lehrbuch*
Cowie, J.M.G. *Friedr. Vieweg Sohn Verlagsgesellschaft mbH, Braunschweig/Wiesbaden* **1997**, p. 43-44

[99]   *Controlling Network Structure in Degradable Thiol-Acrylate Biomaterials to Tune Mass Loss Behavior*
Rydholm, A.E.; Reddy, S.K.; Anseth, K.S.; Bowman, C.N. *Biomacromolecules* **2006**, *7*, 2827-2836

[100]   *Development and characterization of degradable thiol-allyl ether photopolymers*
Rydholm, A.E.; Reddy, S.K.; Anseth, K.S.; Bowman, C.N. *Polymer* **2007**, *48*, 4589-4600

[101]   *An effective method to prepare sucrose polymers by Thiol-Ene photopolymerization*
Ortiz , R.A.; Garcia Valdéz, A.E.; Martinez Aguilar, M.G.; Berlanga Duarte, M.L. *Carbohydrate Polymers* **2009**, *78*, 282-286

[102]   *Preparation of a crosslinked sucrose polymer by thiol–ene photopolymerization using dithiothreitol as comonomer*
Ortiz, R.A.; Ruiz Martinez, A.Y.; García Valdez, A.E.; Berlanga Duarte, M.L. *Carbohydrate Polymers* **2010**, *82*, 822-828

[103]   *Thermal polymerization of thiol–ene network-forming systems*
Cook, W.D.; Chen, F.; Pattison, D.W.; Hopson, P.; Beaujon, M. *Polym Int* **2007**, *56*, 1572-1579

[104] *Radiation Curing – Coatings and Printing Inks*
Gloeckner, P.; Jung, T.; Struck, S.; Studer, K. *Vincentz Network GmbH & Co. KG, Hannover* **2008**, p. 34

[105] *Photochemistry and photoinduced chemical crosslinking activity of type I & II co-reactive photoinitiators in acrylated prepolymers*
Allen, N.S.; Marin, M.C.; Edge, M.; Davies, D.W.; Garrett, J.; Jones, F.; Navaratnam, S.; Parsons, B.J. *J. Photochem. Photobio. A: Chem.* **1999**, *126*, 135-149

[106] *Heteroaromatic Thiols as Co-initiators for Type II Photoinitiating Systems Based on Camphorquinone and Isopropylthioxanthone*
Andrzejewska, E.; Zych-Tomkowiak, D.; Andrzejewski, M.; Hug, G.L.; Marciniak, B. *Macromolecules* **2006**, *39,* 3777-3785

[107] *Camphorquinone–amines photoinitating systems for the initiation of free radical Polymerization*
Jakubiak, J.; Allonas, X.; Fouassier, J.P.; Sionkowska, A.; Andrzejewska, E.; Linden, L.A.; Rabek, J.F. *Polymer* **2003**, *44*, 5219-5226

[108] *The role of oxygen in camphorquinone-initiated photopolymerization*
Andrzejewska, E.; Lindén, L.-A.; Rabek, J.F. *Macromol. Chem. Phys.* **1998**, *199*, 441-449

[109] *Use of α-Diketones as Visible Photoinitiators for the Photocrosslinking of Waterborne Latex Paints*
Bibaut-Renauld, C.; Burget, D.; Fouasier, J.P.; Varelas, C.G.; Thomatos, J.; Tsagaropoulos, G.; Ryrfors, L.O.; Karlsson, O.J. *J. Polym. Sci A: Polym. Chem.* **2002**, *40*, 6171-3181

[110] *Kinetics of Thiol–Ene and Thiol–Acrylate Photopolymerizations with Real-Time Fourier Transform Infrared*
Cramer, N.B.; Bowman, C.N. *J. Polym. Sci. A: Polym. Chem.* **2001**, *39*, 3311-3319

[111] *Initiation and Kinetics of Thiol–ene Photopolymerizations without Photoinitiators*
Cramer, N.B.; Reddy, S.K.; Cole, M.; Hoyle, C.; Bowman, C.N. *J. Polym. Sci. A: Polym. Chem.* **2004**, *42*, 5817-5826

[112] *Influence of the Thiol Structure on the Kinetics of Thiol-ene Photopolymerization with Time-Resolved Infrared Spectroscopy*
Wutticharoenwong, K.; Soucek, M.D. *Macromol. Mater. Eng.* **2008**, *293*, 45-56

[113] *Photopolymerizations of Thiol−Ene Polymers without Photoinitiators*
Cramer, N.B.; Scott, J.P.; Bowman, C.N. *Macromolecules* **2002**, *35*, 5361-5365

[114] *Thiol−Allyl Ether−Methacrylate Ternary Systems. Polymerization Mechanism*
Lee, T.Y.; Smith, Z.; Reddy, S.K.; Cramer, N.B.; Bowman, C.N. *Macromolecules* **2007**, *40*, 1466-1472

[115] *Thiol-Ene Photopolymerization Mechanism and Rate Limiting Step Changes for Various Vinyl Functional Group Chemistries*
Cramer,N.B.; Reddy, S.K.; O'Brien, A.K.; Bowman, C.N. *Macromolecules* **2003**, *36,* 7964-7969

[116] *Photocrosslinked Norbornene-Thiol Copolymers: Synthesis, Mechanical Properties, and Cure Studies*
Jacobine, A.F.; Claser, D.M.; Grabek, P.J.; Mancini, D.; Masterson, M.; Rakas, M.A.; Woods, J.G. *J. Appl. Polym. Sci.* **1992**, *45*, 471-485

[117] *Nonclassical Dependence of Polymerization Rate on Initiation Rate Observed in Thiol-Ene Photopolymerizations*
Scott, T.F.; Kloxin, C.J.; Draughon, R.B.; Bowman, C.N. *Macromolecules* **2008**, *41*, 2987-2989

[118] *Gel Formation in Addition Polymerization*
Walling, C. *J. Am. Chem. Soc.* **1945**, *67*, 441-447

[119] *Physical and Mechanical Properties of Photopolymerized Thiol-Ene/Acrylates*
Senyurt, A.F.; Wei,H.; Phillips, B.; Cole, M.; Nazarenko, S.; Hoyle, C.E.; Piland, S.G.; Gould, T.E.
Macromolecules **2006**, *39*, 6315-6317

[120] *Ternary Thiol-Ene/Acrylate Photopolymers: Effect of Acrylate Structure on Mechanical Properties*
Senyurt, A.F.; Wei,H.; Hoyle, C.E.; Piland, S.G.; Gould, T.E.
Macromolecules **2007**, *40,* 4901-4909

[121] *Thiol–Ene Click Chemistry*
Hoyle, C.E.; Bowman, C.N. *Angew. Chem. Int. Ed.* **2010**, *49*, 1540-1573

[122] *Oxygen Inhibition in Thiol-Acrylate Photopolymerizations*
O'Brien, A.K.; Cramer, N.B.; Bowman, C.N. *J. Polym. Sci. A: Polym. Chem.* **2006**, *44*, 2007-2014

[123] *Untersuchungen zur Thiol-En-Polymerisation: elektronenspinresonanzspektroskopischer Nachweis spontaner Radikalbildung*
Sensfuß, S.; Friedrich, M.; KIemm, E. *Makromol. Chem.* **1991**, *192*, 2895-2900

[124] *Free-radical stabilizers for the thiol/ene-systems*
Klemm, E.; Sensfuß, S.; Holfter, U.; Flammersheim, H.J.
Angew. Makromol. Chem. **1993**, *212*, 121-127

[125] *New results of the self-initiation mechanism of SH/En addition polymerization*
Kuhne, G.; Diesen, J.S.; Klemm, E. *Angew. Makromol. Chem.* **1996**, *242*, 139-145

[126] *The effect of thiol and ene structures on thiol–ene networks: Photopolymerization, physical, mechanical and optical properties*
Li, Q.; Zhou, H.; Hoyle, C.E. *Polymer* **2009**, *50*, 2237-2245

[127] *Structure of Gels as Investigated by Means of Static Scattering Techniques*
Bastide, J.; Candau, S.J. in Cohen Addad J.P. Ed. *The Physical Properties of Polymeric Gels, John Wiley & Sons Ltd.* **1996**

[128] *Dynamic Light Scattering*
Berne, B.J.; Pecora, R. *John Wiley & Sons, Inc.* **1976**

[129] *Polymer Physics*
Rubinstein, M.; Colby, R.H. *Oxford University Press* **2003**, pp.29

[130] *Preparation of Homogeneous Hydrogels by Controlling the Crosslinker Reactivity and Availability*
Abdurrahmanoglu, S.; Okay, O. *J. Macromol. Sci. A: Pure Appl. Chem.* **2008**, *45*, 769-775

[131] *Habilitation Thesis: Fluctuations and Correlations: Dynamic Light Scattering*
Rička, J. *Unknown*, **1994**

[132] *Universality and Specificity of Polymer Gels Viewed by Scattering Methods*
Shibayama, M. *Bull. Chem. Soc. Jpn.* **2006**, *79*, 1799-1819

[133] *Polymer Physics*
Rubinstein, M.; Colby, R.H. *Oxford University Press* **2003**, pp.345

[134] *Teilchengrößen-Bestimmung mittels dynamischer Lichtstreuung*
Wagner, J. *Chem. Ing. Tech.* **1986**, *58*, 578-583

[135] *Particle Sizing by Quasi-Elastic Light Scattering*
Finsy, R. *Adv. Coll. Int. Sci.* **1994**, *52*, 79-143

[136] *Light scattering for particle characterization*
Jones, A.R. *Prog. En. Comb. Sci.* **1999**, *25*, 1-53

[137] *Dynamic Light Scattering by Non-Ergodic Media*
Pusey, P.N.; van Megen, W. *Physica A* **1989**, *157*, 705-741

[138] *Dynamic light scattering by nonergodic Media: Brownian particles trapped in polyacrylamide gels*
Joosten, J.G.H.; Geladé, E.T.F.; Pusey, P.N. *Physical Review A* **1990**, *42*, 2161-2175

[139] *Gel Formation Analyses by Dynamic Light Scattering*
Shibayama, M.; Norisuye, T. *Bull. Chem. Soc. Jpn.* **2002**, *75*, 641-659

[140] *Development of a Heterodyne Photon Correlation Spectroscopy Measuring Probe for Highly Concentrated Dispersions*
Willemse, A.W.; Merkus, H.G.; Scarlett, B. *J. Coll. Int. Sci.* **1998**, *204*, 247-255

[141] *Particle size measurements on turbid latex systems using heterodyne intensity autocorrelation spectroscopy*
Cummins P.G.; Staples, E.J. *J. Phys. E: Sci. Instrum*. **1981**, *14*, 1171-1177

[142] *Photon Correlation Spectroscopy using Optical Heterodyne Detection*
Fletcher, G.C.; Harnett, J.I. *Aust. J. Phys.* **1981**, *34*, 575-584

[143] *Dynamic Light Scattering by Permanent Gels: Heterodyne and Nonergodic Medium Methods of Data Evaluation*
Fang, L.; Brown, W. *Macromolecules* **1992**, *25*, 6897-6903

[144] *Fiber Optic Dynamic Light Scattering, neither Homodyne nor Heterodyne*
Bremer, L.G.B.; Deriemaeker, L.; Finsy, R.; Geladé, E.; Joosten, J.G.H.
Langmuir **1993**, *9*, 2008-2014

[145] *Dynamic and Static Light Scattering by Aqueous Polyacrylamide Gels*
Joosten, J.G.H.; McCarthy, J.L.; Pusey, P.N. *Macromolecules* **1991**, *24*, 6690-6699

[146] *Dynamic Light Scattering Study of Poly(N-isopropylacrylamide-co-acrylic acid) Gels*
Shibayama, M.; Fujikawa, Y.; Nomura, S. *Macromolecules* **1996**, *29*, 6535-6540

[147] *Dynamic Inhomogeneities in Polymer Gels Investigated by Dynamic Light Scattering*
Norisuye, T.; Tran-Cong-Miyata, Q.; Shibayama, M. *Macromolecules* **2004**, *37*, 2944-2953

[148] *Dynamic Fluctuations and Spatial Inhomogeneities in Poly(N-isopropylacrylamide)/Clay Nanocomposite Hydrogels Studied by Dynamic Light Scattering*
Nie, J.; Du, B.; Oppermann, W. *J. Phys. Chem. B* **2006**, *110,* 11167-11175

[149] *Scaling analyses of polyacrylamide gels at swelling equilibrium in water/acetone mixtures by small-angle X-ray scattering*
Sakurai, S.; Hayashi, H.; Hamada, F. *Polymer* **1993**, *34*, 4625-4628

[150] *The swelling and collapse of hydrogen bonded polymer gels*
Shenoy, S.L.; Painter, P.C.; Coleman, M.M. *Polymer* **1999**, *40*, 4853-4863

[151] *Swelling, Elasticity, and Spatial Inhomogeneity of Poly(N-isopropylacrylamide)/Clay Nanocomposite Hydrogels*
Nie, J.; Du, B.; Oppermann, W. *Macromolecules* **2005**, *38,* 5729-5736

[152] *Scattering by an Inhomogeneous Solid*
Debye, P.; Bueche, A.M. *J. Appl.Phys.* **1949**, *20*, 518-525

[153] *Light Scattering Studies of Poly(dimethylsiloxane) Solutions and Swollen Networks*
Soni, V.K.; Stein, R.S. *Macromolecules* **1990**, *23*, 5257-5265

[154] *Comparison between Neutron and Quasielastic Light Scattering by Polyacrylamide Gels*
Geissler, E.; Hecht, A.M.; Duplessix, R. *J. Polym. Sci. Polym. Phys. Ed.* **1982**, *20*, 225-233

[155] *Raman Spectroscopic and Thermal Studies* of *Polyacrylamide Gels with Varying MonomerlComonorner Ratios*
Manoj K. Gupta, M.K.; Bansil, R. *J. Polym. Sci. Polym. Lett. Ed.* **1983**, *21*, 969-977

[156] *Elastic Properties of Highly Cross-Linked Polyacrylamide Gels*
J. Baselga, J.; Hernández-Fuentes, I.; Piérola, I.F.; Llorente, M.A.
Macromolecules **1987**, *20,* 3060-3065

[157] *Water Structure and Changes in Thermal Stability of the System Poly (ethylene oxide)-Water*
Kjellander, R.; Florin, E. *J. Chem. Soc., Faraday Trans. 1* **1981**, *77*, 2053-2077

[158] Presetting of the ALV-Correlator Software ALV-5000/E/EPP & ALV-60X0-WIN V.3.0.2.0
08/2004

[159] *Viscosity of the mixture (1) water; (2) ethanol.*
Wohlfarth, C. in Lechner, M.D. (ed.) *SpringerMaterials - The Landolt-Börnstein Database*
Springer-Verlag Berlin Heidelberg **2008**, DOI: 10.1007/978-3-540-75486-2_447

[160] measured

[161] *Brice Phoenix Differential Refractometer, Visual Laboratory Type Model BP-2000-V* Operation
Manual, Table 1, according to a CAUCHY-plot of the first seven values extrapolating to 632.8 nm

[162] *Polymer Handbook*
Brandrup, J.; Immergut, E.H.; Grulke, E.A. Eds*. John Wiley and Sons, Inc.* **1999**, 4th Edition,
p. VII/595

[163] *Polymer Handbook*
Brandrup, J.; Immergut, E.H.; Grulke, E.A. Eds. *John Wiley and Sons, Inc.* **1999**, 4th Edition,
p. VII/558

[164] *The Effect of Microstructure and Molecular Weight on the Refractive Index Increment Of Polybutadiene in Cyclohexane*
Chen, X.; Hadjichristidis, N.; Fetters, L.J.; Carella, J.; Graessley, W.W.
J. Polym. Sci. Polym. Phys. Ed. **1984**, *22,*777-779

[165] *Specific Refractive Index Increments of Polymer Solutions. Part 11. Scope and Applications*
Huglin, M.B. *J. Appl. Polym. Sci.* **1965**, *9*, 4003-4024

[166] *Variation of refractive index increment with molecular weight*
Margerison, D.; Bain, D.R.; Kiely, B. *Polymer* **1973**, *14*, 133-136

[167] *Effect of molecular weight on the refractive index increment of polystyrenes in solution*
Candau, F.; François, J.; Benoit, H. *Polymer* **1974**, *15*, 626-630

[168] *Refractive Index-Tempera ture Measurements on Anionically Polymerized Polystyrene*
Krause, S.; Lu, Z.-H. *J. Polym. Sci. Polym. Phys. Ed.* **1981**, *19,*1925-1928

[169] *Effect of Molecular Weight on the Refractive Index Increments of Polystyrene, Poly(ethy1ene Glycol), Poly(propy1ene Glycol), and Poly(dichloropheny1ene Oxide) in Solution*
Binboga, N.; Kisakürek, D.; Baysal, B.M. *J. Polym. Sci. Polym. Phys. Ed.* **1985**, *23*, 925-931

[170] *"Steric'' Stabilization of Colloidal Solutions by Adsorption of Flexible Macromolecules*
Heller, W.; Pugh, T.L. *J. Polym. Sci.* **1960**, *47*, 203-217

[171] *Dynamic light scattering with single-mode receivers: partial heterodyning regime*
Flammer, I.; Rička, J. *Appl. Opt.* **1997**, *36*, 7508-7517

[172] *Polymer Handbook*
Brandrup, J.; Immergut, E.H.; Grulke, E.A. Eds. *John Wiley and Sons, Inc.* **1999**, 4th Edition,
p. VII/61

[173] *Structure and Properties of Ionic Hydrogels*
Oppermann, W. *Angew. Makromol. Chem.* **1984**, *123/124*, 229-239

[174] *Correlation between crosslinking efficiency and spatial inhomogeneity in poly(acrylamide) hydrogels*
Orakdogen, N.; Oguz, O. *Pol. Bull.* **2006**, *57*, 631-641

Appendix A: List of Abbreviations and Acronyms

AAm	acrylamide
ACF	autocorrelation function
APS	ammonium peroxydisulfate
BIS	N,N'-methylene-bisacrylamide
CDCl$_3$	chloroform
CQS	camphorquinone-10-sulfonic acid
DAP	diallylated polyethylene glycol
DCTB	*trans*-2-[3-(4-*tert*-butylphenyl)-2-methyl-2-propenylidene]malononitrile
DLS	dynamic light scattering
DMA	dynamic mechanical analysis
DMAAm	N,N-dimethylacrylamide
DSC	differential scanning calorimetry
DT	water soluble dithiol
ETTMP1300	ethoxylated trimethylolpropane tri(3-mercaptopropionate)
FCC	free radical crosslinking copolymerisation
FCF	field correlation function
GDMP	glycol di(mercaptopropionate)
ICF	intensity correlation function
Ini	initiation
ISC	intersystem crossing
KCl	potassium chloride
KTFA	potassium trifluoroacetate
LCST	lower critical solution temperature
LED	light emitting diode
LN	linear thiol-ene polymer
LS	light scattering
MALDI	matrix assisted laser desorption ionisation
NaH	sodium hydride
NMR	nuclear magnetic resonance
PAAm	polyacrylamide
PEG	polyethylene glycol
PEO	polyethylene oxide
PTFE	polytetrafluoroethylene
RII	refractive index increment
SLS	static light scattering
TEMED	N,N,N',N'-tetramethylethylenediamine
TEP	thiol-ene polymerisation
THF	tetrahydrofuran
TOF	time of flight
UV/Vis	ultraviolet/visible
v : v	ratio of volume to volume

Appendix B: List of Symbols

$\langle\ldots\rangle$	average
$\langle\ldots\rangle_E$	ensemble-average
$\langle\ldots\rangle_T$	time-average
$\langle\delta c^2\rangle$	mean square fluctuation of the concentration
$\langle\delta n^2\rangle$	mean square fluctuation of the refractive index
A	amplitude of exponential decay
c	concentration
c^*	overlap concentration
c_{AAm}	concentration of acrylamide
c_{BIS}	concentration of BIS
c_{cross}	concentration of crosslinker functionalities
$c_{DAPX000}$	concentration of DAP1000/DAP2000/DAP3000
c_{DTX000}	concentration of DT1000/DT2000
c_{Etox}	concentration of ethoxy groups
c_{ETTMP}	concentration of ETTMP1300
c_{min}	minimally necessary concentration for formation of a continuous network
c_{pol}	concentration of polymer
c_{TEP}	monomer concentration in thiol-ene polymerisation
D	diffusion coefficient
D_A	apparent diffusion coefficient
dn/dc	refractive index increment
E	electric field amplitude
E^*	conjugate electric field amplitude
$\vec{E}$	electric field
f	functionality
f_{av}	average functionality
$f(q,\infty)$	offset of the FCF as determined by non-ergodic medium method
$f(q,\tau)$	FCF as determined by non-ergodic medium method
$g^{(1)}(q,t)$	field correlation function
$g^{(2)}(q,t)$	intensity correlation function
G	shear modulus
G'	elastic shear modulus / storage modulus
G''	viscous shear modulus / loss modulus
G^*	complex shear modulus
G_0	equilibrium shear modulus
G'_∞	elastic shear modulus, plateau value
G''_∞	viscous shear modulus, plateau value
G_{af}	shear modulus as determined by the affine network model
$G_{af,eff}$	effective shear modulus as determined by the affine network model
G_{ph}	shear modulus as determined by the phantom network model
$G_{ph,eff}$	effective shear modulus as determined by the phantom network model
G'_{th}	theoretically possible maximal elastic modulus
$H(x)$	HEAVISIDE function
I	scattering intensity [Hz]
I_0	intensity of the incident radiation
I_F	scattering intensity of the fluctuating fraction of a network [Hz]
I_S	scattering intensity of the static fraction of a network [Hz]

k_B	BOLTZMANN constant, $1.381 \cdot 10^{-23}$ J/K
K	constant (eq. (56))
m	mass
m_{dry}	mass of the dry network
m_{sw}	mass of the equilibrium swollen network
M	molar mass
M_{branch}	molar mass of the branches in ETTMP1300
M_{chain}	molar mass of network chains as defined in chapter 4.1
$M_{DAPX000}$	molar mass of the dienes DAP1000/DAP2000/DAP3000
M_s	number-average molar mass of network strands
M_{NMR}	molar mass determined from NMR spectrum
M_n	number-average molar mass
M_w	weight-average molar mass
n	refractive index
n	amount of substance [mol] (chapter 3.2.2)
n	relaxation exponent (chapter 2.1.3.2)
n_F	scattering count rate of the fluctuating fraction of a network
n_S	scattering count rate of the static fraction of a network
N	number of molecules
$\aleph$	number of modes
p	conversion
p_{crit}	critical conversion
p_{gp}	conversion at gel point
p_{swell}	conversion determined after swelling
$P(\langle I \rangle_{T,p})$	distribution of the time-average, position-dependent scattering intensity
q	length of the scattering vector
Q_m	mass-related degree of swelling
Q_V	volume-related degree of swelling
r	molar ratio of thiol and ene functional groups (eq. (27))
r	distance (eq. (54))
r_0	end-to-end distance
r_p	reaction rate
R	universal gas constant, 8.314 J/(molK)
R^2	coefficient of determination
$R(q)$	RAYLEIGH-ratio
$R_{ex}(q)$	RAYLEIGH-ratio of the excess scattering
$R_{gel}(q)$	RAYLEIGH-ratio of a polymer gel
$R_{sol}(q)$	RAYLEIGH-ratio of a polymer solution
$R_T(q)$	RAYLEIGH-ratio arising from thermal concentration fluctuations
R_H	hydrodynamic radius
t	time
T	temperature
T_g	glass transition temperature
T_{melt}	melting temperature
u	distance between scattering volume and detector
V_{coil}	volume of a polymer coil
V_{sc}	scattering volume
V_{dry}	volume of the dry polymer network
V_{sw}	volume of the equilibrium swollen network
x_n	degree of polymerisation
z	charge of a molecule in MALDI-TOF

β	coherence factor
δ	phase shift / phase angle
ε	crosslinking efficiency
ϕ_v	volume fraction
γ	shear strain
γ_0	amplitude of shear strain
$\dot{\gamma}$	shear rate
$\gamma(r)$	spatial correlation function
η	dynamic viscosity
λ_0	wavelength of radiation in vacuum
μ	molar density of crosslinker molecules
ν	molar network chain density
ν_{eff}	effective molar network chain density
ν_{th}	theoretical molar network chain density
θ	scattering angle
ρ	density in g/L
ρ_{net}	density of the dry polymer network in g/L
ρ_{solv}	density of the solvent in g/L
σ	shear stress
σ_0	amplitude of shear stress
σ^2	y-axis intercept of the ICF
τ	lag time
$\tau_{(1)}$	correlation time of the FCF
$\tau_{(2)}$	correlation time of the ICF
$\tan\delta$	loss tangent
ω	shear frequency
ξ_D	dynamic correlation length
ξ_S	static correlation length

indices:

coop	cooperative
ho	homodyne
he	heterodyne
Lit	literature value
p-h	partial-heterodyne
p	position-dependent
rb	reactor-batch gel
trans	translational

NMR-abbreviations:

d	doublet
t	triplet
q	quintet
m	multiplet

Appendix C: List of Chemicals

Substance	Abbreviation	Molar Mass in g/mol	Supplier	Purity	Utilisation	Illustration
acrylamide	AAm	71	Sigma-Aldrich	99 %	recrystal-lised from acetone	Scheme 8 left hand side
allyl bromide		121	Aldrich	99 %	used as received	
ammonium peroxydisulfate	APS	228	Aldrich	≥ 98 %	used as received	Scheme 10 left hand side
camphorquinone-10-sulfonic acid monohydrate	CQS	264	molekula	hydrate	used as received	Scheme 9
diethyl ether		74	Merck	≥ 99.7 %	used as received	
ethanol		46	Merck	≥ 99.5 % absolute	used as received	
ethoxylated trimethylolpropane tri(3-mercaptopropionate)	ETTMP1300	1274	donated by BRUNO BOCK Chemische Fabrik GmbH & Co. KG		used as received	Scheme 6 right hand side
glycol di(mercaptopropionate)	GDMP	238	donated by BRUNO BOCK Chemische Fabrik GmbH & Co. KG	98 %	used as received	Scheme 11 top
N,N,N',N'-tetramethylethylenediamine	TEMED	116	Acros Organics	99 %	used as received	Scheme 10 right hand side
N,N'-methylene bisacrylamide	BIS	154	Merck	99.5 %	used as received	Scheme 8 right hand side
n-hexane		86	Sigma-Aldrich	≥ 95 %	dried with KOH and distilled	
polyethylene glycol	PEG	1000, 2000, 3000, 35000	Sigma-Aldrich		used as received	

| Substance	Abbreviation	Molar Mass in g/mol	Supplier	Purity	Utilisation
potassium chloride		74.5	Merck	≥ 99.5 %	used as received
potassium hydroxide		56	Sigma-Aldrich	≥ 90 %	used as received
sodium hydride		24	Aldrich	60 % in mineral oil	purified with n-hexane
sodium sulfate		142	Sigma-Aldrich	≥ 99.0 %	used as received
tetrahydrofurane	THF	72	Sigma-Aldrich	≥ 99.5 %	dried with Na_2SO_4
toluene		92	Acros Organics	99.85 %	used as received
water		18	Sartorius arium 611VF	ultra-purified 18.2 MΩ·cm	

Appendix D: NMR Spectra

1. Diallylated polyethylene glycol, DAP1000: ^{1}H-NMR, 400 MHz, CDCl$_3$
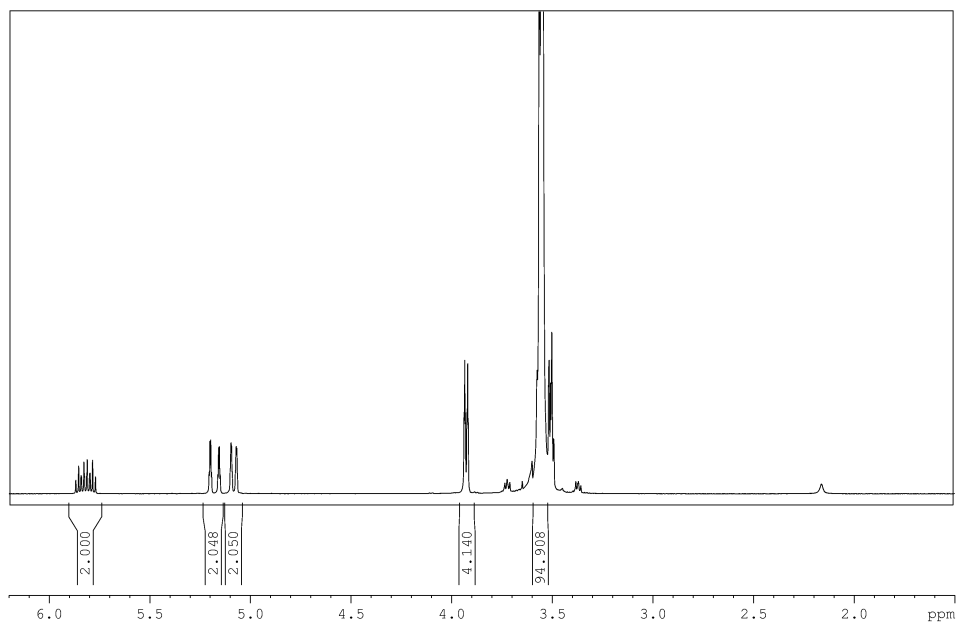
2. Water soluble dithiol, DT1000: ^{1}H-NMR, 400 MHz, CDCl$_3$
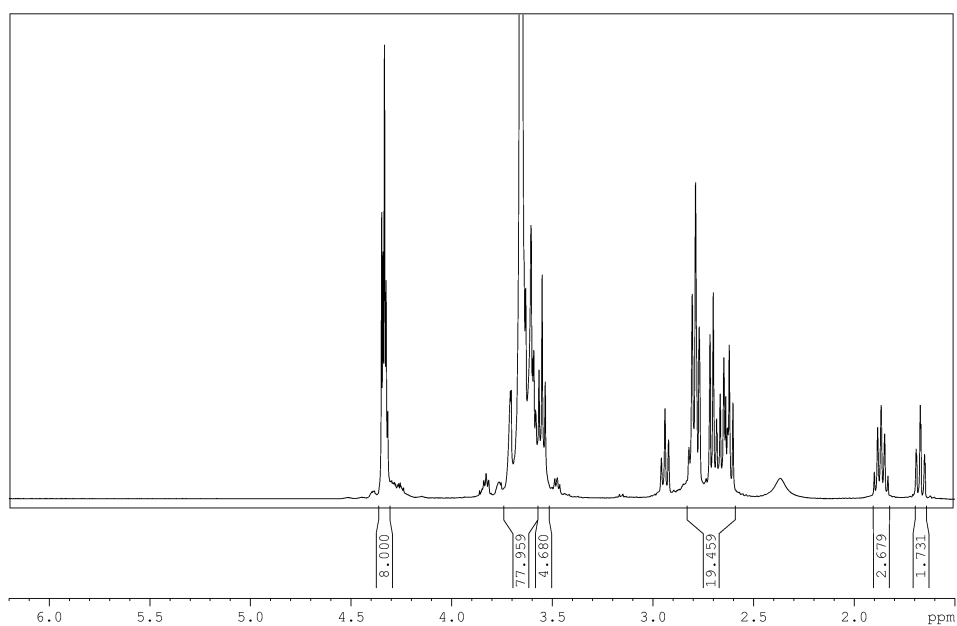
3. Linear thiol-ene polymer, LN11: ^{1}H-NMR, 400 MHz, CDCl$_3$
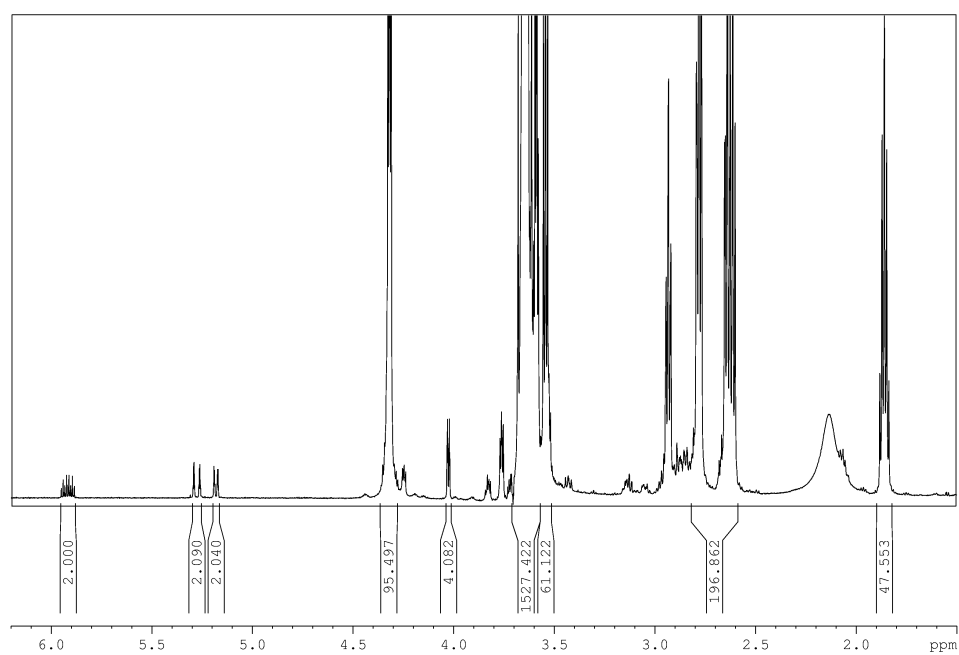
Acknowledgements

First of all I want to thank PROF. WILHELM OPPERMANN for giving me the chance to work on this interesting and challenging topic. The door was always open to talk to him, to discuss problems. After every discussion I gained important insights and new ideas on how to go on.

My thanks also go to DR. JÖRG ADAMS for reviewing my thesis and for being a great office-neighbour who was always willing to help with all kinds of questions and problems.

Furthermore, I thank PROF. DIETER KAUFMANN for taking over the post as chairperson of the board of examiners.

I also owe thanks to DANIEL GROSCH, SANDRA KAUL, PHILIPP SEICHTER, TABEA THÜRNAU, FABIAN UHRNER AND MARTIN SÖFTJE who all of the them, at one time or another, worked with me on this thesis.

I am very grateful to ASTRID PESCHEL for carrying out DSC measurements for me, to LARS NOTHDURFT for performing important MALDI-TOF measurements and to JAN NAMYSLO and his team for quite a lot of NMR measurements.

I am especially indebted to ARNE LANGHOFF, for example for putting together several LED lamps from scratch that were absolutely essential to my work, and MICHAEL TÖLLE, who always provided support and all the things you cannot go without, working in a lab. Without the two of them it would have been a lot harder and less fun to work on this thesis. The same goes for all my other friends and co-workers at the Institute of Physical Chemistry. I had an incredibly good time and it was a treat to go to work every day.

I particularly want to mention some other people, who have been very important to me: ANNE, EVA, KATJA, NADINE, NENA, RIKE, STEFFI, SYLVIA, VOLKAN, I feel blessed that we could go through this crazy, funny, tough time together.

Obviously, I am most grateful to my parents, my brother and my boyfriend, who have always and ever been there for me.

And lastly, I thank ARNE LANGHOFF, KATJA POHL, REBEKKA KÖNIG, ROSS MASPERO and VOLKAN CAN for thoroughly proof-reading my thesis. I know it took up quite a lot of their time!

THANK YOU!